

Time domain identification of the mechanical system of a drive for the purpose of diagnostics

Von der Naturwissenschaftlich – Technischen Fakultät
der Universität Siegen

zur Erlangung des akademischen Grades

Doktor der Ingenieurwissenschaften

(Dr.-Ing.)

genehmigte Dissertation

von

M.Sc. Maria del Carmen Perdomo Arvizu
aus Mexiko, Mexiko Stadt

1. Gutachter: Prof. Dr.-Ing. Mario Pacas
2. Gutachter: Prof. Dr.- Ing. Hubert Roth

Tag der mündlichen Prüfung: 03.03.2015

Index of contents

Index of contents.....	2
Acknowledgements.....	5
Nomenclature.....	6
Abstract.....	9
Zusammenfassung.....	10
1. Introduction.....	11
1.1 Motivation of the work.....	12
1.2 Objectives.....	13
1.3 State of the art.....	14
1.3.1 Identification of mechanical parameters.....	14
1.3.2 Adaptive control.....	16
1.3.3 Machine diagnosis.....	17
1.4 Outline of the chapters.....	21
2. Theoretic fundamentals.....	23
2.1 Modelling and identification of electromechanical drives.....	23
2.1.1 One-mass system.....	25
2.1.2 Two and more mass system.....	26
2.1.3 Generalized coordinates and reduced moment of inertia of multi-body mechanisms.....	27
2.2 Cascade control structure.....	29
2.3 Sensorless speed control techniques.....	32
2.4 Summary of the chapter.....	34
3. Stochastic identification in time domain.....	35
3.1 Stochastic identification: extended Kalman filter.....	35
3.2 Causes of divergence by utilizing Kalman filters.....	39
3.2.1 Causes of divergence due to linearization in extended Kalman filters.....	40
3.3 PRBS as additional excitation to the system.....	41
3.4 Non-linear system model.....	44
3.5 Structure of identification.....	46
3.6 EKF identification of a variable reduced moment of inertia.....	48
3.6.1 Reduced moment of inertia of a vertical crankshaft slider.....	48

3.7	Simulation of EKF identification of a crankshaft slider.....	51
3.8	Summary of the chapter.....	53
4.	Deterministic Identification in time domain	55
4.1	Fourier series for signal representation	55
4.2	Identification of a periodical drive torque	57
4.3	Working hypothesis for the deterministic identification of a periodical load	58
4.4	Mechanical load as function of the angular position of the motor	59
4.5	Sliding window for discrete integration	61
4.6	Structure of identification	64
4.7	Summary of the chapter.....	64
5.	Feed-forward control for a variable inertia system	66
5.1	Feed-forward control structure.....	66
5.2	Model of disturbances and variable reduced inertia effect.....	69
5.3	Summary of the chapter.....	72
6.	Diagnostics.....	73
6.1	Rolling bearing failure detection	74
6.2	Causes and classification of failures in rolling bearings	75
6.3	Diagnostic of failures ball rolling bearings on machines with cyclical process	76
6.4	Effect of the friction in rolling bearings on the load torque to the drive.....	77
6.5	Fault bearings effects on the drive torque of a composed mechanism.....	79
6.6	Summary of the chapter.....	80
7.	Experimental results.....	82
7.1	Identification with the extended Kalman filter	83
7.1.1	EKF identification of variable moment of inertia with measurement of the shaft position.....	83
7.1.2	Identification of the reduced moment of inertia with an EKF and without encoder.....	92
7.2	Identification of the torque by means of a deterministic procedure	99
7.2.1	Deterministic identification using the measured mechanical velocity	100
7.2.2	Deterministic identification in a system without encoder	103
7.3	Feed-forward compensation	105
7.3.1	Feed-forward compensation with encoder feedback	106
7.3.2	Feed-forward compensation in encoderless control scheme	111
7.4	Diagnostics.....	116

7.4.1	Single point bearing damage.....	117
7.4.2	Severe single point fault on bearings	119
7.5	Summary of the chapter.....	122
8.	Conclusions.....	124
9.	Appendix.....	127
9.1	Characterization of the crank slider mechanism for the mass particles model.....	127
9.2	Experimental Platform I.....	129
9.3	Experimental Platform II.....	130
9.4	Kinetic energy analysis	130
10.	References.....	136

Acknowledgements

The present work was realized during my research activities in the Institute of Power Electronics and Electrical Drives of the University of Siegen. This work was carried out thanks to the financial assistance of the German Academic Exchange Service (Deutscher Akademischer Austauschdienst-DAAD) and the Mexican National Council of Science and Technology (Consejo Nacional de Ciencia y Tecnología-CONACyT).

I would like to express my deepest gratitude to Prof. Dr.-Ing. Mario Pacas for his guidance during this project, the great continuous support he gave me and all the useful scientific advices. I really appreciate all his valuable suggestions that made possible the completion of my research.

I also would like to thank Prof. Dr.-Ing. Hubert Roth for his counseling and work as co-examiner. I'm thankful to Prof. Dr.-Ing. Elmar Griese for the guidance of the doctoral procedure. I'm also grateful to Prof. Dr.-Ing. Claus Peter Fritzen, Dr.-Ing. Thomas Eutebach, Dr.-Ing. Klaus Teichmann, Prof. Dr.-Ing. Rainer Lohe, Dr.-Ing. Jürgen Wahrburg and Dr.-Ing. Ahmad Kamal for the all the help and technical discussions.

I want to mention my appreciation to the persons of the institute, Dipl.-Ing. Erhard Oerter, Dipl.-Ing. Walter Bruch, Sabine Leukel, Dipl.-Ing. Manuel Steinbring, Dipl.-Ing. Simon Feuersänger, Dipl.-Ing. Henning Zoubek, M.Sc. Saul Dufoo, M.Sc. Othman Abdulhadi Taha, M.Sc. Marcelo Pozo, Dipl.-Ing. The Minh Phan, M.Sc. Seemaa Fathi, M.Sc. Al-Badrani, and M.Sc. Fernando Ramirez. I'm deeply thankful for the cooperative working environment at the institute that was very important for the realization of this work.

My special acknowledgement to my parents, Manuel y Carmen and special thanks to Laura, Manolo, Jorge, Fernando y Lula.

Nomenclature

Symbols

M	Torque
J	Polar moment of Inertia
ω	Angular frequency
t	Time variable
D	Damping constant
C	Elastic constant
i	Current
Ψ	Flux
α, β	Polar coordinates
γ	Motor angular position
T	Time constant
K_p	Proportional controller gain
\underline{x}	State vector
\underline{u}	Input vector
\underline{y}	Output vector
Q	Process error covariance matrix
R	Measurement error covariance matrix
P	Estimation covariance matrix
K	Kalman filter gain
Φ	Transition Matrix
F(...)	Jacobian Matrix
F	Force
H	Observer Matrix
p	Relative position
J_e	To the shaft of the motor Reduced moment of inertia
θ	Angular crank position
j	Imaginary unit
m	Mass
N	Number of registers on the PRBS generator

Subscripts

M	Motor related quantity
L	Load related quantity
CR	Connecting rod
R	Quantity with radial orientation
N	Quantity with normal orientation

L_f	Related to load friction
V	Related to viscous friction

Superscripts

x^T	Transposed Matrix
\hat{x}	Estimated value
x^*	Reference value
\dot{x}	Derivative

Abbreviations

EKF	Extended Kalman Filter
MRAS	Model reference adaptive system
DOF	Degrees of freedom
PM	Permanent magnet
EMF	Electromotive force
MPC	Model predictive control
FEM	Finite element method
DTC	Direct torque control
FOC	Field Oriented control
PRBS	Pseudo random binary signal
TTL	Transistor-transistor logic
SPI	Serial peripheral Interface

Special terms

L_0	Mechanical angular momentum
T_n	Control parameter, time constant of integration
T_{si}	Equivalent time constant of the closed current control loop
i_q	Torque forming current component
T_H	Mechanical time constant
t_k	Discrete time
T_p	Period
T_{PRBS}	Period of the PRBS
T_t	Interval of the PRBS
ma	Dynamically equivalent mass particle located at the actuator
mb	Dynamically equivalent mass particle located at the crank and connecting rod junction
mc	Dynamically equivalent mass particle located at the slider
r_1	Distance between crank joints

r_2	Distance between connecting rod joints
x_{CR}	Slider displacement
P_f	Power density
ω_0	Fundamental frequency
E_K	Kinetic energy
M_{FB}	Total torque due to friction in the bearing

Abstract

The dynamic behavior of an electrical drive depends largely on its mechanical components. Models of the mechanical parts are often used in the industry to adjust current, velocity and position control. Therefore the identification of the mechanics is of high importance to adequately design the control and to monitor the condition of the drive. The present work, is a contribution on the identification of mechanical parameters in time domain. This dissertation is focused on the identification of drives possessing composed mechanisms that have periodical motion cycles. From the point of view of control, such mechanisms can be described by the reduced moment of inertia, which is a function of the position of the actuator. The identification of this mechanical part was approached in this work by utilizing two different methods: a stochastic and a deterministic procedure.

By utilizing an Extended Kalman Filter the reduced moment of inertia can be estimated as well as the load over the mechanism. A new speed-sensorless scheme for the identification of variable inertia and load with EKF was experimentally evaluated.

Load and inertia have a separated effect on the dynamical response of a drive system. Their effects are even more significant when this parameters are variable. However by defining certain working conditions, the velocity controller of the system can be utilized to characterize the motor torque reference. Based on this idea a novel deterministic identification method with Fourier series was developed. The results of this identification method can be used to calculate a mathematical model of the motor torque of the system. This model can be used to improve the classical PI velocity control with feed forward compensation.

In the industry, faults related to the mechanical components of the electro-mechanical machines represent a high proportion of the total failures within industrial drives. A method for the detection of faults in bearings was outlined within the scope of this work. If the dynamic response of a drive is measured during the commissioning of the machine, this information can be considered the footprint of a healthy system and can be used to be compared with updated measurements during operation.

Zusammenfassung

Das dynamische Verhalten eines Elektroantriebs ist von seinen mechanischen Komponenten abhängig. Mehrere Modellen der mechanische Teil sind an der Industrie oft verwendet um die Steuerung anzupassen. Die Identifikation der mechanischen Parameter ist deswegen für den optimale Steuerungsentwurf und Zustandsüberwachung der Maschinen von große Bedeutung. Dieses Werk ist ein Beitrag an das Thema Identifikation von mechanischen Parametern im Zeitbereich. Die Dissertation konzentriert sich auf die Identifikation Elektromechanischer Antriebe mit ebene Mechanismus und periodischen Bewegungen. Solche Mechanismen lassen sich durch sein reduziertes Trägheitsmoment beschreiben. Die Identifikation der mechanischen Parametern identification wurde durch zwei unterschiedliche Methoden erfolgt: stochastische und deterministische Verfahren.

Anhand Erweiterter Kalman Filtern kann das reduzierte Trägheitsmoment so wie das Lastmoment ermittelt werden. Ein neues Sensorloses Schema für die Identifikation von variable reduziertes Trägheitsmoment und Lastmoment wurde bewertet.

Das Lastmoment und das Trägheitsmoment haben unterschiedliche Effekte über die Dynamik des Antriebsystems. Die Wirkung von solchen Parametern ist sogar starker wenn die Parameter variabel sind. Unter bestimmte Betriebsbedingungen kann der Drehzahlregelung benutzt werden um der Solldrehmoment zu kennzeichnen. Aus diesem Grund wurde eine deterministische Identifikationsmethode mit Fourier-Reihen entwickelt. Die Ergebnisse dieser Identifikationsmethode können in der Berechnung eines mathematischen Modells des Antriebsdrehmoments verwendet werden. Solch ein Modell kann durch eine Vorsteuerung die Dynamik einer klassischen PI-Drehzahlregelung verbessern.

Die Schäden in den mechanischen Komponenten stellen den größten Anteil der gesamten Störungen Elektromechanischer Antriebe in der Industrie dar. Eine Methode für die Erkennung von Wälzlagerschaden wurde beschrieben. Messungen der dynamische Antwort bei der Inbetriebnahme der Maschine können ein Bewertungskriterium sein, dass sich der Antrieb in einem guten Zustand befindet und diese Messungen können jedes Mal mit aktualisierten Messungen verglichen werden.

1. Introduction

The production and handling of goods and materials requiring machines with high dynamics and precision is a rising demand in the industry. Cost reduction and quality of production is related to specific capabilities of these machines. Automatic commissioning, early failure detection, reliability, optimal control and simplification of instrumentation are among others desired characteristics for all machines and processes with a high degree of automation. Electrical drives are key components in such machines and processes and therefore they have to fulfill these characteristics as well.

Nowadays the term “Servo-Drive” designates generally a variable velocity electrical drive that allows velocity and position control. Servo-Drives can be DC-drives or AC-drives. Today in all ranges of power AC- drives are preferred because its robustness and because they exhibit excellent dynamic properties as a result of the progress in power electronics and signal processing during the recent years. The advances in design of frequency converters and motion control have contributed to increase the efficiency and to improve the performance of production machinery.

Beside of the electrical components, production machines requires a mechanical part, axes, gear boxes, guides and often more complex mechanism with specific characteristics for the transmission of forces and movement. The different applications of electro-mechanical drives extend to a large variety of manufacturing machines, to several production stages and to logistic systems. Most of such systems are designed and built in a unique way, with the purpose to execute a particular task. The operation of high automatized production systems is based on the distribution of the whole process in sequential repetitive tasks. These tasks are sometimes so specific that the designed system are so adapted to the individual task that it is difficult to categorize them in a suitable way, but it is important to understand the physical phenomena that occurs on them. The dynamic response of an electro-mechanical drive is influenced by its mechanical parameters. Therefore the optimal design of control for such systems can only be accomplished if information about these parameters is available. Furthermore, the mechanical parameters should be observed and understood for condition monitoring purposes. When disturbances appear on the system, it is crucial to identify their causes. For example, some

mechanical parameters can change during operation of the machine, such changes could be an indication of failure but also it may be proper of the mechanism motion. A correct discernment of the causes of the disturbances and an appropriate interpretation of the mechanical parameter identification allows the development of diagnostics procedures for the early detection of faults in electro-mechanical drives which would make possible to avoid the costs of production interruptions or more severe reparations.

1.1 Motivation of the work

The identification of the mechanical parameters in drive systems has a significant connotation for design of the control especially for the automatic commissioning and for the optimum operation of industrial machines.

In many industrial applications, the mechanical parameters of the mechanical system change during the operation; this can be due to the inherent characteristics of its mechanisms or to the nature of the process. On the other hand, changes of the parameters of a drive during operation can also indicate an emerging failure. For both scenarios, an on-line identification of the mechanical characteristics and parameters of the driven machine is desirable. In the first case, the control scheme must be automatically adapted to the changing mechanical parameters in order to meet the desired dynamic performance. In the second case, the knowledge of a change of the parameters during the operation allows the development of online strategies for condition monitoring.

Cost reduction and reliability in industrial drives are also topics of high importance. Recently, more advanced control methods and techniques for the minimization of the time dedicated to the commissioning and of the number of sensors are being developed with these aims. Since sensors are keen to fail in harsh environments [1] and because of the cost factor that they represent, speed-sensorless control techniques are subject of intensive research. Currently some of such techniques are successfully applied in the praxis [2] [3] [4].

One of the purposes of the present work is to further research identification methods to estimate the mechanical parameters of the system under sensorless control schemes, which would result

in more reliable systems and cost reduction for the assembly and maintenance of the installations.

1.2 Objectives

The present work is a contribution to the area of identification of mechanical parameters in the time domain. This dissertation was developed at the Institute of Power Electronics and Electrical Drives of the University of Siegen, complementing in this way the line of research realized until now that approaches the identification of systems in the frequency domain.

More specifically, the first objective of this dissertation is the identification of mechanical part in electro-mechanical drives with repetitive, periodical motion cycles in the time domain. The task of identification is intended to estimate the mechanical parameters under speed-sensorless control schemes. For this two approaches of identification are utilized: stochastic and deterministic.

The identification results can be utilized to calculate a model of the mechanical load of the system. This model can be used for a feed-forward control in order to improve the dynamic response of the system.

The second objective of this dissertation is the outline of characterization of faults in rolling bearings of electrical drives in composed mechanism. In the time domain, oscillations of the drive torque are unavoidable in mechanism which transforms rotating into linear motion such as crankshafts-sliders, not just because of the change in orientation of the forces but also because of the changing nature of the inertial forces due to the changes in the geometry of the mechanics. The effects of a failure in bearing are therefore not easily recognizable in time domain. However, by taking measurements of the driving torque at the commissioning of the machine a typical pattern of the healthy mechanics can be obtained. This pattern can be compared with updated measurements during operation to detect deviations that may indicate a fault in the mechanics.

1.3 State of the art

This dissertation is oriented to the topic of identification and diagnostics in time domain. In the context of control, the identification results are utilized to improve the dynamics of the system response by implementing feed-forward compensation, a kind of adaptive control. Therefore, a description of the state of the art of identification, adaptive control and diagnostics is presented in this section.

1.3.1 Identification of mechanical parameters

Because of its impact in the dynamic behavior of the electrical drive systems, the identification of the mechanical parameters is the aim of several works that can be found in the literature. Hence, it has been mainly examined and analyzed in control schemes with position or velocity sensor.

In [5] Saarakkala utilizes a discrete-time pulse transfer function calculated from the differential equations of the mechanical part modeled as a two mass system, the mechanical parameters are calculated from the coefficients of the discrete polynomials of the transfer function by using an output error structure for the direct estimation in a close control loop when the velocity control is a single gain. Subsequently, in [6] and [7] Saarakkala and Hinkkanen modified this procedure [5] for indirect closed control loop identification when a state space velocity controller is used, there the matrices of the discretized pulse transfer function are used in an iterative least squares algorithm to calculate the continuous time transfer function of the system. The mechanical parameters are computed from the coefficients of the transfer function. This technique works under the assumption that the load torque is known and it is assumed to be constant or a step function.

Andoh proposed two methods for the identification of the moment of inertia: in the first one [8] the inertia is estimated based on the time average of the product of torque reference input and motor position, in the second one [9] a sinusoidal position reference is utilized for the determinist calculation of the moment of inertia as a function of the amplitude of position reference and of the measured velocity.

Guo and collaborators presented an MRAS algorithm for identification of the moment of inertia [10]. Toyozawa, Harada and Kashiwagi [11] describe the online identification of mechanical parameters from the mechanical function with a steep descent method using an M-sequence as input to the system. Pletschen, Rohr and Kennel [12] [13] describe a method for nonparametric identification in the frequency domain. All these works considered only the cases of constant moment of inertia and velocity control with feedback from sensors or encoders [14].

The behavior of the load torque is also an important factor that impacts the dynamic response of the system, for example when the mechanical dynamics or the load are non-linear or time varying it is hard to achieve a good tracking of the velocity reference. Several strategies have been developed to cope with these issues. Harnefors, Saarakkala and Hinkkanen [15] designed a 2 DOF PI controller to overcome the disadvantages of a standard 1 DOF PI-velocity controller in those cases, they also use a simple load torque estimator for pumps and fans and a model for viscous friction to compensate the load torque in a feed-forward control scheme. De Angelo and coworkers designed a non-linear reduced-order observer for PM-AC electrical drives to estimate the induced EMF and load torque and calculate the rotor position [16]. Janiszewski utilizes an Unscented Kalman filter as observers for the estimation of the load torque [17] [18].

The well-established cascade structure of control with standard PI velocity controller cannot always shape the velocity response as desired when the load or the mechanicals parameters are time variable. Alternative methods are developed to overcome this problem, such as adaptive techniques or additional feedbacks. A comparative study of several techniques, such as different pole placement, the implementation of PID-velocity control, insertion of additional measured feedback and additional feedbacks from disturbance observers (Luenberger observers and Kalman filter) was presented in [19].

Szabat and Orłowska-Kowalska describe in [20] a forced dynamic control strategy where an optimized torque control loop is utilized to calculate the motor torque by taking feedback from the velocity, the load torque, the driving torque and its derivatives. However, the direct measurement of such variables is hard or not possible; therefore the application of an extended Kalman filter (EKF) is used. Also EKF are used in [21] to identify the driving torque, load torque and moment of inertia in order to tune the parameters of an adaptive control, and in [22] and

[23] in order to estimate the load velocity and torque and driving torque to provide an additional feedback for comparison when a Model Predictive Control (MPC) is used to optimize the system behavior with a cost function.

Identification under speed-sensorless schemes is a topic of increasing interest in research. All the consulted works realized under this scheme have identified constant moments of inertia. Some studies on the observability conditions for sensorless schemes have been performed [24], for a particular case because these conditions are dependent on the identification structure. In [25] Zhou and coworkers described the identification for constant mechanical parameters in time domain by using a varying amplitude triangular wave as velocity reference and utilization a least square algorithm to fit the parameters under sensorless control scheme.

In our research group at the University of Siegen, our group has developed and experimentally validated identification methods in the frequency domain. In his dissertation [26], Villwock utilized the Welch-Method to estimate the frequency response of the system. In [27] [28] [3] Zoubek achieved the calculation of the frequency response in a sensorless control scheme with different models of the mechanical part.

1.3.2 Adaptive control

The characteristic of adaptive control is mainly that it automatically adjusts to the plant. In adaptive control the control scheme is based on a mathematical model of the plant, therefore the quality of the control is determined by the accuracy of the model and of its parameters. By continuously monitoring the accuracy of the model and changing it by enhanced models, the properties of the control can be improved, therefore it can be stated that adaptive control contains additional feedback from the observed data of the model. [29]

Adaptive Control can be classified in two main categories [30]:

- a. **Feed-forward adaptive controllers:** This scheme works under the principle that the characteristics of the plant can be attained by only measuring signals acting on the process. A model of the plant can be calculated based on the relation between the

reference signal and the related output signal. The signals of the inner closed control loop are not taken in account. The advantage is that it is fast to track changes on the process; nevertheless a disadvantage is that the effects of disturbances on the unmeasured signals are overlooked.

- b. **Feedback adaptive controllers:** The signals acting on the process are measured as well as the input and output of the plant. In this way, the effect of external disturbances is also considered. The feedback adaptive controller are subdivided into ***dual adaptive controllers***, where the controller provides the desired performance by changing its parameters to reduce the estimation uncertainty by incorporating it into the control strategy [31], and ***non-dual adaptive controllers***, which do not include the uncertainty in the control strategy and only consider present and past values of the control loop signals.

A classification of the feedback adaptive controllers is summarized in Figure 1.1:

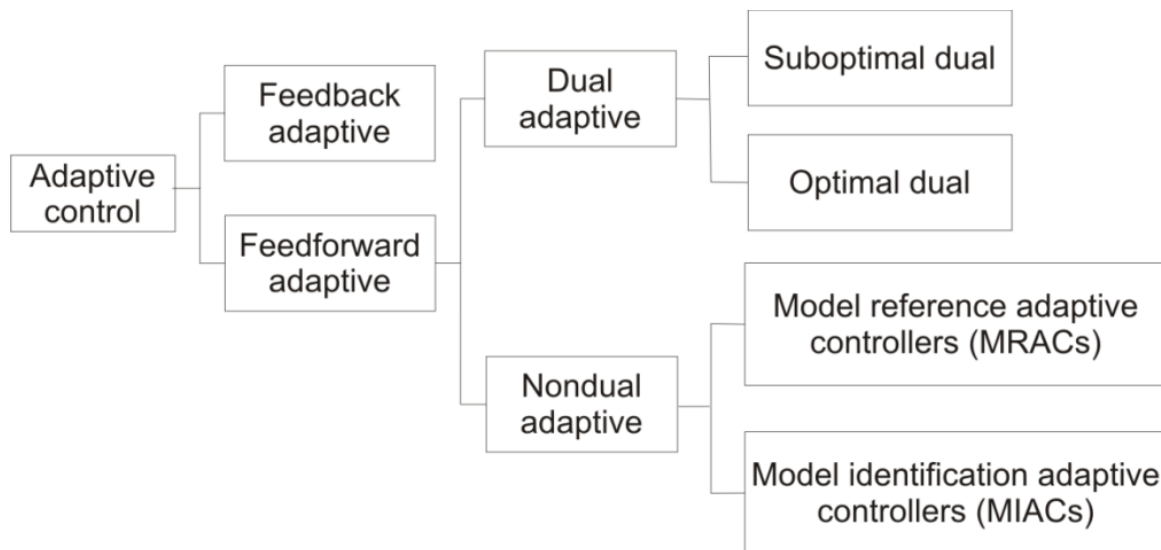


Figure 1.1 Classification of feed-forward adaptive controllers

1.3.3 Machine diagnosis

The breakdown of electrical drives causes financial losses due to repair expenses and unexpected downtime in the production. Therefore the maintenance of the systems is of high importance.

Several surveys about the faults in industrial installations (e.g. [32] and [33]) and a vast research on the causes and detection of such failures have been conducted.

There exist several faults that might happen in an electrical motor, depending on the type and location they can be classified as [34]:

- Stator faults
- Rotor faults
- Static and dynamic eccentricities
- Bearing faults

A survey report about motor reliability on industrial installations was presented by the IEEE Industrial Application Society in [32]. A similar survey was given by the Electric Power Research Institute on Palo Alto California [33]. The surveys were oriented to the more common types of medium-size motors: induction and synchronous motors ([32] included DC Motors). In a similar way, both reports coincide that the higher percentage of failures corresponds to failures related to bearings.

Failed component	IEEE- IAS % of failure	EPRI % of failure
Bearings	43.7	41
Stator related	8.4	36
Rotor related	25.5	9
Others	22.4	14

Table 1 Percentage of faults in electrical drives due to failed components

The causes of several failures on different components are mostly mechanical deterioration (wear and breakage), overheating and insulation break down. For the case of bearing related failure, other factors should be also considered.

In [35] Zhang and colleges made a review of several existing condition monitoring methods for medium-voltage induction motors including thermal protection, stator insulation monitoring,

broken rotor bar detection, air gap eccentricity and bearing failure detection. There they classify the methods for bearing damage detection on intrusive or non-intrusive, depending on if the method require sensors to measure data, or if the method makes use of signal already available within the control loop.

Within the literature, several methods for the diagnosis of bearing failure can be found such as:

- Vibration monitoring [36] [37] [38] [39]
- Shock pulse methods [40]
- Acoustic emission measurement [41]
- Stator current monitoring [42] [43] [44]

Among them, one of the most widely used in the industry utilizes vibration measuring, with the disadvantage that additional sensors are necessary for this and access to the motor is required, which makes this type of diagnostic methods more expensive than the alternatives for example, non-intrusive techniques.

A comparison between vibration signal analysis and current signal monitoring for diagnosis of bearing faults is presented by Bellini and coworkers in [45]. Within that work it is mentioned that the vibration signals caused by the repetitive impact between the damage component and the rolling elements bring information in amplitude and frequency about the location of the fault and are related to the mechanical frequency.

On the subject of current signal analysis, it is still unclear how the physical mechanism of vibration associates to the motor current harmonics, because also other troubles linked to the coupling of the machine with the load cause vibration, so the correlation between them is not straightforward.

Two approaches link the vibration monitoring and the current signal analysis: vibration causes torque ripple resulting in velocity ripple, and vibration causes a stator current component.

Zhou, Habetler and Harley used a noise cancelation technique to remove the dominant components of the stator current with a Wiener filter, so that the remaining components are related to the bearing fault. They also studied the case of a load that changes as a step function,

there the noise cancellation has to track the stator current over the load level, with satisfactory results in this case [46].

In [47] Blödt and coworkers unified the two approaches to the current signal analysis by utilizing the two effects of bearing failure: radial motor movement and load torque variations. First they calculate the air gap permeance as a function of the length variation of the air gap, depending on the fault location then the air gap flux density. The additional flux density is considered equivalent to the additional magnetic flux. The additional flux in each stator phase can be calculated. Under the hypothesis of the imposed stator voltages, the stator current in each phase is given by the derivatives of the corresponding fluxes, so it can be demonstrated that the radial rotor movement due to bearing faults produces additional frequencies in the stator current. In the case of punctual faults, each time a ball passes a hole, a mechanical resistance will appear. The load torque can be expressed in terms of the bearing fault related torque variations if the variations on the mechanical velocity are used to estimate the variations in the rotor MMF. In a different work [48], they utilize the same unified approach to calculate a time-frequency distribution to extract fault indicators for online monitoring, obtaining good results in steady state, in transient state they could execute the procedure under certain difficulties.

The results presented by Villwock [49] and coworkers [50] about the mechanical parameter identification in the frequency domain were applied by Zoubek and coworkers to develop a method for bearing condition monitoring [51]. By assuming the mechanics of an electric drive as a two-mass system, the frequency response can be calculated by applying the Welch method with the periodograms of the system from the transfer equation of the two-mass model and by measuring two signals from the system. A comparison between an actual frequency response with the one obtained during the commissioning of the plant, was used for an automated diagnosis by pattern recognition [52], with this method two types of bearing fault can be detected: generalized rough and single point defects. In a further step, they developed a method based on the frequency response analysis which can be used to identify bearing faults utilizing a broad band of perturbations that can be used as indicator to recognize the bearing failure [53]. Also time domain diagnosis methods for the identification of mechanical backlash were developed within the work group [54] [55] at the University of Siegen. These methods were

integrated with the bearing diagnosis frequency domain methods for the design of an expert system for identification, commissioning and monitoring of electrical drives [56].

1.4 Outline of the chapters

This dissertation is distributed in eight main chapters. This first chapter is an introduction to the subject of identification of mechanical parameters, adaptive control and diagnostics in electro-mechanical drives, also a portrait of the state of the art in these research areas was given.

In chapter 2, the theoretical fundamentals of this work are presented. The most usually applied models for the identification of the mechanical part in industrial drives are explained, following with the description of the cascade control structure and an explanation of the speed-sensorless control techniques for AC machines. An explanation of the reduced moment of inertia of composed mechanism is presented in this chapter as well.

Time domain identification was achieved by utilizing two different approaches: Stochastic and Deterministic procedures.

Chapter 3 is dedicated to describe the stochastic identification method in drives with an extended Kalman filter (EKF). This identification procedure for composed mechanisms with periodical motion estimates the reduced moment of inertia and the load torque. The identification implementation with EKF under speed-sensorless control schemes is also explained in this chapter.

Chapter 4 describes the deterministic identification technique. This method utilizes Fourier series to estimate the mechanical load of the drive under certain working conditions. In this chapter a description of the deterministic identification without encoder is presented.

In chapter 5 the calculation of a model for the drive system is achieved by utilizing the identification results from the deterministic method. Then, the realization of a feed-forward control to improvement of the system response is explained.

As one of the major failure percentages in electro-mechanical systems is caused by faults in the bearings, this work is focused on detection of rolling bearings faults. Diagnostics of fault bearings in electro-mechanical drives is presented in chapter 6. A short review of failure causes is given, as well as a classification of the faults. A method for the detection of faults in bearings on electrical drives with composed mechanism is outlined in the last part of this chapter.

Chapter 7 seven contains the experimental results obtained from the practical implementation of the algorithms and methods described in chapters 3, 4, 5 and 6. In the first part, the results of the experimental identification with the Extended Kalman filter are presented; then the deterministic identification experimental results with Fourier series are given as well.

The calculated model from those results was experimentally tested also for feed-forward control. The last part of chapter 7 contains the experimental results obtained when the measurements were performed with a healthy bearing and contrasted to the measurements obtained by utilizing a damaged one. The results can be used for diagnostic purposes.

The chapter 8 corresponds to the conclusions attained at the end of this work and the possible future work within this line of research. The chapter 9 and 10 correspond to the appendix and to the literature references.

2. Theoretic fundamentals

The purpose of this chapter is to introduce fundamental concepts that constitute the theoretical foundation of the present work.

Modeling electromechanical drives as a set of mass systems is a typical approach to describe its dynamic behavior. The models of a single mass system and two or more mass system are explained in the first part of this chapter. Then the concept of reduced moment of inertia for the case of machines with composed mechanism is introduced. This is used to explain how a multi-body mechanism can be represented in the time domain as a variable moment of inertia from the point of view of the velocity controller.

An explanation of the classical cascade control is given in the present chapter. The description of this structure of control is presented for a better understanding of the control and measured variables that were utilized for the identification.

2.1 Modelling and identification of electromechanical drives

Models are descriptions of physical systems that allow engineers to handle reality. Idealized models are usually utilized to analyze dynamical systems, such as electromechanical drives. Modelling opens a way to understand the relations between inputs, outputs and state variables within the limits of the described system. The approach to obtain a model of a dynamical system can be theoretical i.e. by mathematical formulation of processes, or experimental i.e. based on measurements of the signal process, but usually it is the combination of both.

Identification is the experimental approach to model a system from measurements [57] [58]. The identification of a system usually follows the theoretical formulations or a model constructed from *a-priori* knowledge about the process and physical laws. The identification methods are usually classified depending on the used model: Parametric models or Non-Parametric Models [26]. Non-parametric identification can be obtained straightforward from frequency domain measurements; a direct estimation of the characteristics of the system without previous

knowledge can be achieved by this way in the frequency domain [59]. Parametric models are often used to obtain an identification of the system in the time domain [6]. These models usually inherit their structure from the differential equations describing the dynamical system.

The measured data used for the identification is supposed to provide information about the dynamics of the system; however, all measured data contain noise as well as measurement errors coming from the sensors and the interfaces. At the same time, the model used for the identification is always an idealized and simplified version of the real system. Absolutely accurate models do not exist anywhere in the world and the deviation of the model with respect to the actual plant is called model error. Another classification of identification methods is based on the way the method handle the model, measurement and estimation errors [60]:

- Stochastic methods.
- Deterministic methods

Within the scope of this work, both approaches were applied for different identification procedures. The stochastic methods consider the errors stochastic, i.e. uncorrelated; the deterministic methods assume that the errors are limited and that the input determines the behavior of the system.

A parametric model of the mechanical system was utilized in the stochastic method of identification.

The mechanical components of electrical drives are usually modelled as a one, two or more mass system. This approach is a usual procedure in engineering in order to understand the dynamical behavior of complex mechanism. Such models of one or two elastically coupled masses may include non-linearities such as friction or backlash depending on the application and are described in the following.

2.1.1 One-mass system

The simplest model structure used to model a mechanical system is a single mass system that consists of just one integrator and is therefore a first order system.

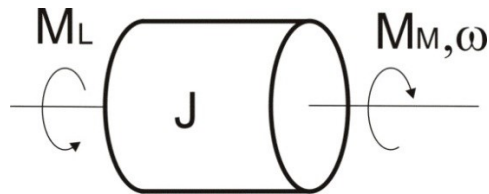


Figure 2.1 Rotary movement scheme

It is derived from the fundamental kinetic law of angular momentum when applied to a rotary motion of a body:

$$\frac{dL_0}{dt} = M_M - M_L = J \frac{d\omega}{dt} + \omega \frac{dJ}{dt} \quad (2.1)$$

Where the variables are:

L_0 – Mechanical angular momentum

M_M – Driving torque

M_L – Load torque

J - Moment of inertia

ω – Mechanical angular velocity

In many cases, the moment of inertia can be supposed to be constant, therefore its derivative can be neglected and the equation (2.1) is simplified. The classical expression of the one mass model depicted in (2.2) is:

$$\frac{d\omega}{dt} = \frac{1}{J} (M_M - M_L) \quad (2.2)$$

This model is accurate enough when the motor and the load are coupled with a stiff joint and the moment of inertia of the mechanism does not change during operation.

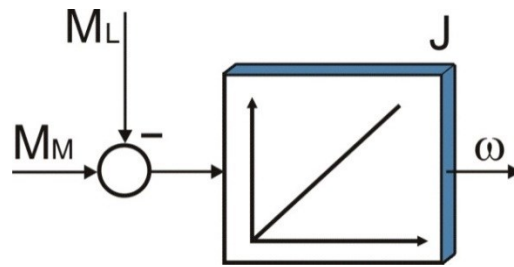


Figure 2.2 Block representation of one mass system

2.1.2 Two and more mass system

In several industrial applications the model of a single mass system is not enough because the joint between the drive motor and the last mechanism is elastic. The two or more mass system models are utilized to gain information about the system and its torsional oscillations. Figure 2.3 illustrates the model of the elastic coupling of two masses with the parameters C designating the elastic constant and D , the damping constant of the mechanical joint between load and actuator.

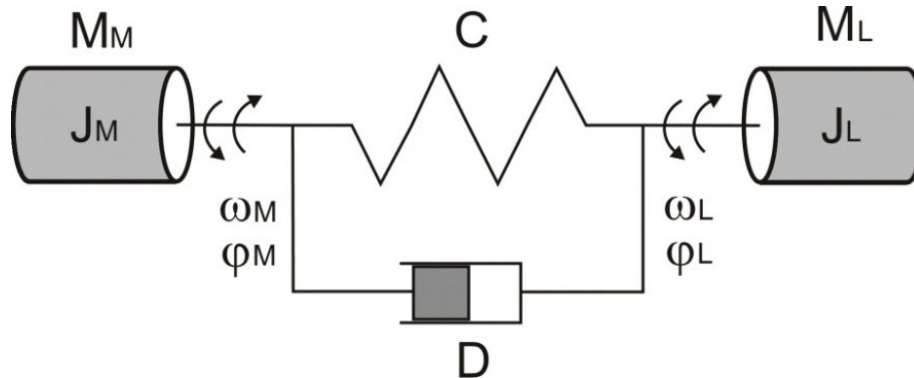


Figure 2.3 Two mass system scheme

In the case of more complex machines, the model with two masses cannot be enough, therefore a FEM analysis can be implemented, but this procedure has the disadvantage that the resulting model can have a very high order and non-linearities that are difficult to be included. Certainly, it is possible to reduce the order of such models [61] but under this approach, the resulting system may not be physically interpretable and internal states are not observable. Therefore, it is a usual practice, to describe the physics of the arrangement of masses joint by elastic couplings,

underlying the parameters and non linearities that are relevant to describe the dynamic behavior of the system [62].

Under this logic, the description of the two mass systems shown above can be extended for three, four or more mass system as shown in Figure 2.4 for a system with three concentrated masses that include as an example the backlash and the friction as non-linear elements.

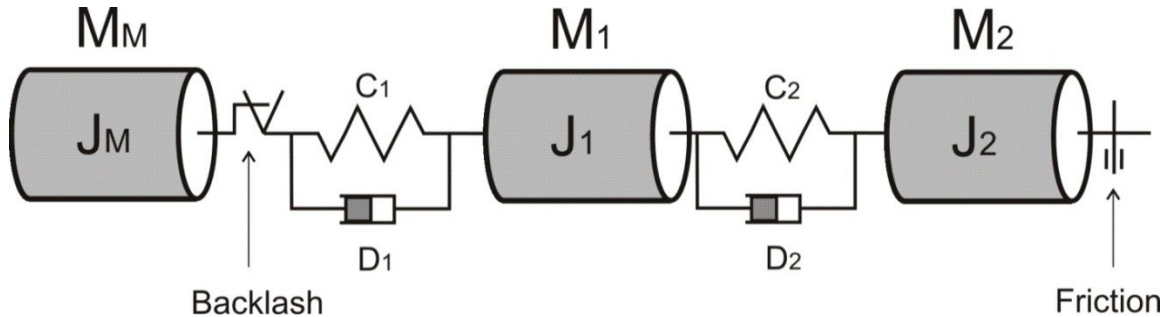


Figure 2.4 Three mass system scheme with two examples of possible causes of non-linearities.

The extended model of several masses is suitable for the study of torsional oscillation in complex systems with constant moment of inertia. Electrical drives in machines with composed mechanism where the rotatory movement is transformed in linear motion or transferred by displacement of mechanical elements usually have repetitive cycles of motion. They typically have a change in the geometry of the mechanical system, meaning that the position of the elements changes with respect to the actuator. This structure makes the equivalent moment of inertia, as reduced to the motor shaft, of the whole system to be a variable quantity. Thus the resultant equivalent moment of inertia can be expressed as a function of the position of the actuator.

2.1.3 Generalized coordinates and reduced moment of inertia of multi-body mechanisms

A generalized coordinate frame is sufficient to describe the position of a single body. Rigid bodies have characteristic mass parameters, center of mass, mass and moment of inertia. Generally the moment of inertia of a body and its position are defined with respect to a frame on the center of mass or a local frame.

In the case of mechanisms composed by rigid bodies moving around parallel axes and connected by revolute joints of one degree of freedom, the geometrical relation between the position of the actuator and the position of each component is determined by the structure of the mechanism and by the dimensions of its components. In those mechanisms, the generalized coordinate frame is located in the actuator and the local coordinate frames used to describe the relative position of the particular elements are located at the joints. The position of each component in a local frame \mathbf{p}_i can be expressed as function of the position of the actuator. Where the position of the actuator in generalized coordinates $\boldsymbol{\gamma}(t)$ is a function of time:

$$\mathbf{p}_i = \mathbf{p}_i(\boldsymbol{\gamma}(t)) \quad (2.3)$$

The velocity is calculated as the derivative of the position with respect to time:

$$\dot{\mathbf{p}}_i = \dot{\mathbf{p}}_i(\boldsymbol{\gamma}(t)) = \frac{d\mathbf{p}_i}{d\boldsymbol{\gamma}} \frac{d\boldsymbol{\gamma}}{dt} = \mathbf{p}'_i \dot{\boldsymbol{\gamma}} \quad (2.4)$$

The Kinetic energy of the whole mechanism is the sum of the kinetic energy of all components of the mechanism:

$$E_K = \frac{1}{2} \sum_i^I (m_i \cdot \dot{\mathbf{p}}_i^2) = \frac{1}{2} \sum_i^I (m_i \cdot \mathbf{p}'_i^2) \dot{\boldsymbol{\gamma}}^2 = \frac{1}{2} J_e(\boldsymbol{\gamma}) \dot{\boldsymbol{\gamma}}^2 \quad (2.5)$$

From the Kinetic Energy equation an expression for the reduced moment of inertia is obtained. This equation describes the apparent inertial change of the whole mechanism due to the displacement of the components with respect to the actuator:

$$J_e(s) = \sum_i^I (m_i \cdot \mathbf{p}'_i^2) \quad (2.6)$$

$J_e(\boldsymbol{\gamma})$ is the equivalent moment of inertia which is a function of the actuator position and represents all the inertial changes of every single element of the mechanism with respect to the

generalized coordinate frame due to the elements motion. This kinematic analysis makes possible to represent a composed mechanism as a single variable inertia system.

2.2 Cascade control structure

The cascade control is one of the most effective methods to stabilize and optimize process with time constants [63] of different ranges of magnitude, it is also the usual structure applied for the control of electrical drives. The cascade control scheme as shown in Figure 2.5 is a nested structure of underlying control loops [62] [64]. This is the common structure of an industrial electrical drive in which **C1** is the current or torque controller, **C2** the velocity controller and **C3** the position controller. V-FF and M-FF are eventual feed-forward blocks. The mechanical part is modelled as a single mass mechanical part with a mechanical time constant T_H ; the electrical machine is modelled as a first order lag with the time constant T_{si} , the torque and velocity constants k_M and k_ω respectively and a dead time block with the delay T_t . The integrator with the arbitrary time constant T_x delivers the linear or angular position as output of the system.

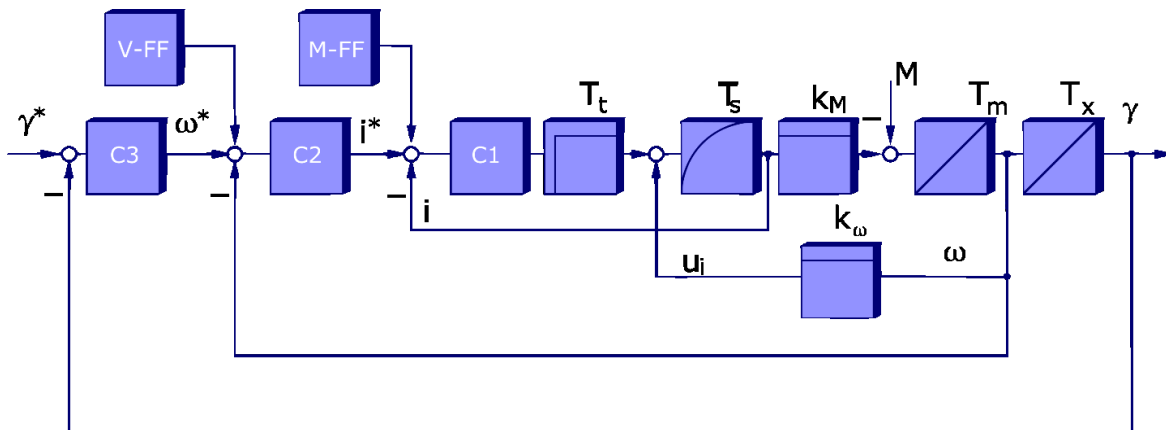


Figure 2.5 Cascade control structure

The current control is governed by the short time constant T_{si} of the electrical machine and demands therefore a fast control. Thus, this control loop can be nested within the slower control loops for the velocity ω and position γ .

In DC machines, the armature current control substitutes the torque control, as the torque itself is usually not measured and proportionality between torque and armature current can be assumed as long as the field is kept constant.

In the case of AC-machines the torque can be also controlled by means of a current control. A well established method for the control of the torque is the field oriented control, developed by Haase [65] and Blaschke [66] and whose structure is depicted in Figure 2.6.

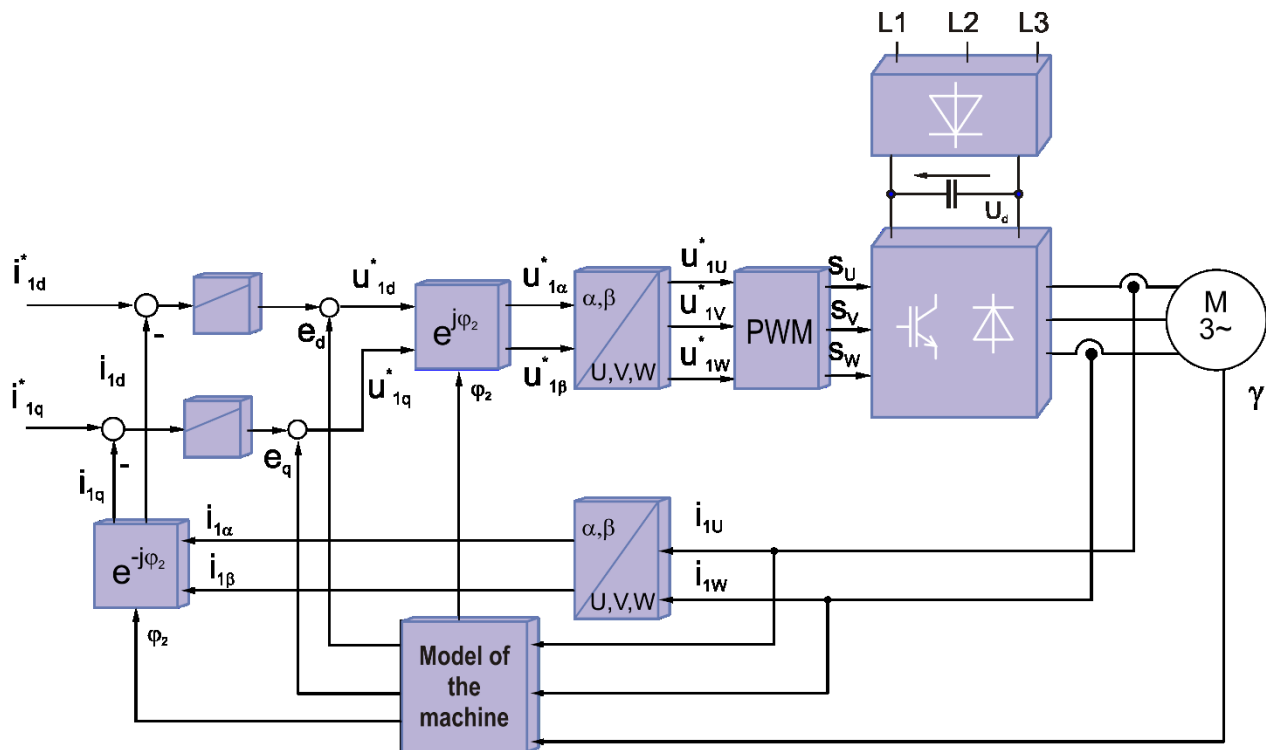


Figure 2.6 Diagram of Field Oriented Control with PI velocity control.

In this case the torque of the machines is indirectly controlled in a rotating frame of coordinates aligned to the rotor flux of the machine through i_q , the imaginary component of the stator current space phasor whereas the flux in the machine is controlled through the i_d , the real component of the stator current space phasor.

An alternative to the field oriented control is the direct torque control developed by Depenbrock [67] and Takahashi [68] in which the torque and the stator flux of the machine are directly

controlled with an hysteresis control and the stator voltages as manipulated variables as depicted in Figure 2.7.

In both cases the torque control is independent of the velocity control and builds the fast inner control loop of the cascade. If required this structure can be extended to include a velocity and a position control superimposed to the torque control.

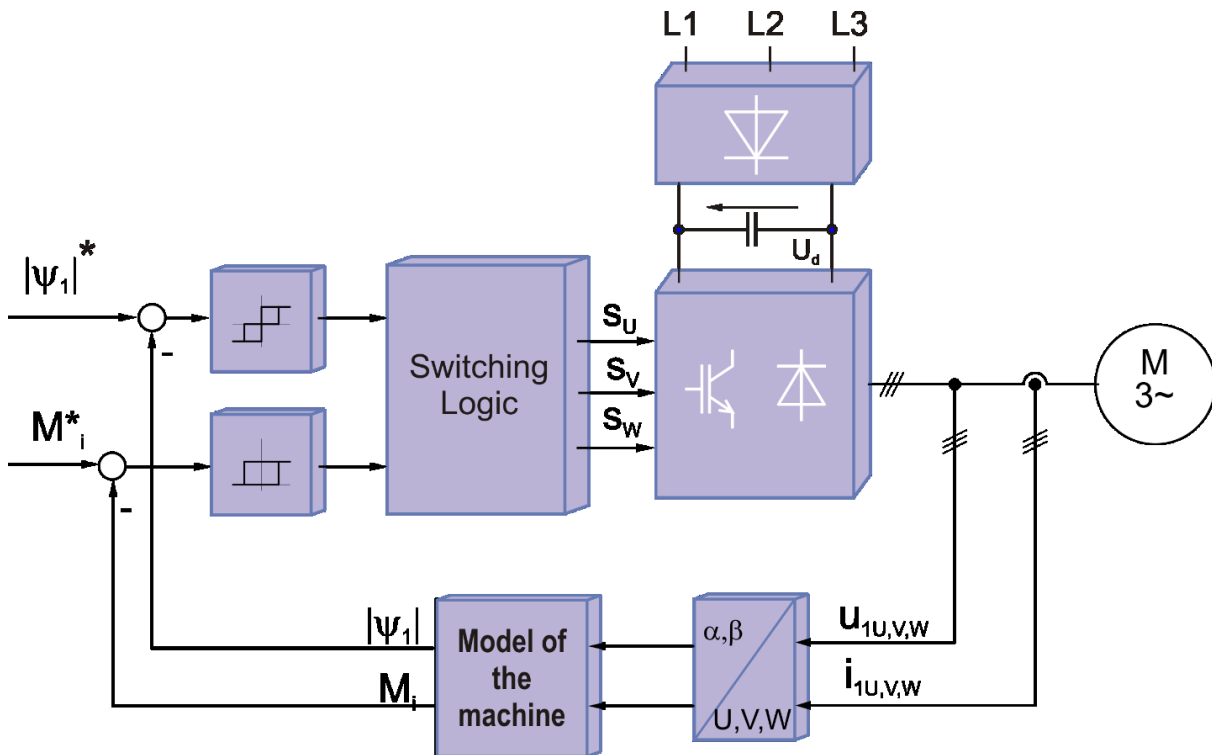


Figure 2.7 Diagram of Direct Torque control

If only the velocity and the position control are examined, the cascade structure can be approximated by a simplified one in which the torque control is represented by a first order lag that represents the closed control loop of the innermost current control as shown in the Figure 2.8.

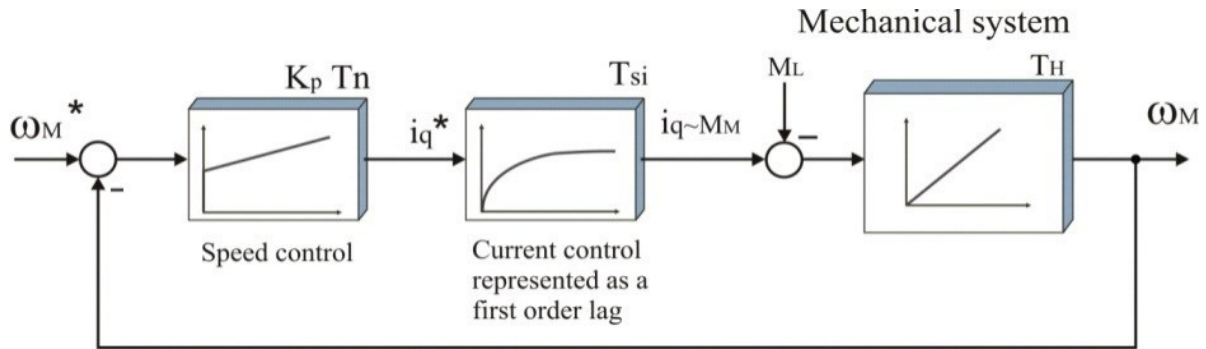


Figure 2.8 Typical cascade control configuration for electrical drives

The feedback for the velocity control can be obtained from an optical or magnetic encoder, from a resolver or from some other kind of velocity sensor attached to the shaft of the electrical machine. Yet there exist already developed techniques that allow the estimation of the position and velocity of the shaft of electrical machines from the measurement of voltages and currents on its terminals. The main advantage of this approach is that the mechanical velocity or position sensor is not required anymore and the robustness of the system is enhanced. An overview of these techniques is given in the following.

2.3 Sensorless speed control techniques.

Permanent magnet excited synchronous machines as well as induction machines require the continuous information of the rotor position or of the machine flux to control the magnitude of the magnetic flux and the torque produced by the machine in a proper way and with high dynamics. The strategies that make possible torque control without an installed mechanical sensor, the so-called sensorless control methods or control of a self-sensing machine can be grouped into two main classes: methods with signal injection and techniques based on fundamental wave models [28]:

- a) **Methods with signal injection:** These methods exploit the anisotropies of the machine and apply high frequency signals on the stator of the motor. This does not affect the operation of the machine but allows the detection of magnetic asymmetries due to the geometry of the machine or to the saturation of the main flux path or of the slotting.

Since the detected asymmetry is associated to the position of the rotor or of the flux, it can be used for the derivation of these angular positions in a mathematical model. These techniques work and are stable even at low or zero speed, but are highly sophisticated and the distinction of different anisotropies can be a difficult task.

b) ***Fundamental wave model based methods***: These methods are based on the fundamental machine equations [69]. They utilize the current and voltage at the terminals of the machine to deliver an estimate of flux position and of the mechanical velocity. The fundamental wave methods are mostly based on the measurement of the electromotive force (EMF) that is induced in the stator windings. Unfortunately, the AC machine becomes unobservable at low frequency of operation and the methods based on the EMF fail. Some of the sensorless schemes based on the fundamental wave model or the electrical machine are:

- Open loop models as the simplest subcategory of this group, directly constructed from the machine equations. Since there is no feedback, these methods are very sensitive to variations of the parameters of the electrical machine, require an excellent tuning of the model and an adaption of the parameters during the operation.
- Other methods within this group are Model Reference Adaptive Systems (MRAS) which compare outputs of two different models, one dependent and the other one independent of the machine velocity, by tuning the model the compared outputs are the same when the right velocity is used for the estimation.
- Observers based schemes constitute a third approach [3]. In an observer a model of the machine is supplied with the inputs to the machine and produces estimates of outputs. The error between the measured and the estimated outputs is fed back in a control loop that corrects the system until the error between estimated and measured variables vanishes. Several works explore this approach: in [70] Solsana

describes the application of a closed loop observer to a sinusoidal PM machine and several others techniques [71] have been proposed to overcome the starting problem. However at standstill and low velocity operation the limitations remain.

2.4 Summary of the chapter

Within this chapter the typical engineering approach to model the mechanical system of electrical drives as a single or two or more mass system is elucidated. These models can be utilized within the control structure also with the purpose of identification. The single mass system is of advantage for inertia identification, this can be extended to a two or more mass system to identify the elasticity of the shaft when torsional oscillations are present in the drive. In the case of an electrical drive with a composed mechanism, the concept of reduced moment of inertia can be utilized to model the inertia variation of the whole mechanism when it is calculated with respect to the actuator.

The cascade control structure is the most widely utilized scheme in electrical drives [57]. A general description of this structure was presented in order to clarify the source of the control and measured signals that will be used for the identification and diagnosis algorithms. A review of speed-sensorless scheme is presented as well, with emphasis on permanent magnet synchronous machines, which require during operation constantly updated information of the rotor position for velocity and torque control.

3. Stochastic identification in time domain

System identification in time domain usually implies parametric methods. The literature describes different techniques for the system identification in the time domain [72] [58]. All of them are based on the mathematical representation of the dynamical behavior of the system. The identification utilizes data measured on the physical system and processes this information for obtaining the mathematical model of the system respectively parameters of such model.

Within this work, two techniques were utilized for the identification of the system.

The first approach is stochastic and proposes a new procedure to achieve a speed-sensorless identification of the mechanical part of the system in the time domain with an extended Kalman filter (EKF). By comparing the calculations of a simplified model of the system with measurements from the actual system, the extended Kalman filter estimates the states of the system. For this purpose the mechanical parameters of the system are considered states.

Since its first publication in 1960 [73] , the Kalman filter has been utilized in several applications. The aim of this algorithm is to estimate the state of a process by mathematically reducing the mean of the squared error, based on past estimations, a model of the system and measurements from the actual system [74]. The extended Kalman filter works under the same principles of the original Kalman filter, and can be utilized for online identification of the mechanical system of a drive.

3.1 Stochastic identification: extended Kalman filter

The Kalman filter has a great importance in the area of estimation. This method was initially proposed for linear systems but can be also extended for non-linear systems. The extended Kalman filter is a recursive procedure used to obtain the best possible estimation of the state vector of a system [75] [30]. This is achieved by minimizing the error between the estimated states and the obtained measurements. The Kalman filter can be extended for non-linear systems by

using a Taylor approximation for the linearization. The block diagram of a discrete EKF is illustrated in Figure 3.1

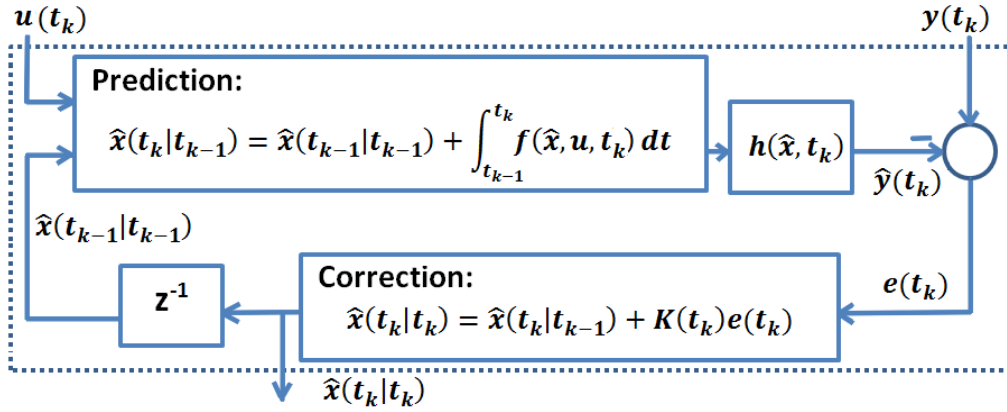


Figure 3.1 Extended Kalman Filter structure

The continuous system to be identified is described by the non-linear equations:

$$\begin{aligned} \frac{d}{dx} \underline{x} &= f(\underline{x}, \underline{u}, t) + \underline{q}(t) \\ \underline{y}(t_k) &= h(\underline{x}, \underline{u}, t) + \underline{r}(t) \end{aligned} \quad (3.1)$$

Where $\underline{q}(t)$ and $\underline{r}(t)$ are stochastic variables representing the process error covariance and the measurement error covariance respectively. The Kalman filter assumes that $\underline{q}(t)$ and $\underline{r}(t)$ are Gaussian noise.

The mathematical equations describing the system behavior are represented by the non-linear matrix function $f(\underline{x}, \underline{u}, t)$ depending on the inputs to the system \underline{u} , the space states \underline{x} and the time variable. It is in continuous time because it represents the actual system.

The observation matrix is designated by $h(\underline{x}, \underline{u}, t)$ and describes the relation between \underline{u} the output of the system, \underline{x} the space states and t time variable.

Based on these mathematical relations, the EKF gives an estimation of the system states $\underline{\hat{x}}$ by minimizing the error between the measured signals and the observed states. The Kalman gain is the weight operator used to minimize the error.

The following terms have to be defined:

- The *a-priori* values of $\underline{\hat{x}}(t_k|t_{k-1})$ and $\widehat{\mathbf{P}}(t_k|t_{k-1})$ are the extrapolation of the state estimation and its covariance up to time t_{k-1} correspondently
- The *a-posteriori* values of $\underline{\hat{x}}(t_k|t_k)$ and $\widehat{\mathbf{P}}(t_k|t_k)$ are the corrected prediction of the state vector and the covariance of the estimation after the measurement in time t_k correspondently.

The identification utilizing the EKF executes two recursive steps: prediction and correction.

- 1) **Prediction:** The a-priori estimation can be obtained from the numerical integration the system. This initial estimation $\underline{\hat{x}}(t_{k+1}|t_k)$ is determined by $\underline{\hat{x}}(t_k|t_k)$ the initial value of the state vector estimation at the current step and $f(\underline{\hat{x}}(t|t_k), \underline{u}, t_k)$ the model of the system dynamics. The model of the system dynamics is evaluated at the current step. This implies that the system is linearized at the current states. The duration between the current time instant t_k and the next t_{k+1} is the duration of one EKF-step. The estimation covariance matrix of this a-priori estimation $\widehat{\mathbf{P}}(t_{k+1}|t_k)$ is obtained extrapolating $\widehat{\mathbf{P}}(t_k|t_k)$ the estimation covariance related to the previous state vector estimation and adding the process error covariance $\widehat{\mathbf{Q}}(t_k)$. The process error covariance is an estimation of the error due to the limitations of the model of the system $f(\underline{\hat{x}}(t|t_k), \underline{u}, t_k)$.

The expressions used to calculate $\underline{\hat{x}}(t_{k+1}|t_k)$ the a-priori estimation and its covariance $\widehat{\mathbf{P}}(t_{k+1}|t_k)$ are:

$$\underline{\hat{x}}(t_{k+1}|t_k) = \underline{\hat{x}}(t_k|t_k) + \int_{t_k}^{t_{k+1}} f(\underline{\hat{x}}(t|t_k), \underline{u}, t_k) dt \quad (3.2)$$

$$\hat{\mathbf{P}}(t_{k+1}|t_k) = \mathbf{\Phi}(t_k)\hat{\mathbf{P}}(t_k|t_k)\mathbf{\Phi}^T(t_k) + \hat{\mathbf{Q}}(t_k) \quad (3.3)$$

The transition matrix $\mathbf{\Phi}(t_k)$, expresses the linearized dynamics of the system. The operating point of this linearization is the previous estimate. This simplifies the calculations. The transition matrix can be used to find the of the a-priori estimation covariance $\hat{\mathbf{P}}(t_{k+1}|t_k)$. The transition matrix is obtained by a Taylor linearization of the dynamics model:

$$\mathbf{\Phi}(t_k) \approx \mathbf{\Phi}(T, \hat{\underline{x}}(t_k|t_k)) = \sum_{m=0}^{\infty} \frac{\left(\mathbf{F}(\hat{\underline{x}}(t_k|t_k), t_k)\right)^m \cdot T^m}{m!} \quad (3.4)$$

Where T is the time interval $T = t_{k+1} - t_{k-1}$ and $\mathbf{F}(\hat{\underline{x}}(t_k|t_k), t_k)$ is the Jacobi Matrix which contains expressions of the state changes linearized at the current estimate:

$$\mathbf{F}(\hat{\underline{x}}(t_k|t_k), t_k) = \left. \frac{\partial}{\partial \underline{x}} f(\underline{x}, \underline{u}, t_k) \right|_{\underline{x}=\hat{\underline{x}}(t_k|t_k), t=t_k} \quad (3.5)$$

- 2) **Correction:** In this second step of the algorithm, the a-priori estimation $\hat{\underline{x}}(t_{k+1}|t_k)$ obtained in the prediction step is corrected using the Kalman gain to calculate the final estimation of the EKF main step the uncertainty of this estimation $\hat{\mathbf{P}}(t_k|t_k)$ is also calculated.

$$\hat{\underline{x}}(t_k|t_k) = \hat{\underline{x}}(t_k|t_{k-1}) + \mathbf{K}(t_k) \left[\underline{y}(t_k) - h(\hat{\underline{x}}, \underline{u}, t_k) \right] \quad (3.6)$$

$$\hat{\mathbf{P}}(t_k|t_k) = [\mathbf{I} - \mathbf{K}(t_k)\mathbf{H}(t_k)]\hat{\mathbf{P}}(t_k|t_{k-1}) \quad (3.7)$$

Where \mathbf{I} designates the identity matrix.

These two expressions represent the output of the EKF, and will be used as initial values for the next step of prediction within the EKF algorithm execution.

The covariance estimation $\hat{\mathbf{P}}(t_k|t_k)$ depends on the Kalman gain and on the observation matrix $\mathbf{H}(t_k)$ linearized and evaluated at the a-priori vector state estimation $\hat{\underline{\mathbf{x}}}(t_{k+1}|t_k)$.

$$\mathbf{H}(t_k) = \left. \frac{\partial}{\partial \hat{\underline{\mathbf{x}}}} h(\hat{\underline{\mathbf{x}}}, \underline{\mathbf{u}}, t_k) \right|_{\hat{\underline{\mathbf{x}}}=\hat{\underline{\mathbf{x}}}(t_k|t_{k-1})} \quad (3.8)$$

The Kalman gain is calculated in terms of the observation matrix $\mathbf{H}(t_k)$, the error covariance $\mathbf{R}(t_k)$ related to the measurement and the error covariance $\hat{\mathbf{P}}(t_k|t_{k-1})$ related to the a-priori state estimation:

$$\mathbf{K}(t_k) = \hat{\mathbf{P}}(t_k|t_{k-1})\mathbf{H}^T(t_k) [\mathbf{H}(t_k)\hat{\mathbf{P}}(t_k|t_{k-1})\mathbf{H}^T(t_k) + \mathbf{R}(t_k)]^{-1} \quad (3.9)$$

The Kalman gain operates as a weight function evaluating which information is more reliable, either measured data or estimation based on the model of the system.

3.2 Causes of divergence by utilizing Kalman filters

The central problem of estimation with the extended Kalman filter is to separate the actual signal from the combination of signal and noise by minimizing the mean-square error in the time domain. The extended Kalman filter approaches in the praxis this problem by considering the noisy measurement to be a discrete sequence of data in time and by utilizing a discrete space model of the non-linear system [76]. The accuracy of the estimation with EKF depends on the parameterization of the covariance matrixes and on other factors.

The Kalman filter may not always converge to the actual values of a real system. Two of the main causes for the failure are *finite precision arithmetic* and *modeling errors*. The Kalman filter arithmetic is assumed to be infinite precise in the theory, but computers and digital microprocessors only have a certain word length to represent the numbers. The theory also

assumes that the error of the system model is precisely known, as well as the measurement error, and that the noises are pure white, zero-mean and uncorrelated. Real implementations do not fit these assumptions; therefore, the estimation is not always optimal.

There are some strategies to improve the performance of the EKF [77]:

- **Increase of the arithmetic precision:** It forces the digital implementation to more closely match the analog model.
- **Initialize the estimation covariance matrix \hat{P} at each time step to avoid large changes:** This usually does not result in major improvements but it is recommended to avoid instability on the estimation.
- **Use a fading-memory filter:** Is a way to force the filter to “forget” measurements in the distant past and place more weight on recent measurements. This makes the filter more responsive to measurements, and less sensitive to modeling errors.
- **Use fictitious process noise:** This is mathematically equivalent to the fading-memory. Adding fictitious process noise is a way of indicating the filter to have less confidence on the system model. This especially useful when the model assumes some states to remain constant but in reality they change.

3.2.1 Causes of divergence due to linearization in extended Kalman filters

In the general case of non-linear systems, the extended Kalman filter can be used for the estimation of the discrete space state vector. For the EKF algorithm, the state vector a priori estimation is a function of the previous states, the input to the system and the stochastic variable $q(t_k)$ representing the uncertainty of the process:

$$\underline{x}(t_k) = g(\underline{x}(t_{k-1}), \underline{u}, q(t_k)) \quad (3.10)$$

According to the formulation of the Kalman filter algorithm, the states of the system can be calculated from the model of the dynamics of the system evaluated at the previous state and then solving this model by numerical integration as expressed in equation (3.2).

However, this *a-priori* estimation and is just an approximation of the actual state. The covariance of the process noise is determined by the linearization of the system to the current estimate as well, which is also an approximation to the actual covariance of the estimation.

$$\underline{x}(t_k) \approx g(x(t_{k-1}), \underline{u}, q(t_k)) \quad (3.11)$$

$$\hat{P}(t_{k+1}|t_k) = \Phi(t_k)\hat{P}(t_k|t_k)\Phi^T(t_k) + \hat{Q}(t_k) \quad (3.12)$$

The state distribution is propagated by the first order linearization of the transition matrix $\Phi(t_k)$. These approximations can bring considerable errors when the non-linearities are large.

The estimation covariance $\hat{P}(t_{k+1}|t_k)$ is a linearized approximation and it is used to the calculation of the Kalman gain which weights the reliability of the model and measured data.

If the process error covariance $\hat{Q}(t_k)$ has small values then the covariance \hat{P} may not increase very much between cycles. Then the Kalman gain $\mathbf{K}(t_k)$ will be small or close to zero and the measurements will not weight too much. If $\hat{Q}(t_k)$ the covariance increases between cycles, the Kalman gain $\mathbf{K}(t_k)$ will converge to a larger value. A larger value of this gain $\mathbf{K}(t_k)$ implies that the updated value of the estimation $\hat{\underline{x}}(t_k|t_k)$ was calculated pondering high reliability on the measurement. Therefore, large non-linearities on the system may lead to an incorrect weighting causing a suboptimal performance of the Extended Kalman filter.

3.3 PRBS as additional excitation to the system

As explained in the section 3.2, additional excitation to the system can help to compensate the EKF divergences due to model limitations and linearization. Artificial test signals are used when the natural input to the system does not offer enough excitation to the system for identification. The most often utilized test signals are step functions, sinus functions, square wave functions and stochastic signals [72]. The Kalman filter assumes that the noise in the system is Gaussian, this is

stochastically. Stochastic signals are random by definition, in contrast to deterministic signals that are predictable.

However, artificial generated “random” signals are computed by deterministic algorithms. Identical initial conditions will produce identical time series. [78] As the name indicates, pseudorandom signals are not truly random, but they are a good enough deterministic approximation of a random process. A pseudorandom signal can be described as obtained by sampling a Gaussian process for a finite length duration and then folding the recorded data into a loop. This signal is periodical and deterministic but when only a small portion of the loop is considered, it would look like a random signal for an external observer [76]. A pseudorandom binary signal (PRBS) is a signal with those characteristics and only can deliver two values as output.

From several methods described in the literature, two procedures to generate PRBS have gained greater significance for system identification: quadratic residuals and shift registers. [79]

In this work, a PRBS generated by shift registers was used to produce the required additional excitation to the system for the identification with EKF. The utilized PRBS-generator has the structure shown in Figure 3.2

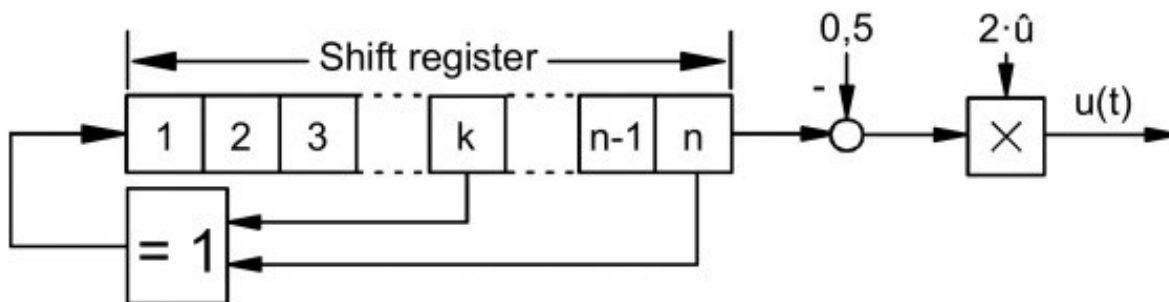


Figure 3.2 PRBS sequence generator

The PRBS generator performs a right shift of one bit and produces a new output every time interval T_t between execution steps. Two bit registers are sampled to feedback a logical operator to produce the input to the shift registers.

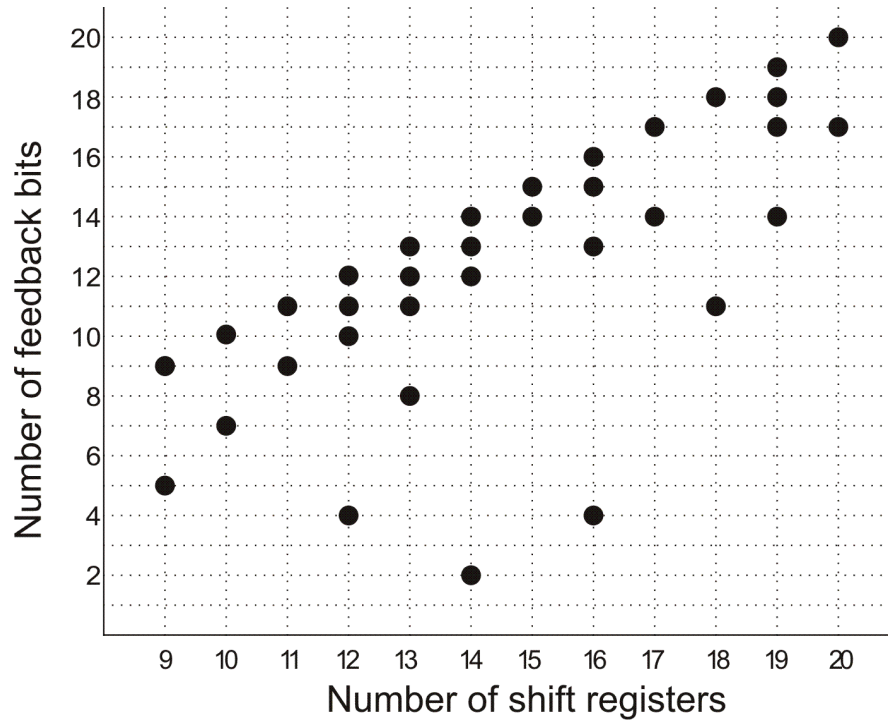


Figure 3.4 Possible feedback combinations for PRBS generators with different registers

3.4 Non-linear system model

The model of the continuous system is described by the non-linear equations:

$$\begin{aligned} \frac{d}{dx} \underline{x} &= f(\underline{x}, \underline{u}, t) + \underline{q}(t) \\ \underline{y}(t) &= h(\underline{x}, \underline{u}, t) + \underline{r}(t) \end{aligned} \quad (3.14)$$

As explained above, $\underline{q}(t)$ and $\underline{r}(t)$ represent the process and the measurement noises of the actual system correspondently.

In the first approach, the time derivative of the moment of inertia and of the load torque are neglected in order to simplify the mechanical equation of the single mass system without friction; thus the motion equation results as:

$$M_M - M_L = J_\Sigma \cdot \frac{d\omega_M}{dt} \quad (3.15)$$

The state vector is extended to include the inverse of the moment of inertia $\left(\frac{1}{J_\Sigma}\right)(t)$ and the load torque $M_L(t)$ as states to be estimated:

$$[\underline{x}]^T = \left[\omega_M(t) \quad M_L(t) \quad \left(\frac{1}{J_\Sigma}\right)(t) \right] \quad (3.16)$$

Thus, the discretized non-linear model is defined as:

$$\begin{aligned} \frac{d}{dt} \underline{x} &= f(\underline{x}, \underline{u}, t_k) + \underline{q}(t_k) \\ \frac{d}{dt} \underline{x} &= \begin{bmatrix} \left(\frac{1}{J_\Sigma}\right)(t_k) \cdot (M_M(t_k) - M_L(t_k)) \\ 0 \\ 0 \end{bmatrix} + \begin{bmatrix} q_{\omega_M}(t_k) \\ q_{M_L}(t_k) \\ q_{J_\Sigma}(t_k) \end{bmatrix} \end{aligned} \quad (3.17)$$

$$\underline{y}(t_k) = h(\underline{x}, t_k) + \underline{r}(t_k) = \omega_M(t_k) + r(t_k) \quad (3.18)$$

In this case, the input of the system is the motor torque $M_M(t_k)$. It can be noticed that the time derivatives of the load torque and the inverse of the moment of inertia are only linked to the stochastic signals $q_{M_L}(t_k)$ and $q_{J_\Sigma}(t_k)$, which represent the noise of the model related to this states and not related to other variables of the system.

In this system, the observation matrix $h(\underline{x}, t_k)$ contains only one element $\omega_M(t_k)$ the mechanical velocity of the motor, and the measurement noise $r(t_k)$ depends on the encoder resolution.

The output of the system is designated by the variable $\underline{y}(t_k)$ and the derivative of the state vector by $\frac{d}{dt} \underline{x}$, which represents the change in time of the states according to the mathematical model of the system. This model is actually inaccurate because the reduced moment of inertia and load torque variation in time are considered to be disturbances i.e. noise. The EKF is continually trying to fit the wrong model to the measured data, but the estimation succeed because more weight is given to the measurements and the values in the Q matrix are chosen large enough to allow the identified state to have the varying behavior calculated from measured data.

3.5 Structure of identification

The EKF algorithm requires the input to the real system and the measured output to calculate an estimation of the system states. The input to the real system is the driving torque delivered for the motor and the output of the system is the mechanical velocity. First, an identification structure with velocity measurement from an encoder was tested.

The control structure and the EKF identification is depicted in Figure 3.5 . The artificial excitation to the system was created with PRBS as described in section 3.3.

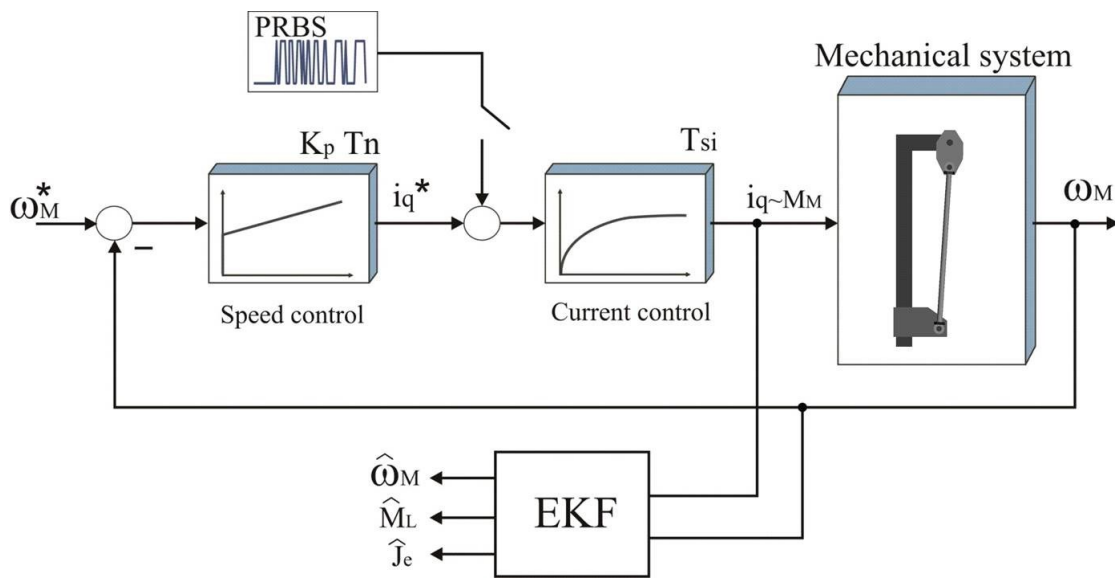


Figure 3.5 Control and identification structure

The artificial excitation to the system with PRBS is added to the reference value of the stator current component i_q^* that is proportional to the motor torque, under Field Oriented Control. The inner current control is approximated as a first order lag element as explained in section 2.2. The inputs to the EKF algorithm are the torque developed by the drive M_M and the mechanical velocity of the motor ω_M . The motor velocity is measured with an encoder and fed back to the control.

A new structure of identification was designed, in order to evaluate the EKF under a speed-sensorless control scheme. An estimation of the mechanical velocity was used instead of encoder measurements. In a similar way, the additional excitation to the system was created with PRBS,

added to the motor torque reference value. The torque control and the estimation of the mechanical velocity of the motor were undertaken by a commercial motion control drive which operates with DTC. This is special aspect of this work that it relies on the commercial available sensorless methods and examines their suitability in identification tasks.

The speed-sensorless identification structure is depicted in Figure 3.6.

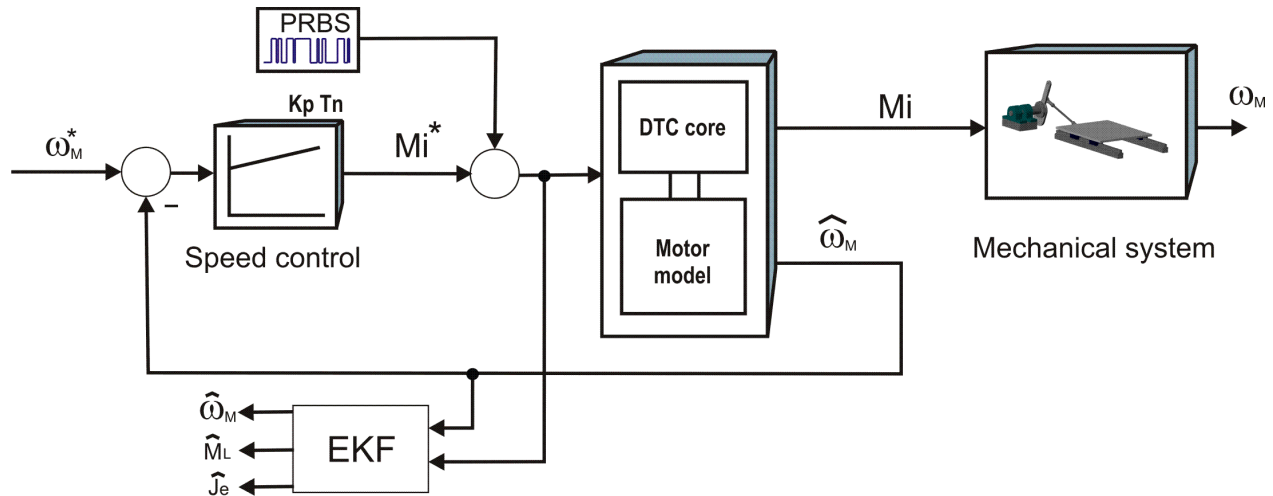


Figure 3.6 Speed-sensorless identification structure

The EKF requires the input and output of the mechanical system, these are the torque developed by the electrical machine, and the mechanical velocity that is also calculated by the drive by using a sensorless technique.

Unfortunately, the actual input to the system, the motor torque, was not available due to interface limitations on the experimental setup. Instead, the reference value of the motor torque was utilized and the delay to the actual value compensated. As explained above, the output of the system, the mechanical velocity, was estimated in the commercial motor control drive with a model of the motor.

The EKF identification method was tested with two configurations of the mechanical system. The mechanical configurations and hardware details are explained in the description of the experimental setup in section 7.

3.6 EKF identification of a variable reduced moment of inertia

In this section, the EKF procedure for the identification of the reduced moment of inertia of a mechanism is explained. First, the reduced moment of inertia is calculated from with a model of mass particles dynamically equivalent to the crankshaft mechanism. By doing so, the reduced moment of inertia can be expressed as a function of the position of the crank. This function can be used to be compared with the estimation of the EKF.

Then, the non-linear model of the mechanical system is used within the EKF algorithm to calculate the a-priori estimation of the prediction step. The non-linear model considers three state variables: the mechanical velocity, the inverse of the reduced moment of inertia, and the load torque. The limitation of this model is that the inertia and load torque are considered to be constant values. Because of this, the model estimation is corrected with the measurements from the system. The measured output of the mechanical system is the mechanical velocity.

Finally, the structure of identification is described. There, the input signals to the EKF algorithm are specified. The structure of control with measured velocity feedback and the speed- sensorless control scheme are explained. Within the structure of identification, the additional excitation to the system with PRBS is also depicted.

3.6.1 Reduced moment of inertia of a vertical crankshaft slider

The kinetic energy analysis of any mechanism, for example a vertical crankshaft, can be carried out by utilizing a dynamically equivalent model of mass particles as depicted in Figure 3.7 . Then, the reduced moment of inertia for the whole mechanism can be obtained from the kinetic energy analysis.

For the EKF estimation the modeling of the vertical slider-crank mechanism as a single variable inertia is utilized. The mass particles depicted in Figure 3.7 were calculated in terms of the slider-crank elements masses by using the dynamically equivalent model described in the literature [80].

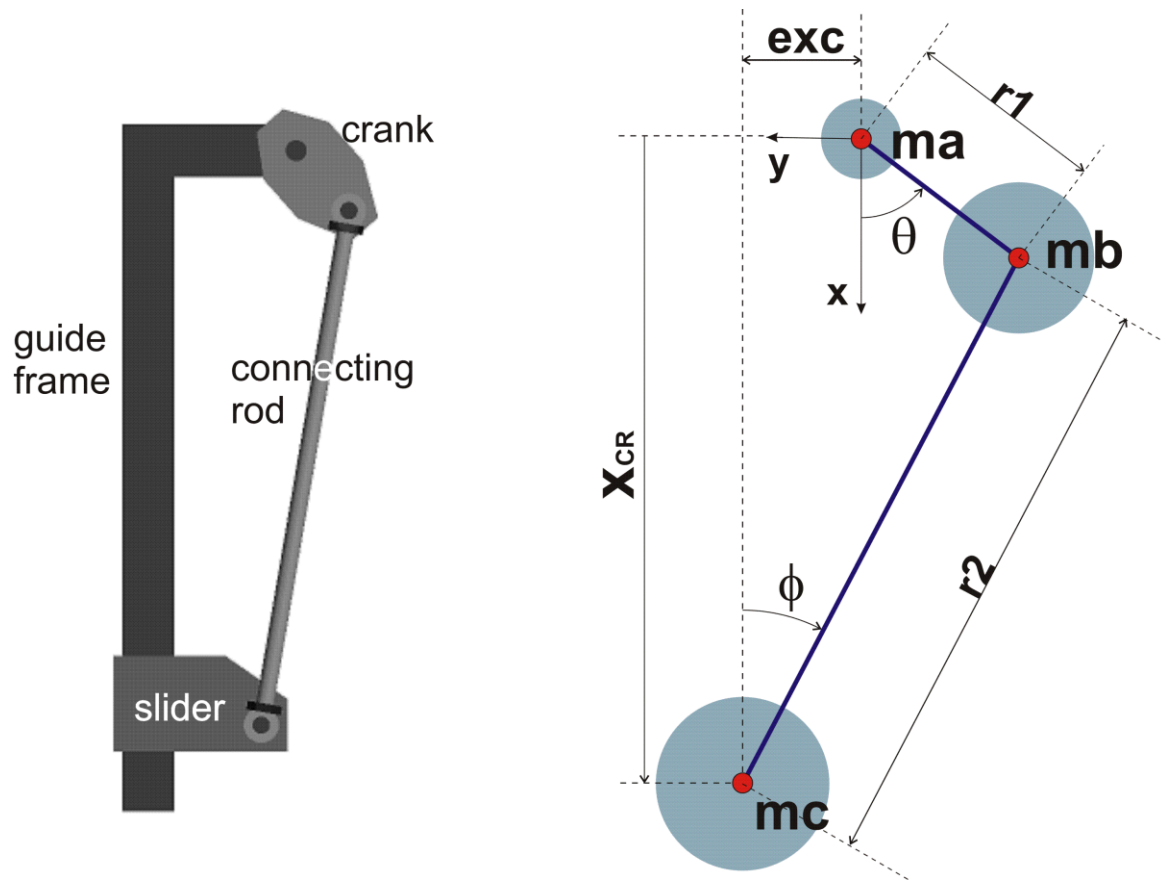


Figure 3.7 Mass particle model of the crank shaft

The mass particles m_a , m_b , m_c are located at the joints of the mechanism. The distances between rotational joints are designated by r_1 and r_2 that correspond to the crank and connecting rod lengths. The variables describing the displacement of the components are θ the angular position of the crank, ϕ the angular position of the connecting rod, and x_{CR} the linear displacement of the slider. The parameter exc is a geometrical constriction of the mechanism, designating the distance between the crank rotation axis and the fixed frame guide of the slider.

The mass particles were calculated following the standard procedure described on literature [80] according to the geometry of the components described on Appendix 9.1. The expression of the mass particles on terms of the mass components are:

$$ma = \frac{4}{5} m_{crank} \quad (3.19)$$

$$mb = \frac{1}{5} m_{crank} + \frac{1}{2} m_{CR} \quad (3.20)$$

$$mc = \frac{1}{2} m_{CR} + m_{slider} \quad (3.21)$$

According to the kinematic analysis and the static forces evaluation, both the equivalent moment of inertia and the load torque can be expressed as functions of the crank position:

$$J_e = mb(r_1)^2 + mc \left[r_1 \sin\theta + \frac{\frac{r_1 \cos\theta}{r_2}}{\sqrt{1 - \left(\frac{exc + r_1 \sin\theta}{r_2}\right)^2}} (exc + r_1 \sin\theta) \right]^2 \quad (3.22)$$

$$M_L = \left(\frac{1}{5} W_{crank} + W_{CR} + W_S \right) r_1 \sin\theta + F_N r_1 \sin\theta \quad (3.23)$$

Where W designates the weight of the components.

The total moment of inertia results as the addition of the motor moment of inertia, the mechanical coupling inertia and the equivalent inertia of the whole composed mechanism:

$$J_\Sigma = J_{motor} + J_{coupling} + J_e \quad (3.24)$$

A graphical representation of the load torque and total moment of inertia is depicted in Figure 3.8. The equations were evaluated utilizing the dimensions and masses of the vertical slider-crank that can be found in the appendix section 9.1.

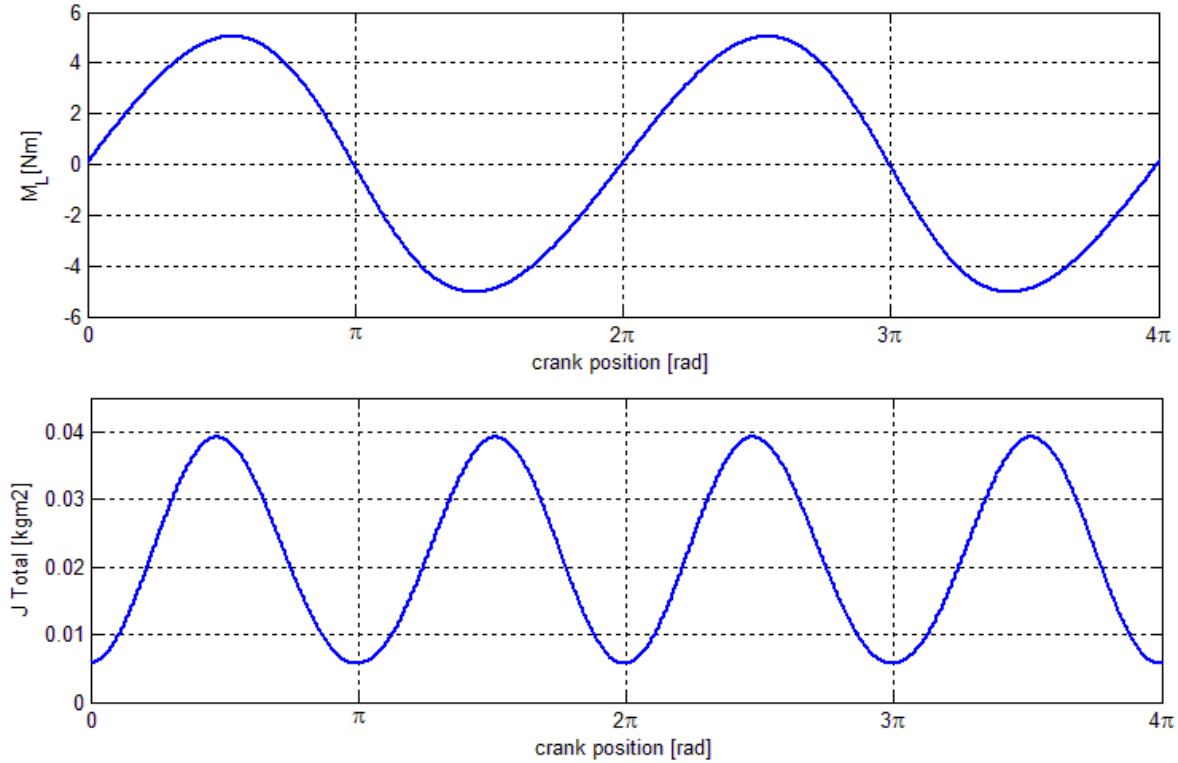


Figure 3.8 Load torque and equivalent moment of inertia as function of the position

3.7 Simulation of EKF identification of a crankshaft slider

The EKF identification method was simulated based on the structure described in the section 3.5. The load torque and reduced moment of inertia correspond to the experimental platform described in section 7.1.1.1. The mechanical system was simulated under the considerations described in section 3.6.1.

The simulations were performed considering the motor velocity reference set to 10 min^{-1} . Initially a simulation without additional excitation to the system was executed. The identification with EKF estimated the mechanical velocity, the load torque and the reduced moment of inertia correspondent in descendent order to the three graphics depicted in Figure 3.9.

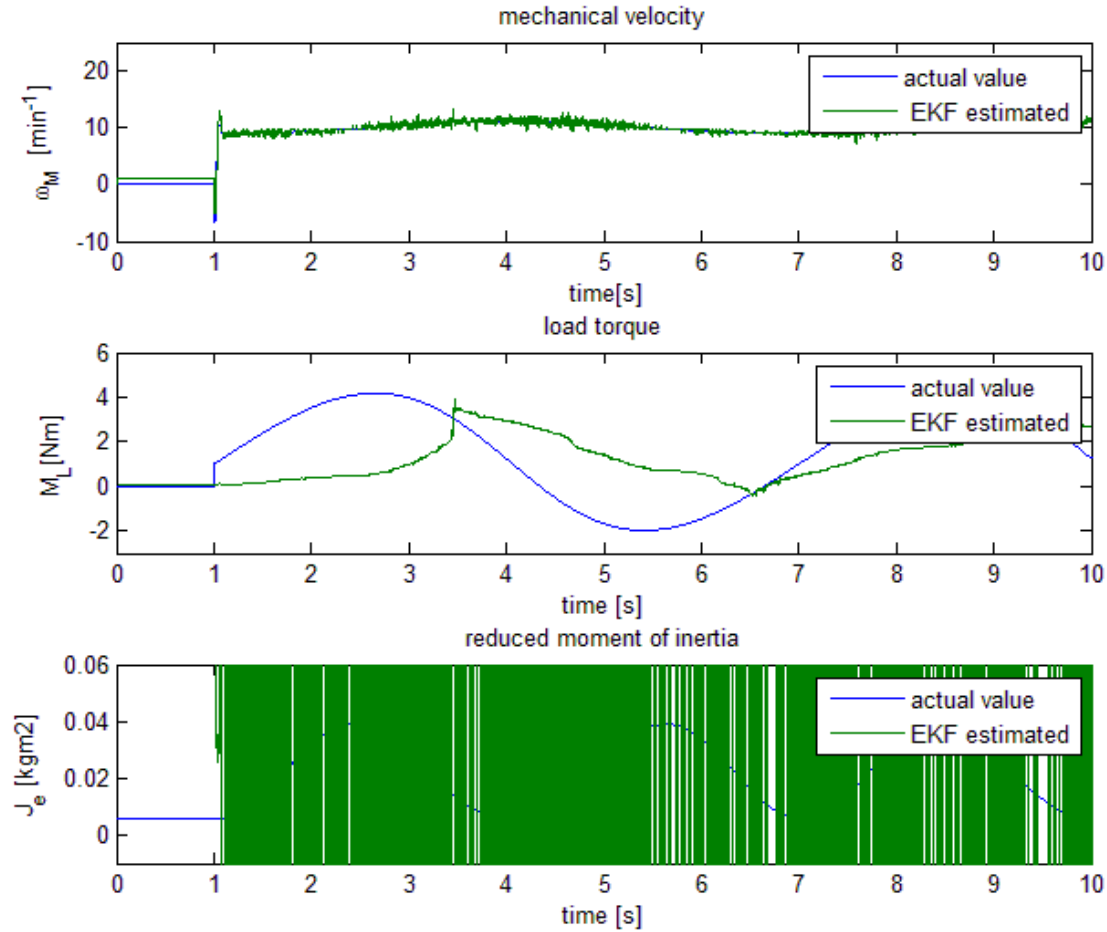


Figure 3.9: Simulation results without additional excitation to the system

The values estimated with the EKF identification are compared with the actual values. It can be noticed that without additional excitation the estimation of the load torque and reduced moment of inertia does not converge to the actual values, the estimated moment of inertia varies between positive and negative values and the estimated load torque diverges.

As the simulation indicated that it was necessary to add artificial excitation to the system, PRBS with amplitudes between 0.1 pu and 0.5 pu were added to the i_q^* current reference value which is proportional to the torque delivered by the motor.

The identification started to converge in the simulation when PRBS with an amplitude of 0.4 pu were utilized. The EKF estimated values in this simulation are shown in the Figure 3.10.

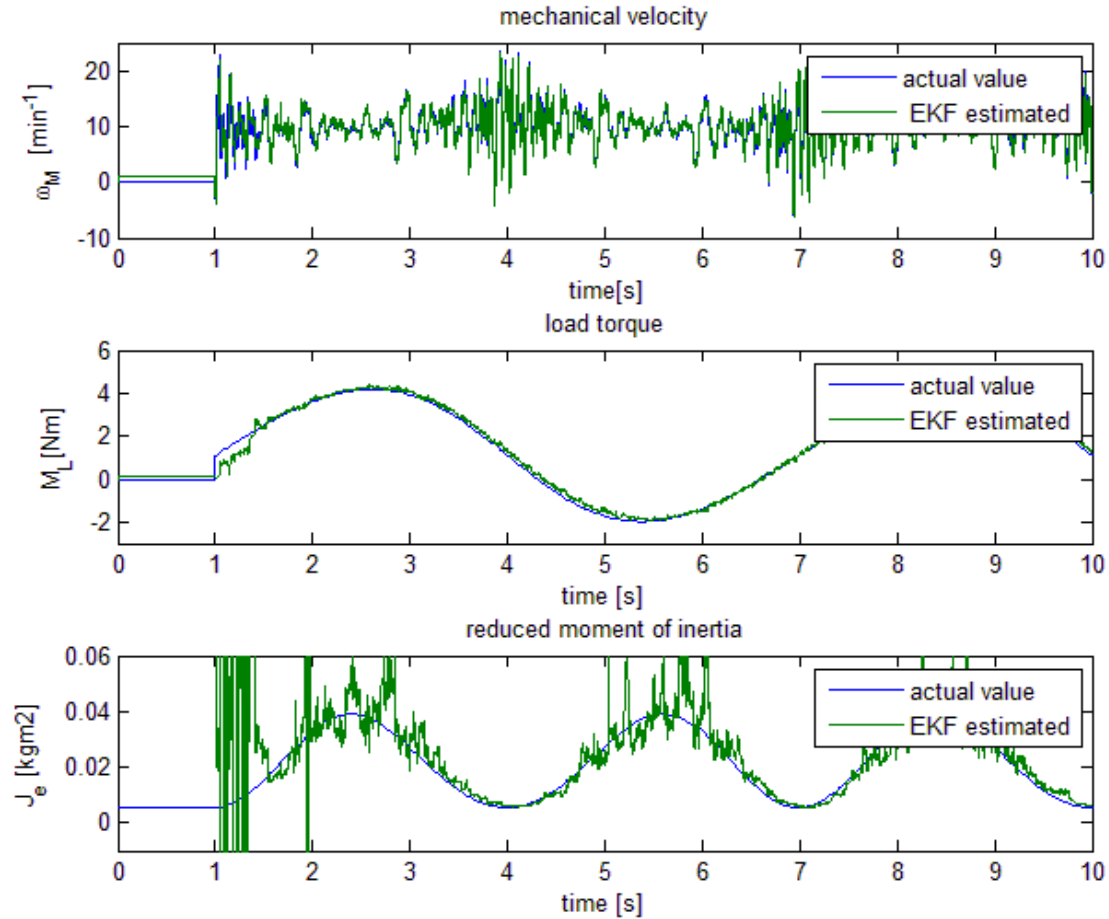


Figure 3.10: Simulation results of the EKF identification with PRBS of 0.4 pu as additional excitation

The simulation indicated that the additional excitation to the system has a significant effect on the EKF identification. However, experimental procedures were required to validate and extend the information gained with the simulation.

3.8 Summary of the chapter

In this chapter, a stochastic method for the identification of the variable reduced moment of inertia and variable load torque by using an extended Kalman filter was presented. In order to achieve the identification of the mechanical system; the information of the position of the drive

has to be known. In this work, it will be assumed that instead of the measurements of the shaft position, a motor drive equipped with a sensorless control scheme is used.

The Extended Kalman Filter is applied as a space state estimator for non-linear systems. By augmenting the state vector to include the load torque and the moment of inertia, these variables can be estimated. However the estimation requires additional excitation to the system, because the composed mechanism has a varying inertia, the single inertia model does not match the actual value and must be corrected in each step of estimation. Other divergence issues are explained. An additional excitation of the system with PRBS, which was also successfully utilized in identification procedures in the frequency domain, is proposed here for the time domain, and evaluated with simulation.

4. Deterministic Identification in time domain

The second identification method proposed in this work follows a deterministic approach. This method utilizes the available variables of the velocity control for achieving the identification.

The mechanical equation of the system, defines the equilibrium condition between the forces interacting at the motor. These forces are related to load, moment of inertia, moment of inertia changes, speed and speed changes. Therefore, in the case of a velocity control, the reference value of the motor torque is kind of “observer” that reflects the load torque or load force under equilibrium conditions. In other words, if steady state accuracy of the velocity control is assumed, the output of the velocity controller corresponds to the mechanical load applied to the drive. If the changes of the load are slower than the dynamics of the control, the reference value of the torque is not equal to the load torque but a good approximation.

In many mechanical systems, like those to be found in production machines, a further assumption can be made: the changes on the load and on the moment of inertia are cyclical and periodical. Thus, the reduced moment of inertia of multi-body mechanism with repetitive cycles of motion is periodical. This is because the reduced moment of inertia is a function of the position of the actuator. By taking all these facts into account, the periodicity of motion was utilized in the proposed method for characterizing the mechanical load of the drive with Fourier series.

4.1 Fourier series for signal representation

This deterministic identification method utilizes the periodical motor torque respectively its reference value as the signal to be characterized. Periodic signals can be always represented by Fourier series and any signal can be described as an infinite sum of sine and cosine sequences or their equivalent weighted harmonically related complex exponentials. The complex expression of the Fourier series is given by the following equation:

In this equation, the complex exponentials represent the harmonics of the periodical signal. The

$$f(t) = \sum_{k=-\infty}^{\infty} c_k e^{jk\omega t} \quad (4.1)$$

weight of each harmonic is determined by the Fourier coefficients c_k . The fundamental frequency is the reciprocal of the signal period [81].

If the periodic signal is real c_k and c_{-k} are complex conjugates, and the Fourier series can be represented according to Euler:

$$f(t) = c_0 + 2 \sum_{k=1}^{\infty} |c_k| \cdot \cos(k\omega t + \gamma_k) \quad (4.2)$$

This expression can be expanded in sinusoidal and cosines terms:

$$f(t) = \frac{a_0}{2} + \sum_{k=1}^{\infty} a_k \cdot \cos(k\omega t) + \sum_{k=1}^{\infty} b_k \cdot \sin(k\omega t) \quad (4.3)$$

Where the coefficients of the Fourier series are defined by the expressions:

$$\frac{a_0}{2} = c_0 \quad (4.4)$$

$$a_k = 2|c_k| \cos \gamma_k \quad (4.5)$$

$$b_k = -2|c_k| \sin \gamma_k \quad (4.6)$$

By representing the motor torque with Fourier series, the coefficients i.e. the harmonics reflect the dynamic behavior of the mechanical system. Under determined working conditions, the

harmonics related to the reduced moment of inertia of the mechanism are dominant and can be indirectly identified by inspection of their values and by comparing with the periodical terms contained in the model of the mechanics. The working conditions for the utilization of this method are defined in section 4.3.

4.2 Identification of a periodical drive torque

As expressed above, in the case of a closed loop velocity control steady state the torque delivered by the motor-drive compensates the torque produced by the forces in the mechanical part of the system. The forces acting on the mechanisms can be classified as [82]:

- **Internal forces:** Are the action and reaction between the components of the mechanism. Because the components are rigid bodies, the forces are fully transmitted through the elements, just changing their direction according to the geometry. When analyzing the forces on each single component for the kinetostatic analysis, these forces are usually represented in pairs (action-reaction).
- **External forces:** They are caused by every external physical load applied on any component of the system. External forces can be considered weights, forces caused by friction, externally applied forces or torque. Because the components are rigid bodies, this forces are also fully transmitted by the internal forces to the actuator, just changing the direction of the force or the displacement vector when producing a torque. They are the cause of the load torque which can be therefore variable as a function of the actuator position because it determines the displacement vector of the load torque.
- **Forces due to the moment of inertia:** They depend on the instantaneous geometry of the mechanism, on the velocity and on the acceleration; this forces can be understood from the impulse and angular momentum law. The forces due to the moment of inertia of the mechanism must be distinguished from the forces causing the load torque.

In the case of machines with repetitive cycles of movement, load torque caused by constant external forces can be described as a periodical function. As it is described in chapter 2, the

reduced moment of inertia of a composed mechanism is a function of the actuator position. Therefore both, load torque and the torque due to inertial forces, are periodical.

The mechanical equation of the system describes the equilibrium conditions of the interacting torques on the actuator. In the next section, the conditions for the characterization of the driving torque produced by the motor given and the working hypothesis are explained by means of the mechanical equation of the system.

4.3 Working hypothesis for the deterministic identification of a periodical load

The differential equation describing the mechanical part of a drive system is derived from the angular momentum of the system.

The angular momentum law was originally formulated for rigid bodies and can be expressed as follows:

$$\frac{dL_0}{dt} = M_0 = \frac{d}{dt} [J \dot{\gamma}] \quad (4.7)$$

Where L_0 denotes the angular momentum, M_0 designates the summation of all torques interacting at the point O , J is the moment of inertia, and $\dot{\gamma}$ the angular velocity. For the purpose of identification for control design, the concept of reduced moment of inertia is used in this work. This allows to obtain an approximation of the dynamics of composed mechanisms, such as a crank-shaft mechanism.

As explained in section 2.1.3, the general dynamic model of a multi-body mechanism can be represented by its generalized moment of inertia with respect to the actuation axis. This way the reduced moment of inertia becomes an explicit function of the actuator position γ and therefore an implicit function of the time:

$$\frac{dL_0}{dt} = M_M - M_L = J(\gamma)\ddot{\gamma} + \frac{dJ}{d\gamma}\dot{\gamma}^2 \quad (4.8)$$

If the angular velocity is kept constant e.g. by means of a velocity control, the term related to the acceleration $\ddot{\gamma}$ can be consequently neglected and the difference between M_M the torque delivered by the drive and M_L the load torque. The difference between both corresponds to the derivative of the moment of inertia with respect to the angular position $\frac{dJ(\gamma)}{d\gamma}$ multiplied with the square of the mechanical velocity.

$$M_M - M_L = \frac{dJ(\gamma)}{d\gamma} \dot{\gamma}^2 = \dot{\gamma} \cdot \frac{dJ(\gamma)}{dt} \quad (4.9)$$

In the case of the horizontal slider-crank mechanism the only significant force actuating as a load is the dry friction on the slider. The dry friction is independent of the velocity; therefore the resulting friction torque transmitted to the actuator axis can be expressed as a function of the angular position of the electrical machine:

$$M_M = M_L(\gamma) + \dot{\gamma} \cdot \frac{dJ(\gamma)}{dt} = M_M(\gamma, \dot{\gamma}) \quad (4.10)$$

As it can be inferred from this expression, the effect of the mechanical velocity is mainly related to the change in time of the moment of inertia. The load torque is a periodical function. Considering this two facts, the motor torque can be characterized in time domain for each velocity as a periodical function.

$$M_M(\gamma, \dot{\gamma}) = M_M(\gamma(t))|_{\dot{\gamma}} \quad (4.11)$$

4.4 Mechanical load as function of the angular position of the motor

As shown above in a machine with repetitive cycles of operation, the drive torque can be described as a periodical function of the angular position of the actuator given for each given mechanical velocity of the motor. As mentioned in section 4.1, periodical functions can be

replicated by infinite Fourier harmonic series. The actual motor torque is a continuous-time signal that can be approximated from the Fourier series of the drive torque reference value which is the output of the velocity controller and it is, therefore, in digital control a discrete-time signal. Hence the approximation with Fourier series has to be carried out in the discretized system by sampling a finite number of terms N that corresponds to one cycle of the machine.

The discrete Fourier series is expressed as follows [72]:

$$f(t) \cong \frac{a_0}{2} + \sum_{v=1}^{N-1} a_v \cdot \cos(v\omega_0 t) + \sum_{v=1}^{N-1} b_v \cdot \sin(v\omega_0 t) \quad (4.12)$$

The frequency of the fundamental oscillation is:

$$\omega_0 = \frac{2\pi}{T_p} \quad (4.13)$$

The Fourier coefficients are calculated by solving the integrations:

$$a_v = \frac{2}{T_p} \int_0^{T_p} f(t) \cdot \cos(v\omega_0 t) dt \quad (4.14)$$

$$b_v = \frac{2}{T_p} \int_0^{T_p} f(t) \cdot \sin(v\omega_0 t) dt \quad (4.15)$$

For the calculation of the coefficient of the Fourier series the limits of integration must theoretically correspond to the exact duration of a period. This is a problem if the integration is performed by considering the period of the system in the time domain, because small oscillations in the velocity would make the duration of period to differ from the calculated one based on the velocity reference value. Therefore, it is preferred to use the angular periodicity of the system and to perform the integration with respect to the angular position:

$$\gamma(t) = \int \omega_0 dt \quad (4.16)$$

By this substitution, the Fourier coefficients of the periodical drive torque at a given velocity can be calculated in terms of the angular position:

$$a_v = \frac{2}{N} \int_{\gamma_0}^{2\pi+\gamma_0} M_M(\gamma) \cdot \cos(v\gamma) d\gamma \quad (4.17)$$

$$b_v = \frac{2}{N} \int_{\gamma_0}^{2\pi+\gamma_0} M_M(\gamma) \cdot \sin(v\gamma) d\gamma \quad (4.18)$$

4.5 Sliding window for discrete integration

The integration for the calculation of the Fourier coefficients can be numerically evaluated by utilizing a sliding window. One property of the Fourier transformation is its cyclical shifting, this means that a time displacement of the signal does not affect the amplitude of the Fourier transform but just the phase angle. By taking advantage of this property, the calculation of the Fourier coefficients can be achieved by using a sliding window for discrete integration. Sliding window indicates that the integration limits are continuously shifted to the positive side of the time axis.

The Figure 4.1 illustrates the concept of a sliding window for the Fourier coefficients calculation. As it can be seen in the picture, for there an increment in time corresponds an increment in the discrete measurement of the angular position.

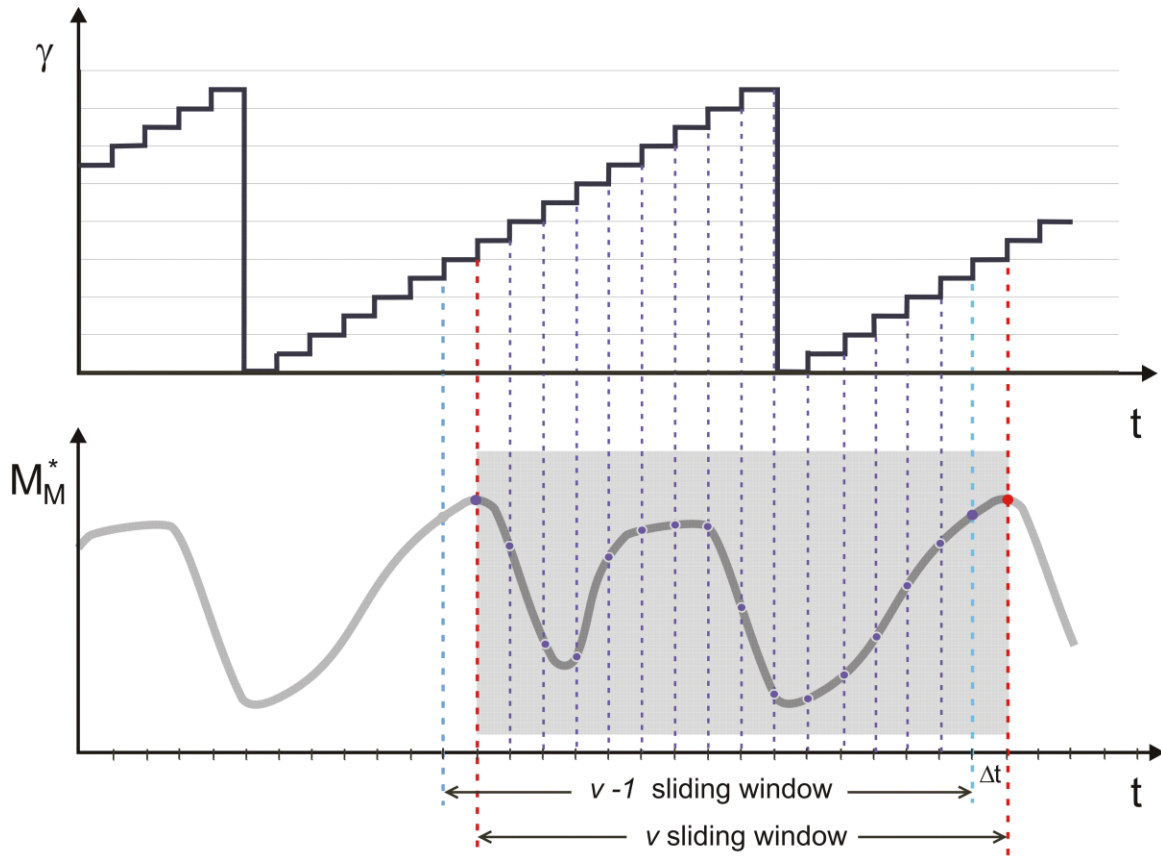


Figure 4.1 Sliding window

The increment of the angular position is a constant value determined by the number of elements to be considered within the sliding window. This can be calculated by simple division:

$$\Delta\gamma = \frac{2\pi}{N} \quad (4.19)$$

In this way, the length of the sliding window is not related to the time. The shifting speed between windows depends on the mechanical velocity, therefore the output value of the sliding window might be hold depending on the selected value of $\Delta\gamma$ and the mechanical velocity.

After the substitution of variables from time to discretized angular position the equation (4.17) and equation (4.18) can be solved.

The Fourier coefficients are calculated by the following equations:

$$a_v = \sum_{i=0}^{N-1} a_{v,i} = \sum_{i=0}^{N-1} \frac{2}{N} M_M(i \cdot \Delta\gamma) \cdot \cos(v \cdot i \cdot \Delta\gamma) \quad (4.20)$$

$$b_v = \sum_{i=0}^{N-1} b_{v,i} = \sum_{i=0}^{N-1} \frac{2}{N} M_M(i \cdot \Delta\gamma) \cdot \sin(v \cdot i \cdot \Delta\gamma) \quad (4.21)$$

The calculation of the coefficient is the addition of all the terms within the integration limits. When the sliding window of integration is shifted $\Delta\gamma$ a new term must be added to, and the oldest summand is subtracted from the total summation of the “old” window. As example, a sliding window with $N=16$ is displayed in Figure 4.2:

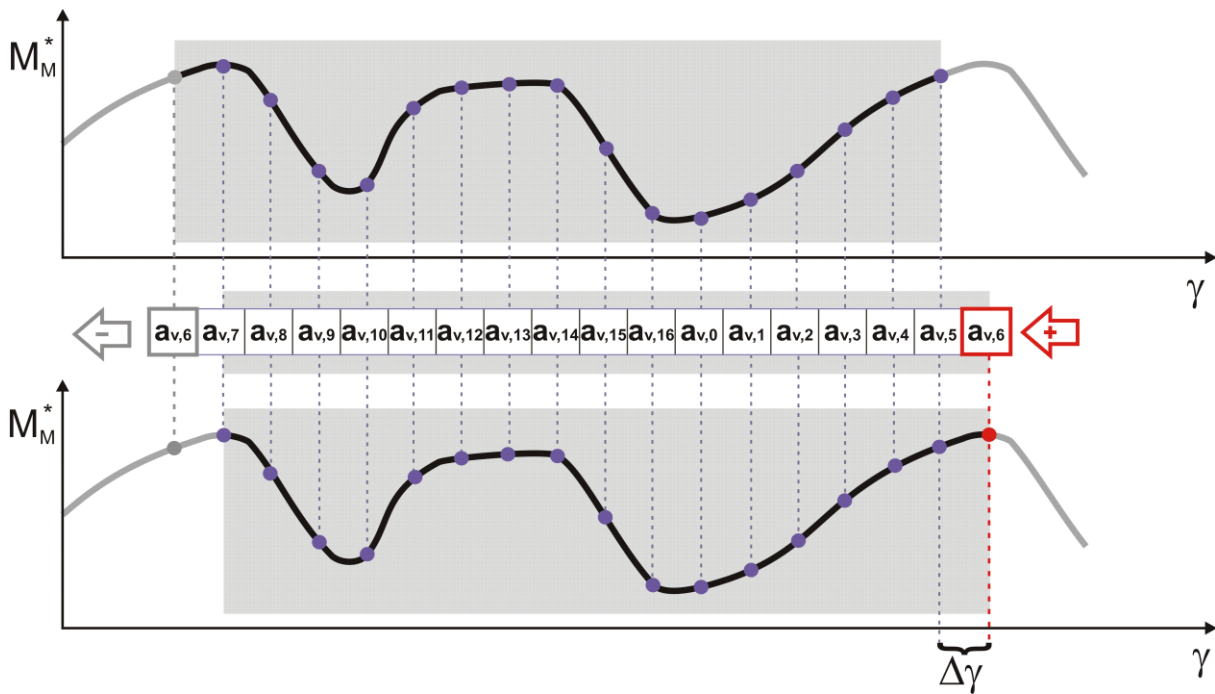


Figure 4.2 Summation elements within the sliding window for integration

The number of terms in the summation is represented by N and it depends on the size of the discretized angle. The larger the number of terms in the summation is, the smaller the discretized

angle $\Delta\varphi$ will be and the higher the precision of the calculated coefficients will be, which also implies a higher calculation effort and the corresponding memory for the storage of the samples.

4.6 Structure of identification

By using the experimental platform with a crank mechanism, with a comparable configuration as the one described in 3.6.1, the identification of a periodical load and its representation by Fourier series was implemented. The control and identification structure is described in Figure 4.3.

The inputs to the identification algorithm are a defined discretized angular position of the motor $\Delta\gamma$, which is calculated as described in section 4.5, and the reference value for the driving torque. In the practical implementation a delay is included to correctly consider the delay between the reference and the actual torque.

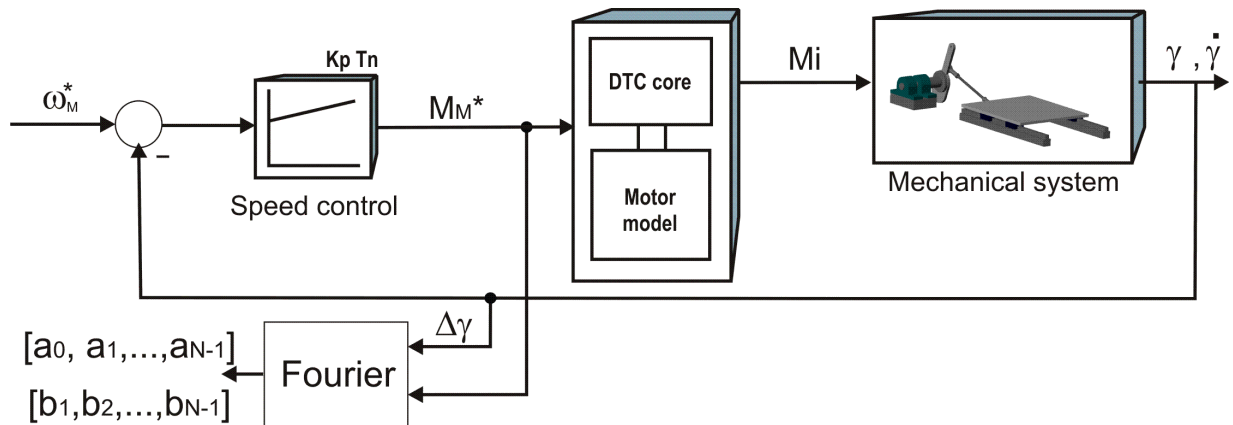


Figure 4.3 Velocity control and Fourier identification diagram

4.7 Summary of the chapter

A novel deterministic identification method to achieve the plant identification in the time domain was developed. This method utilizes the Fourier series for describing the identified total torque that consist of the load torque and the torque due to inertial forces. It was demonstrated that for such mechanism described in section 2.1.3 the driving torque for a given mechanical velocity can

be represented by a periodical function of the angular position of the shaft. The results obtained with this identification technique can be used to calculate a mathematical model of the mechanics of the drive with the purpose of feed-forward control.

5. Feed-forward control for a variable inertia system

The classical cascade control structure frequently contains a proportional-integrating (PI) controller of velocity, whose output is the reference value for the driving torque delivered by the motor [83]. However, under certain operation condition this kind of control may not be enough to track the velocity reference signal. Thus the performance of this controller can be improved. One technique for achieving this objective is the utilization of feed-forward compensation. The main idea of a feed-forward compensation relies on the fact that if the disturbances to the system can be identified, they can be compensated as well.

In given cases, not only disturbances can cause instability or degrade the performance of the system during operation a change of the parameters occur, the controller has to develop a different effort to track the reference. Moreover, non-linear phenomenon, like friction in reciprocating elements, generates oscillations in the load torque. These changes can be included in the identification of the variable load and in the feed-forward compensation.

The variable dynamics and disturbances of the system can be estimated by utilizing the controller of velocity for the identification. The driving torque delivered by the motor for given operation velocities in a closed loop control of the velocity contain the information that is necessary for obtaining a simplified model of the load dynamics and disturbances, and afterwards in a feed-forward scheme for enhancing the behavior of the system.

5.1 Feed-forward control structure

The classical cascade control structure was presented in section 2.2. The input to the PI velocity controller is the difference between the velocity reference and the actual monitored velocity. The actual monitored value is frequently obtained as feedback delivered by position sensors or encoders.

The parameterization of the PI controller of velocity is in the praxis usually performed by symmetrical stabilization. By following this method, the time constant of integration T_n is

calculated in direct proportion to the equivalent time constant of the closed loop current control of the machine, and the proportional controller gain K_p , to the mechanical constant T_H that represents the run-up time of the drive. The symmetrical stabilization usually assures a good step and disturbance response, but when large oscillations are present in the load or when the mechanical parameters of the system change during the operation, it is hard for a classical PI feedback control to achieve a good velocity reference tracking [15].

A feed-forward controller can be used to enhance the dynamic behavior of a system especially to reject disturbances by adapting the system to the dynamic demands. The feed-forward in the velocity control loop achieves a reduction of the tracking error also in the case of a variable reference. Such structures are special cases of the model based control [64] and can be used provided that a model exists and can be used as an adaptation mechanism.

The basic feed-forward control structure is depicted in Figure 5.1. The input to the digital control at the sampling time k is the difference between the reference signal $w(k)$ and the actual output of the system $y(k)$. The adaptation mechanism delivers information about the disturbances. By this, the command signal $u(k)$ can be adapted to better compensate the disturbances, allowing a better tracking of the reference signal.

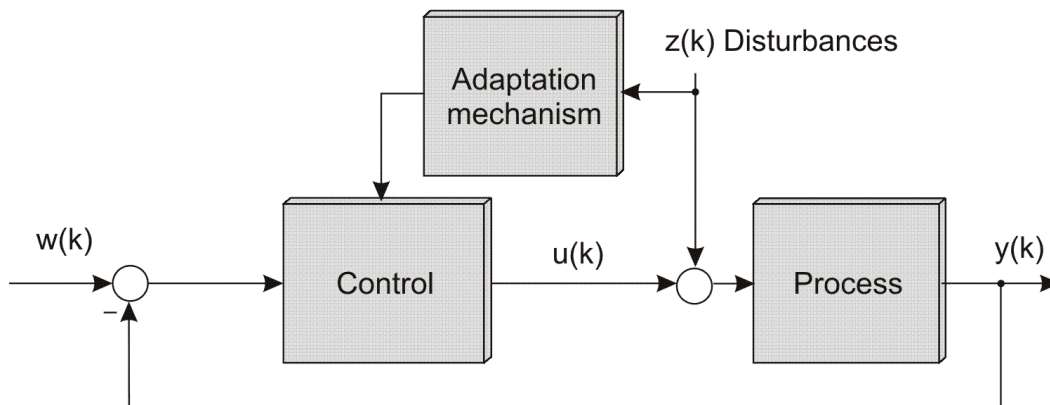


Figure 5.1 Basic structure of digital feed-forward control

This strategy of enhancing the linear control by using the knowledge of the dynamics of the plant can be applied for machines and systems with variable load. If the dynamic behavior of the load

torque M_L is known the velocity controller can be biased in a way that the linear control e.g. PI only rejects the remaining differences between model and real plant.

In the case of a mechanism where the rotation is transformed in linear displacement the changing moment of inertia is a key factor determining the system dynamics. At the same time, the non-linear forces due to friction derive in load torque to the motor that from the point of view of control are disturbances.

The case to be analyzed is a crank-shaft-slider mechanism such as depicted in Figure 5.2. The method presented in this work consist in utilizing the characterized motor torque reference signal, as described in section 4, to design a model for feed-forward control. The system dynamics are reproducible by a mathematical model which is a function of the position of the motor and the mechanical velocity.

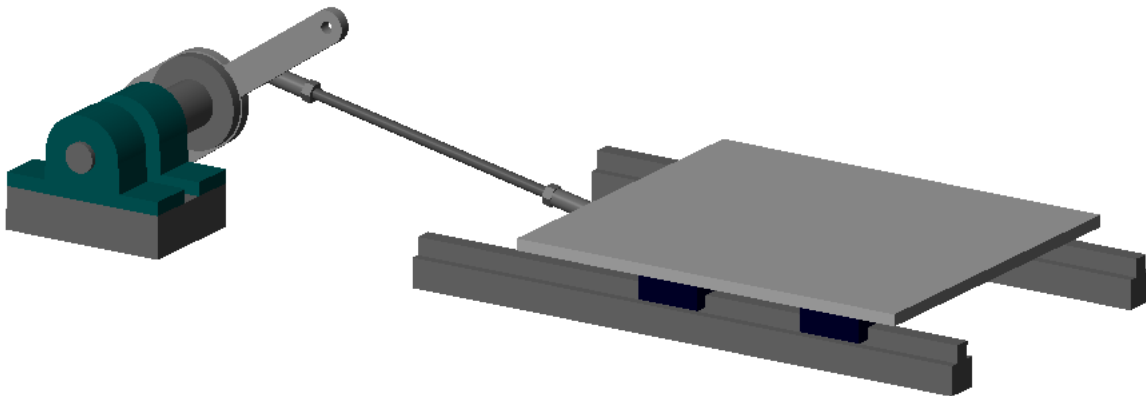


Figure 5.2 Crank-shaft slider mechanism

An ideal model would perfectly reproduce the behavior and disturbances of the system and when applied in the feed-forward control would make the output of the system, in this case the velocity to be equal to the reference.

However, a model that perfectly resembles the behavior of the plant and the disturbances is not possible to achieve. There are several factors, such as the accuracy of the parameters, the consideration of non-linearities, second order effects, the noise in measured data, the numerical

resolution and the memory space for data processing among others that reduce the quality of a model.

The model presented in the present work aims the compensation of the disturbances i.e. of the varying load and mechanical parameters. These are the main factors determining the dynamical response of the mechanical system. A model including such factors is enough for feed-forward control integrated to the classical PI velocity controller.

In the model used for the feed-forward strategy, the following main physical effects are considered:

- The non-linear load due to friction.
- The effect of the varying inertia of the composed mechanism.

By introducing the feed-forward compensation into the cascade control structure of the drive, the diagram of control is modified as depicted in Figure 5.3:

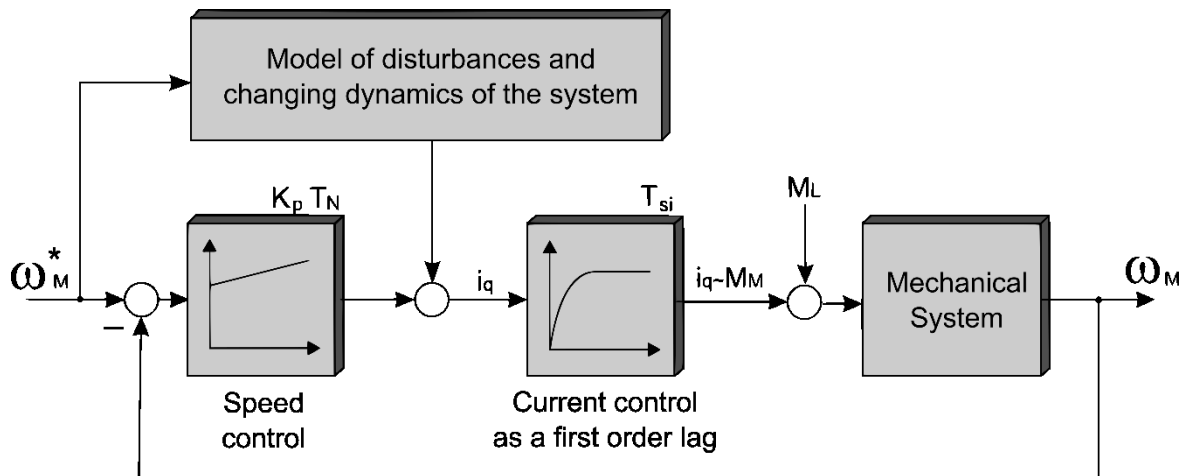


Figure 5.3 Feed-forward compensation structure

5.2 Model of disturbances and variable reduced inertia effect

As explained in section 4.2, the motor torque reference signal is can be characterized for a given mechanical velocity of operation as a function of the position of the motor. As this signal is the output of the velocity controller, it contains information about the load torque and inertial effects

of the mechanism under the equilibrium conditions defined in 4.3. By executing the identification method with Fourier series at several velocities of operation, the inertial effects can be detected and included in a functional model of the system disturbances for a whole velocity range.

With this purpose, the characteristic motor torque for the slider-crank mechanism was identified at several velocities within the range 0 to 100 min^{-1} .

The reduced moment of inertia is a function of the crank angular position. The reduced moment of inertia function of a crank-shaft is expressed in equation (3.22). The graphical representation of this function evaluated with the mechanism dimensions of the experimental platform II (Appendix) is depicted in Figure 5.4 .

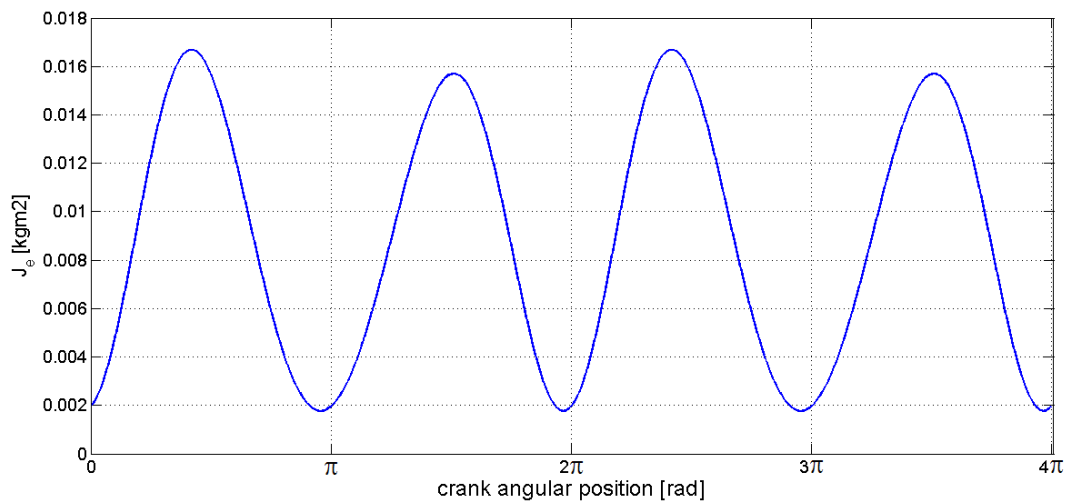


Figure 5.4 Reduced moment of inertia representation with respect to the crank angular position

An apparent double periodicity with respect to the angular position of the crank, which is the same as the angular position of the motor, can be noticed from the graphic. From the mathematical point of view this is explained with the equivalence of trigonometric expressions. The most significant summand in equation (3.22) is a product of a square function, equivalent to a cosine function of twice the angle [84]:

$$\sin^2(\alpha) = \frac{1}{2} \cdot (1 - \cos(2 \cdot \alpha)) \quad (5.1)$$

Therefore, the reduced moment of inertia can be approximated by a negative cosine function with the double of the rotation frequency of the motor shaft. For the derivative of the moment of inertia can be written:

$$\frac{dJ(\gamma)}{dt} = \hat{A} \cdot \sin[2 \cdot (\gamma)] \quad (5.2)$$

As mentioned in section 4.3, if the mechanical velocity of the drive is kept constant by means of an appropriate and fast control, in this way the torque delivered by the motor drive is approximately equal to the load torque plus the product of time derivative of the moment of inertia times the angular velocity, as expressed in equation (4.10).

By substituting equation (5.2) into equation (4.10) , the motor torque expression can be rewritten as equation (5.3):

$$M_M(\gamma, \dot{\gamma}) = M_L(\gamma) + \dot{\gamma} \cdot \frac{dJ(\gamma)}{dt} = M_L(\gamma) + \dot{\gamma} \cdot \hat{A} \cdot \sin[2 \cdot (\gamma)] \quad (5.3)$$

The rate of change of the moment of inertia is a sinus function with double frequency of rotation. This indicates that, within the Fourier approximation of the motor torque expression, the coefficient related to the term $\sin[2 \cdot (\gamma)]$ should show a direct proportional relation to the mechanical velocity $\dot{\gamma}$.

By using the motor torque reference signal approximated by Fourier:

$$\widehat{M}_M(\gamma, \dot{\gamma}) = \frac{a_0}{2} + \sum_{v=1}^N a_v \cdot \cos(v\omega_0 t) + \sum_{v=1}^N b_v \cdot \sin(v\omega_0 t) \quad (5.4)$$

It can be inferred that the coefficient b_2 , related to the term $\sin[2\omega_0 t_v]$, is a function of the mechanical velocity:

$$b_2 = b_{2ML} + \dot{\gamma} \cdot \hat{A} = b_2(\dot{\gamma}) \quad (5.5)$$

Where b_{2ML} is the coefficient of the sinusoidal component related to the load torque.

The deterministic identification procedure with Fourier series can be carried out for several velocities to determine which one of the Fourier coefficients presents a direct proportional relation to the mechanical angular velocity of the motor. Then the values b_{2ML} and \hat{A} are obtained by interpolation.

5.3 Summary of the chapter

The classical linear control with a PI- controller is the most used structure for the velocity control in electrical drives. It is often realized within a cascade control with a current respectively torque control in the innermost loop. In applications with moderate dynamics of the load torque, its performance is excellent and a large bandwidth can be achieved. Nevertheless, depending on the application, the dynamic response cannot always be sufficient. Especially in case of changing parameters, variable moment of inertia, non-linearities or strong and fast changing disturbances the dynamics of the velocity control can become inadequate.

In this chapter, the concept of feed-forward control together with an identification procedure for the variable load torque for compensating such phenomena in a system with a composed mechanism such a crank-shaft-slider was presented. To improve the system response, the velocity control with a linear PI algorithm is extended to include feed-forward compensation.

A new technique for designing a model to describe the dynamical behavior of such system and its disturbances under certain constraints was introduced. By utilizing the results of the proposed deterministic identification technique, the drive torque of the system can be approximated as a periodic function by Fourier series. The coefficients of the Fourier series are calculated at different velocities. By inspecting the Fourier coefficients at the different speeds, the coefficient related to the inertial effect can be detected. Based on this information, the parameters for a model of the mechanical load can be interpolated.

6. Diagnostics

Condition monitoring is the permanent or periodical observation of the physical state of a machine or technical system. The early detection of failures or incipient faults in the components of an automated system is important in order to avoid the difficulties and cost derived from the interruption of operation and the effort of repair when serious failures occurred. As already mentioned, electrical drives are key components in automation and therefore they deserve a special attention regarding diagnostics.

There are several different causes for failures in an electrical drive, some associated to the electrical part of the drives, some associated to the electrical part, but also others related to the mechanical elements between the motor and the load. Such failures can affect the dynamical response of the whole system at certain velocity ranges e.g. start, stop or resonance points or even lead to a fatal failure of the system and eventually to the shutdown of the whole process [85].

Due to the important role of electrical drives in automated processes and machines, many research works have been dedicated their condition monitoring, some of them oriented to electrical faults in the machine [86], and other to the mechanical part of electrical drives [26].

The IEEE Large Motor Reliability Survey of Industrial and Commercial Installation reports that faults related to bearings are the most often failures found on electrical drive systems [32]. The state of the art of the methods for detecting failures in bearings of electrical motors was described in the first chapter.

In the last years, the research group of Electrical Drives and Power Electronics in the University of Siegen has developed frequency domain procedures for the detection of failures in the bearings of electrical drives, the present work focuses on fault detection on rolling bearings in the time domain. If the system under healthy condition of the bearings is characterized, this information can be used to compare when changes on the system behavior appear. By recognizing this changes, fault condition of the bearings can be detected.

6.1 Rolling bearing failure detection

Rolling bearings are machine elements that utilize the rolling interaction of balls or rollers with a fixed element to permit minimum friction for the constrained motion relative to another [87].

There are several types of rolling bearings, its construction depends on the type of movement they allow and the orientation of the load they have to support. The classification depending on the load forces orientation can be large to enumerate [88], the main types are however the radial and axial bearings.

The most popular rolling bearing type is the single-row deep-groove ball bearing [89]. A radial ball bearing of this type is depicted in Figure 6.1. The load force F_r acts radially to the rotating axis.

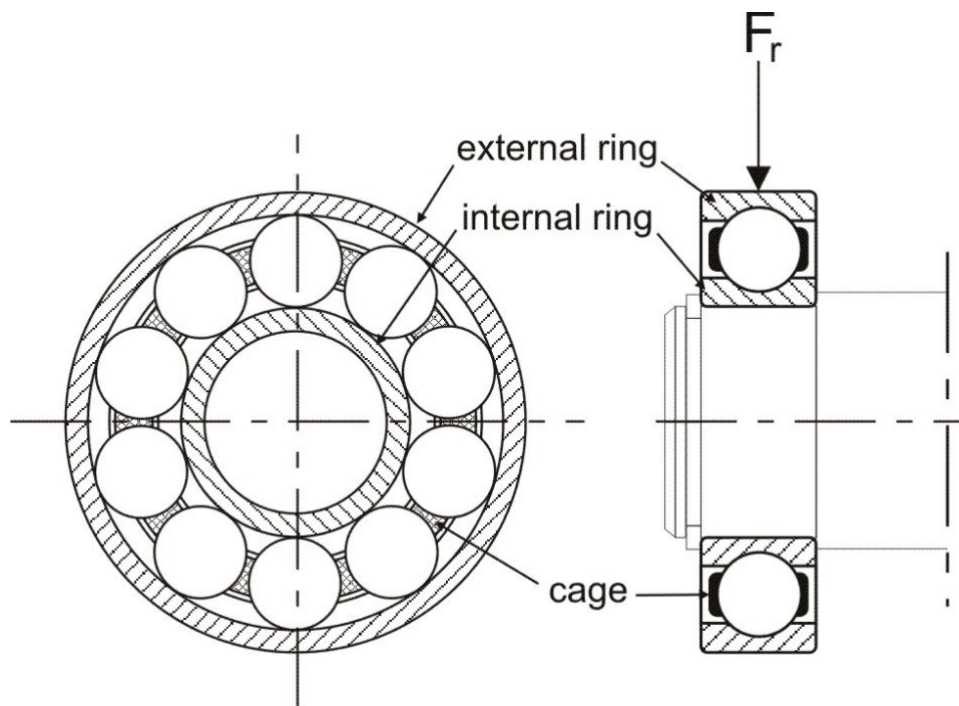


Figure 6.1 Mechanical construction of a radial ball rolling bearing

The ball bearing is composed of two rings one external ring and one internal ring. The rolling elements are located between both rings and are held angularly spaced by a cage to avoid the

contact between the balls. The rolling elements are lubricated, with oil or solid lubrication and for this reason some bearings have also sealing components.

6.2 Causes and classification of failures in rolling bearings

When the condition of operation meet those considered during the design for the specific application, the operation life of the bearings should last as long as calculated, but in many cases, damages or failures in the rolling bearings can emerge.

The major causes of bearing failures during operation are given in the pertinent literature [90]:

- Thermal stresses: overheating degrades lubrication and extreme temperature oscillation causes material fatigue. Also hard coating on balls can be formed by grease polymerization by sliding under high contact stresses and high temperature.
- Mechanical stresses: Vibration is a cause of fatigue, especially for large operations torques. Mechanical stresses are reflected in fretting and wear which can lead to the fracture of the cage or bearing rings.
- Electrical stresses: a cause of lubrication deterioration.
- Shaft currents
- Chemical or particle contamination: Hard particle contamination can cause indentations in the rolling contact surfaces. Chemical contamination can degrade the lubrication or directly cause pitting damage.

One possible classification of bearing failures considers the location on the failure as the criteria for categorization, different frequencies are produced depending on the failure location which can be detected with vibration analysis [53] [47]:

- internal ring
- external ring
- cage
- balls

Other way to categorize the bearing failures takes into account the physical characteristics of the fault. This classification is also useful to discern the different effects that the physical failures produce [52] [36]:

- Single point failure: are localized punctual defects surrounded by a relatively undamaged vicinity surface, they can be a hard coating formation or a fracture. When a bearing ball passes over a single point failure, a shock impulse is generated when the ball tries to leave the hole or to overcome the obstacle. The effect of this is manifested as torque disturbances and velocity fluctuation.
- Generalized rough: This kind of fault may be not visible to bare eye, and as there is no punctual defect, there is nothing to excite characteristic fault frequencies in the torque and it causes that roughly and difficult spinning because of the increase of friction. These faults may also produce in long term single point failures [91].

As mentioned in the first chapter, the detection of bearing faults has been mainly achieved by utilizing vibration analysis methods for what vibration transducers are required, mainly accelerometers which represent an additional costs.

6.3 Diagnostic of failures ball rolling bearings on machines with cyclical process

In industry and in commercial installations, most of the machines perform cyclical coordinated movements often governed by a superimposed open- or closed-loop position control. Several manufacturing process require machines with mechanism for precise and coordinated force transmission, most frequently such mechanisms are crank-shafts [92]. Usually this kind of complex machines operates at a limited velocity range because their movement can induce vibration, can cause noise and wear as well as undesired frame load [93]. These are important aspects especially for high performance machines with and long operation times, in which a high availability is demanded.

The vibration in such machines, where the translation movements are achieved by composed mechanisms with a rotating crank can arise from the changing reduced moment of inertia of the

whole mechanism that results in a disturbance of the velocity and position control that react trying to compensate the variations of torque related to the inertial effect. As it was discussed in section 4.3 the variation in amplitude of the driving torque reference is also related to the velocity of rotation of the crank due to the inertial effect.

Bearing faults can also cause vibrations, distortions in the load torque and fluctuations in the velocity. Nevertheless, depending on the applications, the load torque may be not constant and also inertia related forces can vary. Therefore, it is necessary to recognize the disturbances due to bearing faults and distinguish them from the torque oscillations due to load fluctuation and those due to inertia related forces in the mechanism.

A method for discerning the effect of a damage in the bearings from the load and inertia related effects is the monitoring of the torque produced by the electrical drive. For this purpose, the output of the velocity control can be used as indicator for the load torque and inertial effect. Under the assumption of a sufficient bandwidth of the velocity control resulting in a control error $\omega_M^*(t) - \omega_M(t) \approx 0$, the I-part of the velocity controller is a good approximation of the load torque and inertial effect. This can be acquired during the commissioning of the drive for a complete cycle of the machine as characteristic pattern, and then continuously compared with the actual measurement. If a difference between the characteristic patterns of the machine at the time of the erection and the actual one would indicate a change in the mechanics and can be used as indicator for a failure.

6.4 Effect of the friction in rolling bearings on the load torque to the drive

The friction in rolling bearings is indeed very low on healthy rolling bearings. However, friction in all cases is a very complex phenomenon to describe. When a body rolls over a surface, certain forces act at the contact points of the body opposing to the movement. In rolling bearings there are several movements of the components that cause friction; also the certain viscous friction arises from the lubrication. In general, there are different factors that influence the friction torque in bearings such as the construction and dimension of the bearing, the axial and radial load, the rotational velocity, the type of lubrication and the temperature of the environment [94].

The total friction torque of bearings M_{FB} is usually estimated by the sum of the load friction and the viscous friction [89] [94] [95]:

$$M_{FB} = M_{lf} + M_v \quad (6.1)$$

Where M_{lf} corresponds to the load friction due to the applied load on the bearing and M_v to the viscous friction due to the lubrication. The calculation of both is based on empirical formulas.

The equation used to estimate the friction due to viscous lubricants, up to 2000 min^{-1} is given by:

$$M_v = 10^{-7} f_o (v_0 n)^{2/3} d_m^3 \quad (6.2)$$

Where v_0 and f_o are empirically calculated factors related to the type of bearing and the lubrication, d_m is the bearing pitch diameter and n is the rotational speed in min^{-1} [89].

At high velocity the friction is mainly viscous, but at low velocity the friction is principally caused by the applied load on the bearing.

The equation that calculates the friction torque due to the applied load on the bearing is expressed as follow:

$$M_{lf} = f_l F_\beta d_m \quad (6.3)$$

The load component F_β depends on the magnitude and direction of the applied load; in radial ball bearings it is equal to the total load at the bearing F_r . In the case of rotating mechanism such as crank shafts, there are mathematical equations for the calculation of the oscillating load on the bearing [95] . The f_l factor depends on the bearing design and the static bearing load, this and other calculation factors can be read from manufacturer's catalogs [96].

The total friction torque on the bearing is a component of the total load torque to the drive. On healthy bearings the friction torque is expected to remain within certain tolerance range. An increase on the friction torque would result in load torque change and therefore the reference of

the driving torque delivered the motor would not match the characteristic pattern of the machine which can be used for diagnosis purposes.

6.5 Fault bearings effects on the drive torque of a composed mechanism

As previously mentioned, a motor drive coupled to a composed mechanism, that involves the transformation of rotational movement into linear displacement, will present oscillations in its behavior. Therefore, the diagnosis of fault bearings is especially difficult in such drives. However, unexpected changes on the drive torque of the drive can serve as indicators for a damaged rolling bearing.

- Single point failure: significant punctual defects can produce a pulsating load torque. When the bearing ball tries to overcome the obstacle during the rotation of the machine an instantaneous demand of higher torque produces a rise in the torque of the drive. This effect is detectable only for severe punctual defects; in case that the single point fault is incipient it will not produce a noticeable pulsation on the drive torque.

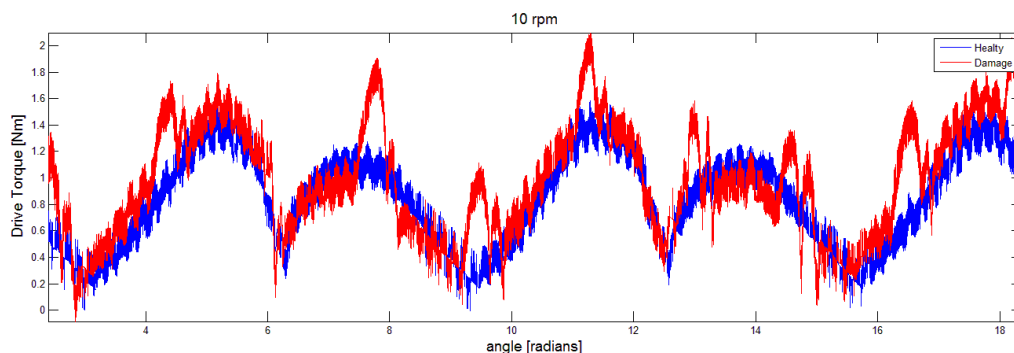


Figure 6.2 Comparison between measurements of the drive torque reference with healthy and damaged bearing with severe single point failure

- Generalized rough or slight single point failure: Generalized rough increases the friction torque on the rolling bearing. At steady state, this friction component remains constant and the effect on torque of the drive can be recognized as the addition of a constant component to the normal pattern of the machine. By comparing measurements

performed with a healthy bearing the measured drive torque with the damaged bearing would appear to have an offset. Incipient single point failures that are too weak to produce a visible pulsation of the drive torque would display a similar same effect.

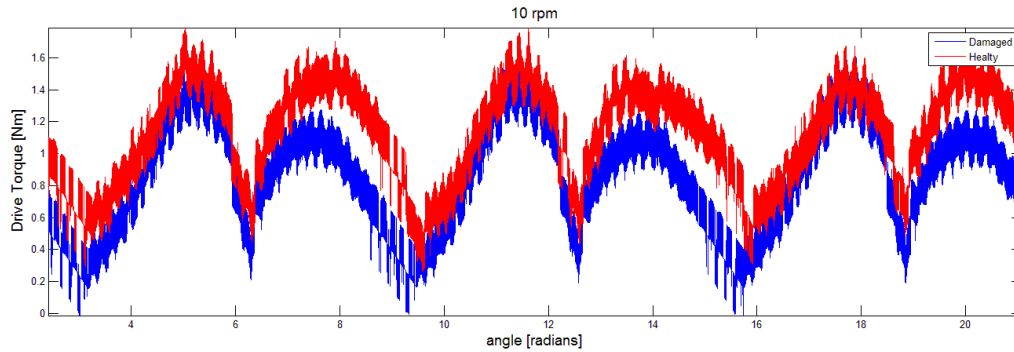


Figure 6.3 Comparison between measurements of the drive torque reference with healthy and damaged bearing with slight single point failure or generalized rough.

6.6 Summary of the chapter

This chapter deals with possible disturbances originated in a drive when a mechanical component fails. The most frequently faults detected in electrical drives are reported to be related to failures in bearings. Ball rolling bearings are the most common type of bearings used in industrial installations. A basic description of the mechanical construction of this type of bearing was presented, for a better understanding of the location and kind of possible damages.

A general explanation of the friction in ball bearings was presented. In composed mechanisms where the movement is transformed from rotation to translation, there are changing loads on the bearing and oscillations that are proper to the mechanism operation, Therefore, the detection of the harmonics related to bearing faults in such systems is not straight forward,

In the literature, several ways to categorize bearing faults are detailed. The classification of the faults in to single point faults and generalized rough was selected for the purposes of diagnosis within the scope of this work.

Several methods for the diagnosis of bearing faults are used in the praxis. One of the most common, vibration monitoring requires the use of special sensors that represent an extra cost.

A criterion for the diagnosis of ball rolling bearing in drives with composed mechanism is presented. This method does not require the installation of additional sensors to those already installed at the commission of the drive. For this, the reference value of the driving torque delivered by the motor is utilized.

A comparison between measurements with a healthy bearing at the commissioning of the plant, with actual measurements taken at a subsequently moment, can be used for the diagnosis of bearing faults. An increment as an apparent offset in the drive torque when compared to the measurements at the commissioning of the system would indicate increment of friction due to generalized rough. Incipient single point failures in bearings produce, in a similar way a increment in the friction. This kind of faults produces an increment in the signal of the reference value of the driving torque delivered by the motor as a constant value, it appears as an offset to the signal with healthy bearings. Only severe single point faults will create a pulsation in the driving torque of the motor.

7. Experimental results

The identification procedures proposed in this work and explained in detail in chapter 3, the feed-forward control explained in chapter 5 and the diagnostic method for rolling bearings explained in chapter 6 were experimentally verified.

The experimentation was carried out in two different platforms, designated as experimental platform I and II correspondently. In both platforms, the mechanism utilized was a slider crank shaft, but with different orientation in order to change the conditions of load. Besides, the motor-drive and the drive control were different for each platform. The initial tests of identification were performed with the experimental platform I described in section 7.1.1.1. The identification tests under the speed-sensorless control scheme, as well as those corresponding to the feed-forward control and diagnostic procedures were carried out on the experimental platform II described in section 7.1.2.1.

The dSpace 1104 rapid prototyping system was utilized in all experiments to execute the programs developed for each procedure. The utilization of this board has the advantage that program parameters can be adjusted during the program execution, not requiring the program to be compiled after parameters changes. The communication between the dSpace 1104 board and the drive control of each experimental platform was done through different interfaces in each case. In the case of the experimental platform I, the development of a particular solution for the communication between both devices was necessary.

The first part of this chapter present the results obtained from the experimental evaluation of the stochastic identification. Initially, the EKF identification was tested with velocity feedback from an encoder. Later, the EKF identification under the speed-sensorless control scheme was evaluated.

In section 7.2, the results of the deterministic identification method with Fourier series are presented. Based on the Fourier coefficients obtained from this identification, a model of the dynamics of the system is calculated. This model was utilized for the feed-forward control

implementation. The results of the feed-forward control combined with the classical PI speed controller are presented in section 7.3.

The experimental procedure for diagnosis of rolling bearings and the measured results are discussed in the last part of this chapter.

7.1 Identification with the extended Kalman filter

The identification procedure with EKF described in section 3 was tested in order to evaluate the effect of several parameters such as:

- The mechanical speed of the motor.
- The PRBS as additional excitation to the system.
- The structure of the PRBS generator.
- The mass addition to one element of the mechanism.

The experimental test were carried out utilizing a slider-crankshaft, a mechanical system with a repetitive production cycle that often can be found in many industrial application.

Two control schemes were considered for the experimentation. First, encoder feedback was utilized to analyze the sensitivity of the EKF procedure to the previously mentioned factors [97]. Later, the EKF identification was achieved under a speed sensorless control scheme. In both cases the variable reduced moment of inertia of a slider-crankshaft was identified.

7.1.1 EKF identification of variable moment of inertia with measurement of the shaft position

The EKF algorithm requires two inputs: the torque developed by the drive M_M and the mechanical velocity of the motor ω_M . The complete identification and control structure utilized for the experimentation was described in section 3.5.

The initial test, was executed by measuring the motor velocity with an encoder and carried out on the experimental platform I which is described in the following section.

7.1.1.1 Description of the experimental platform I

The experimental platform I allowed the experimentation for the identification of a variable reduced moment of inertia and a variable load torque. This laboratory set-up consisted on two separated mechanical systems, each one driven by a PM synchronous motor fed by an IGBT-inverter and equipped with vector control. The Figure 7.1 depicts the two separated mechanisms. According to the numeration in the picture the mechanism are:

- 1) A vertical slider-crank, which shifts a load up and down
- 2) A horizontal slider-crank, which moves a pair of jaws of a clamping fixture.

The experiments were performed on the vertical slider-crank mechanism. As explained in [98] it is possible to characterize the dynamics of composed mechanism, whose elements move around parallel axes as a system of a single equivalent moment of inertia or reduced moment of inertia.

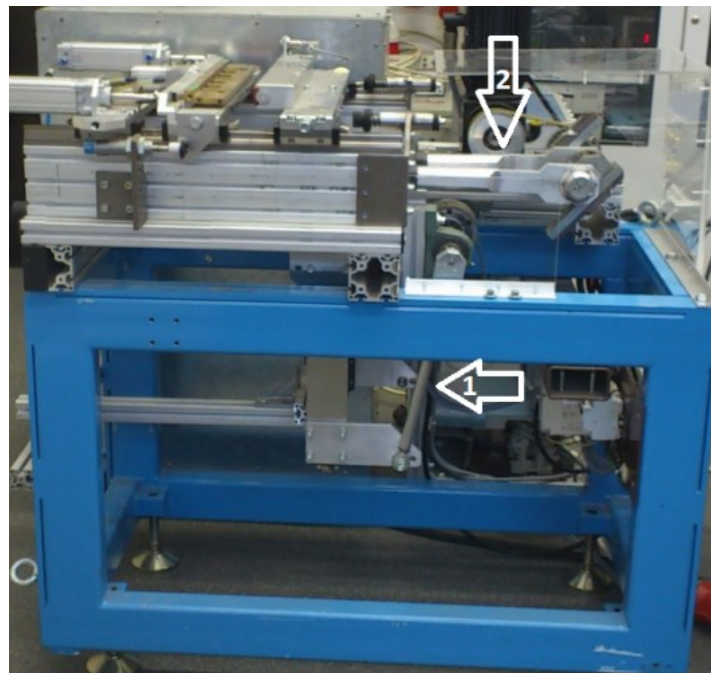


Figure 7.1 Front view of the mechanical experimental setup

The EKF algorithm was programmed in MATLAB Embedded code on a Simulink program which also included the PRBS generator required to create the artificial excitation to the system. This program was executed in the dSpace 1104 board. The velocity and current/torque control of the PMS Motor was performed by a servo drive LF 9400 which could be connected to an external PC for control parameter monitoring.

The communication between the dSpace 1104 and the servo drive LF9400 is depicted in Figure 7.2. The current component i_q which is proportional to the motor torque M_M was communicated through a Serial Peripheral Interphase (SPI), where the LF 9400 was the master and the dSpace board the slave. Due to limitations of the of the dSpace platform, complementary hardware had to be developed. The mechanical velocity of the motor ω_M was acquired through an encoder interface. The PRBS was inserted to the reference value i_q^* of the current control through an analog interface. The identification results were obtained during operation and the graphical interphase of the dSpace allowed the real-time graphical display of the results.

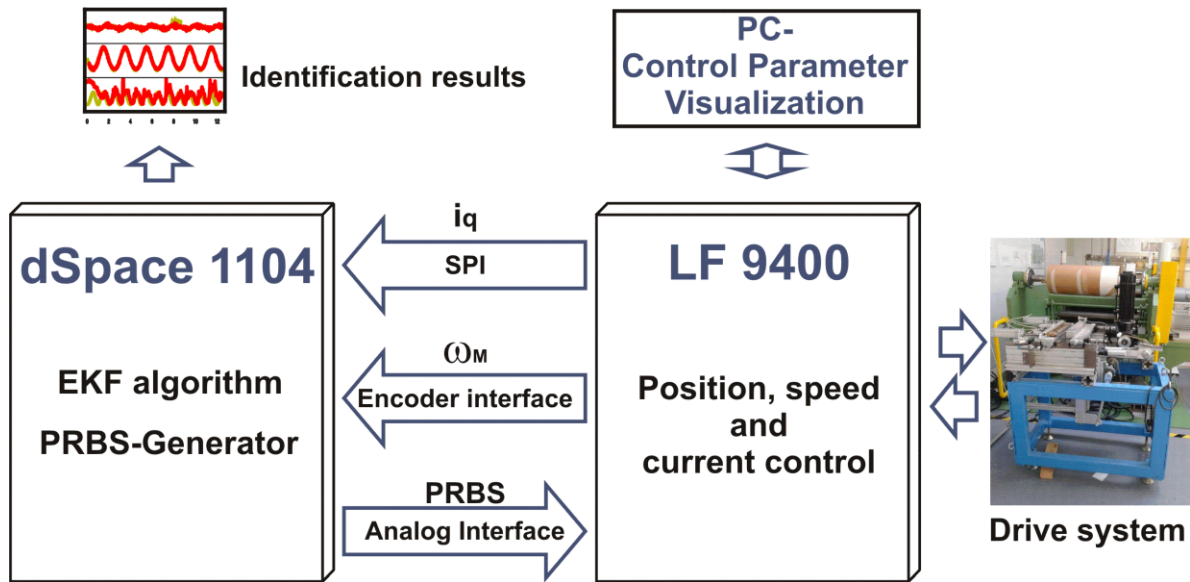


Figure 7.2 Communication diagram between control and identification board

By utilizing the described experimental platform, the EKF identification with encoder feedback was evaluated with respect to different conditions of additional excitation and mechanical velocity of the motor.

7.1.1.2 Influence of additional excitation

Experience has shown that the natural noise of the system is not sufficient for the proper function of the EKF. Therefore, an additional excitation is necessary for the identification of the variable parameters [99].

As mentioned in section 3.4, the EKF gives estimates of 3 states of the system. The estimation results are presented in the following in three graphics vertically arranged and corresponding to:

- Mechanical velocity $\hat{\omega}_M$ in min^{-1}
- Load torque \hat{M}_L in Nm
- Equivalent moment of inertia \hat{J}_e in kgm^2

Figure 7.3 shows the estimation results when no additional excitation is utilized. For comparison the known and measured values are also depicted.

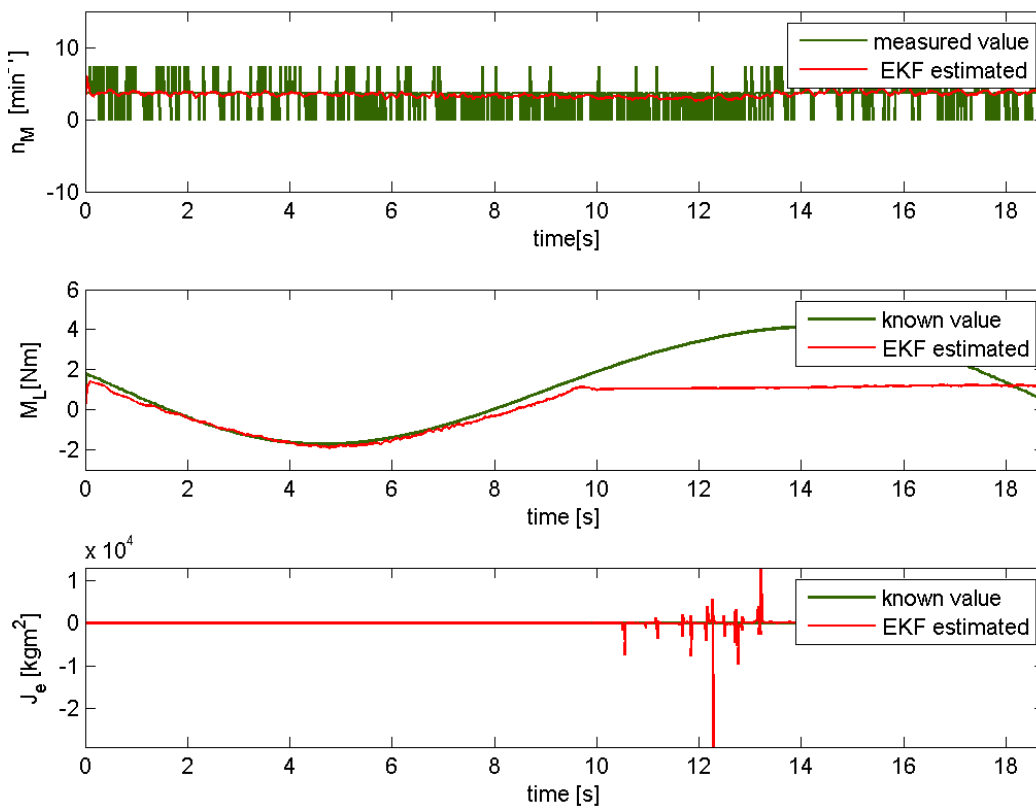


Figure 7.3: Estimation results without additional excitation to the system

The mechanical velocity of the motor was set to 3 min^{-1} for all test of different PRBS amplitude. It can be noticed that the estimated moment of inertia diverges to largely disperse values. The load torque and the reduced moment of inertia in the EKF model are considered constant values as explained in section 3.4. These limitations of the model are supposed to be corrected within the EKF algorithm by the measurements of the actual system. However, there is not enough estimation to compensate the model errors. The estimation of the load torque initially converge to the expected value but later drift to a constant value. In the case of the moment of inertia, the EKF estimation drifts between large positive and negative values.

In order to achieve the desired identification, additional excitation as PRBS of different amplitudes is added to the current reference value i_q^* through the analog interface. Several tests were done incrementing the amplitude of the PRBS. Signals with amplitude 0.48A, 0.72A, 0.96A and 1.2A were tested correspondently to a current of 0.21 pu, 0.31 pu, 0.41 pu and 0.52 pu.

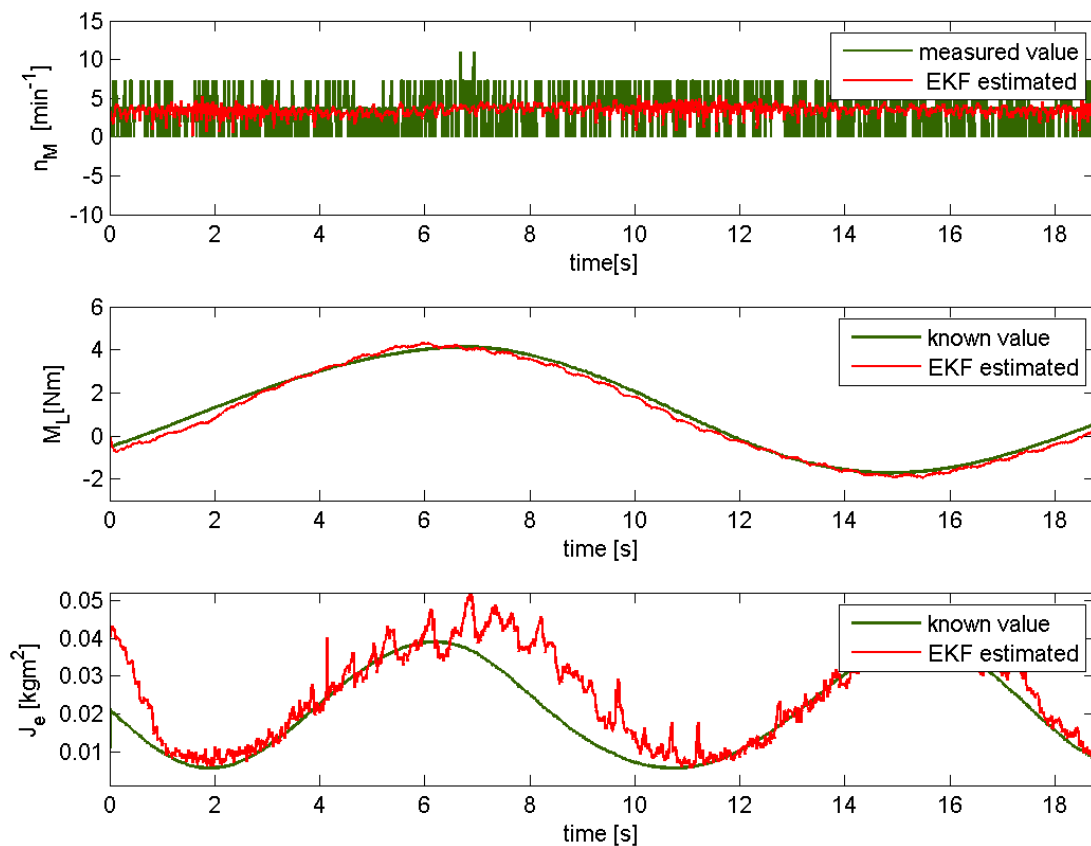


Figure 7.4: Estimation results when using PRBS with amplitude of 0.48A – 0.1 pu.

Initially, PRBS of 0.24A (0.1 pu) of amplitude were used. The small amplitude of the PRBS was not large enough to produce the necessary excitation to the system. Yet, by increasing the amplitude of the PRBS better estimations can be achieved.

The estimation results obtained with PRBS of 0.48A are depicted in Figure 7.4. The improved estimation results are due to the larger amplitude of excitation as explained in section 3.2.1.

The best estimation results were found by utilizing PRBS of 1.2A (0.52 pu) and are depicted in Figure 7.5 . The EKF estimation is improved with the larger artificial excitation which forces the measured data to have a more dense distribution. This makes the EKF to put more confidence on the measurements than on the system model which assumes the load torque and the reduced moment of inertia to be constant signals.

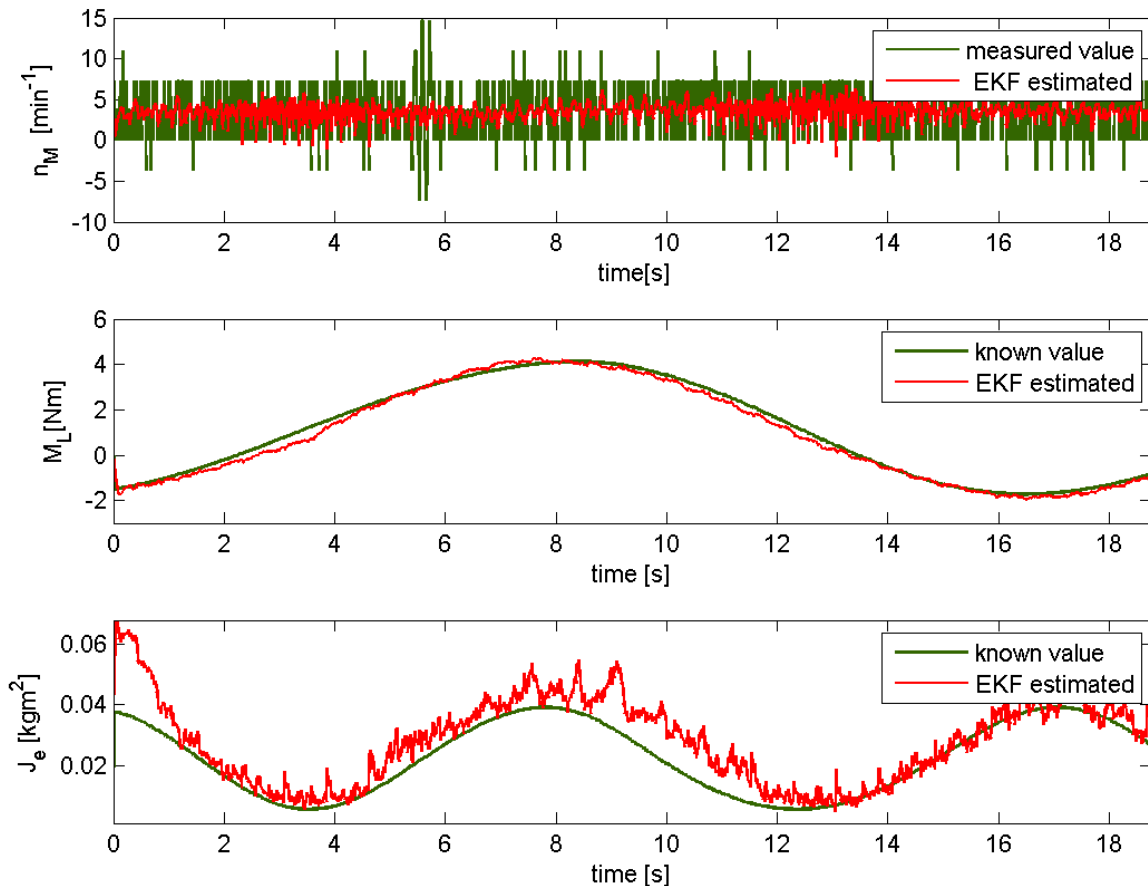


Figure 7.5: Estimation results when using PRBS with an amplitude of 1.2A - 0.52pu.

Structure of PRBS generator

As explained in section 3.3, PRBS were generated using shift registers. Because the number of bits used to create the PRBS has reported a relevant influence when used for some identification techniques in the frequency domain [26], several tests were executed changing the number of the shift registers. PRBS from 9 up to 20 shift registers were tested at the angular velocity reference of 3 min^{-1} . Afterwards, it was intended to examine how the number of shift registers could improve the identification results depending on the angular velocity. With this purpose, the previous experiment completed at the angular velocity reference of 3 min^{-1} was executed for different angular velocities. In this way, all the possible combinations between the number of shift registers of the PRBS-generator and the angular velocity were analyzed. In a similar way to the experiment described above, better results were obtained at lower angular velocities independent from the number of shift register.

The number of bit registers determines the frequency of the additional excitation signal. According to the experimentation it does not exert any influence on the estimation; it should be enough to ensure that this frequency is lower than the frequency of change of the states.

7.1.1.3 Influence of the mechanical velocity

The influence of the motor mechanical velocity over the EKF identification was also experimentally evaluated.

An analog interface in the drive control LF 9400 allows the user to change the reference value of the motor mechanical velocity between 0 and 200 min^{-1} . Test of the estimation procedure for different angular velocity reference within this range where carried out.

The best estimations were obtained at the lowest angular velocity. It must be remarked that the angular velocity determines the rate of change of the equivalent moment of inertia of the slider-crank because it is a function of the mechanism position. The relationship is a proportional one i.e. the faster the angular velocity, the faster the change of the equivalent moment of inertia. At

higher velocity the estimation produces poor results; the best estimations were obtained in the low velocity range up to 30 min^{-1} .

Figure 7.6 presents the test results at different velocities up to 30 min^{-1} . These results are compared with the measured angular velocity, the expected moment of inertia and load torque of the equivalent model of the system. It can be seen that the EKF required almost 1 second to yield an acceptable estimation besides the measurement points out that for faster changing variables in industrial devices, such as the reduced moment of inertia in this case, it may require some modifications to produce better results.

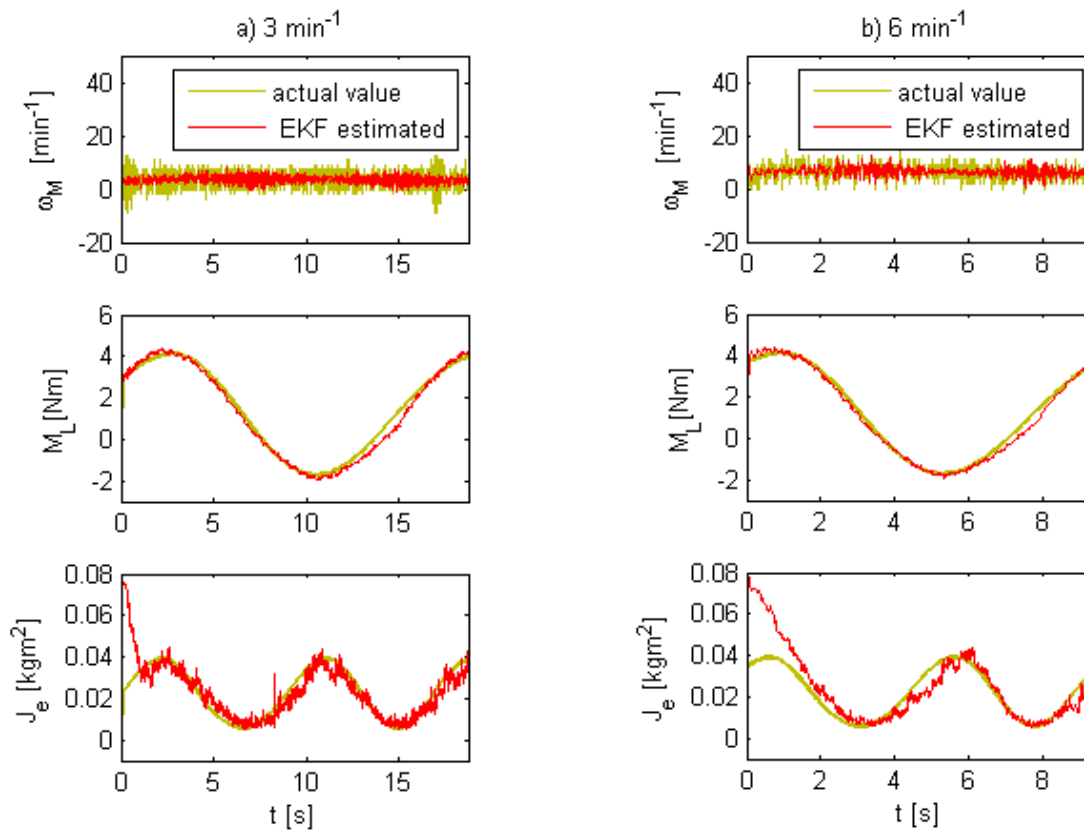


Figure 7.6: Experimental results at: a) 3 min^{-1} b) 6 min^{-1}

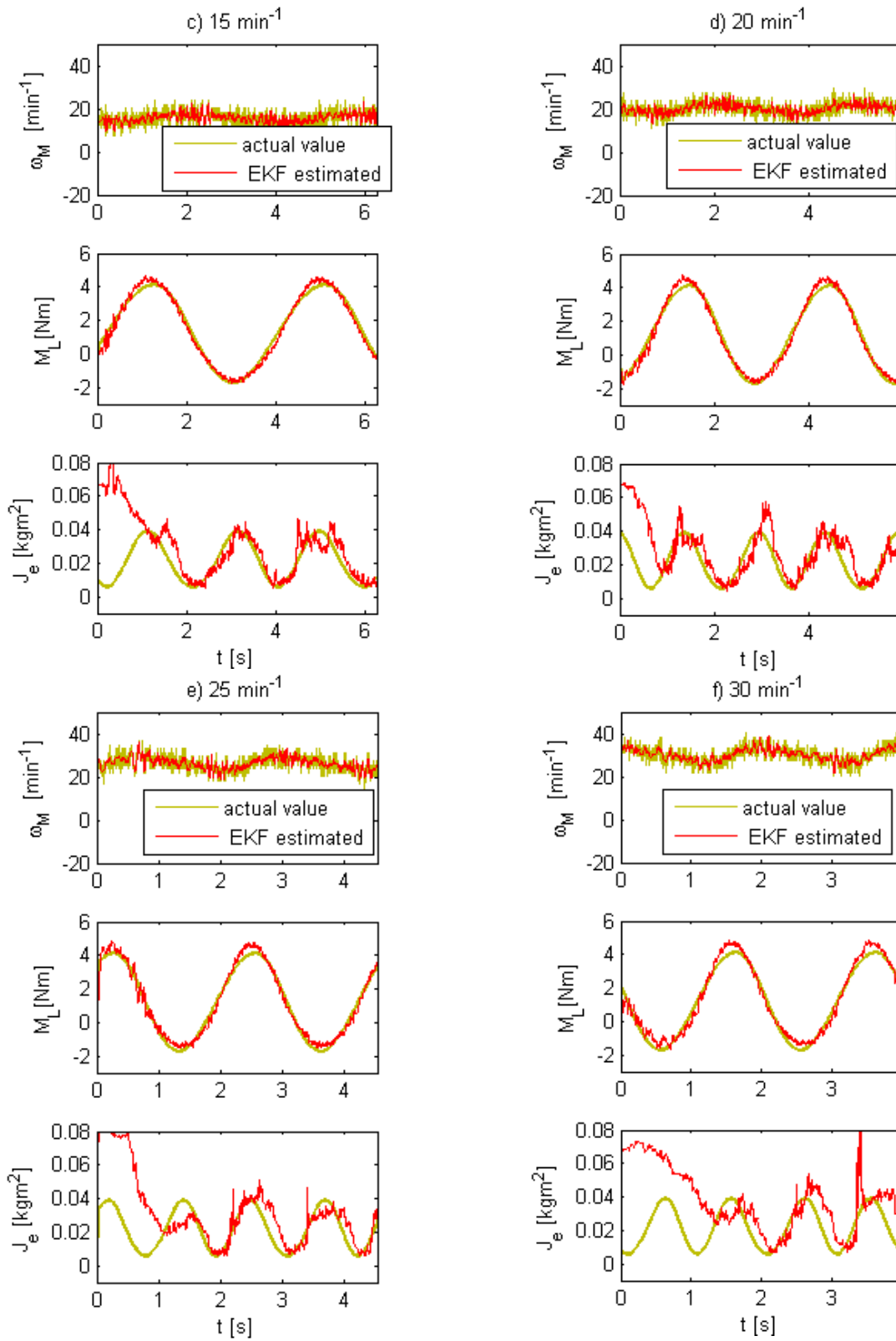


Figure 7.6: Experimental results at: c)15 min⁻¹ d)20 min⁻¹ d)25 min⁻¹ f)30 min⁻¹

7.1.1.4 Estimation of the moment of inertia as function of the crank position

The reduced moment of inertia of the slider-crankshaft mechanism is fundamentally a periodical function of the position of the crank. Therefore, the obtained estimation can be represented in a graphic as a function of the angular position such as depicted in Figure 7.7.

If the reduced moment of inertia is expressed as a function of the position the time is not necessary for describing its change and the results can be compared in a single graphic. Furthermore, this characteristic of the reduced moment of inertia will be used with the purpose of diagnostic and of adjustment of the control parameters.

In this graphic, it can be noticed that the estimation of the reduced moment of inertia at the lower range of motor velocity is more accurate than those obtained at the highest velocity range.

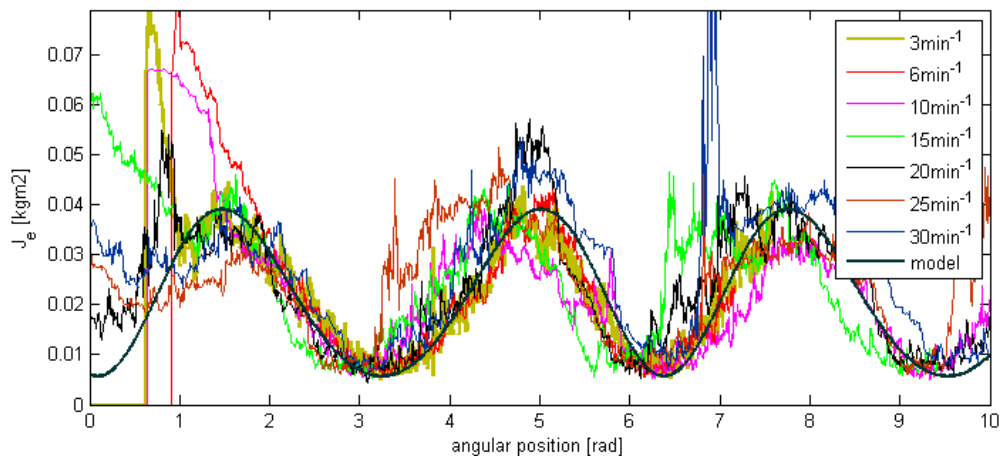


Figure 7.7: Estimation of the reduced moment of inertia at different velocities and model as function of the crank position

7.1.2 Identification of the reduced moment of inertia with an EKF and without encoder

The speed-sensorless EKF identification was achieved by utilizing an estimation of the mechanical velocity of the motor instead of encoder measurements. The identification and control structure will be explained in section 7.1.2.2.

This method was tested with the experimental platform II which is described in the following section.

7.1.2.1 Description of the experimental platform II

A new platform was assembled for the experimental test of the identification without encoder for the measurement of the shaft position. The mechanical part consists of a horizontal slider-crankshaft mechanism with a sliding plate as depicted in Figure 7.8. The mechanism is coupled to a 1.5KW permanent magnet synchronous motor which is connected to a commercial frequency converter and drive control ACSM1-04.

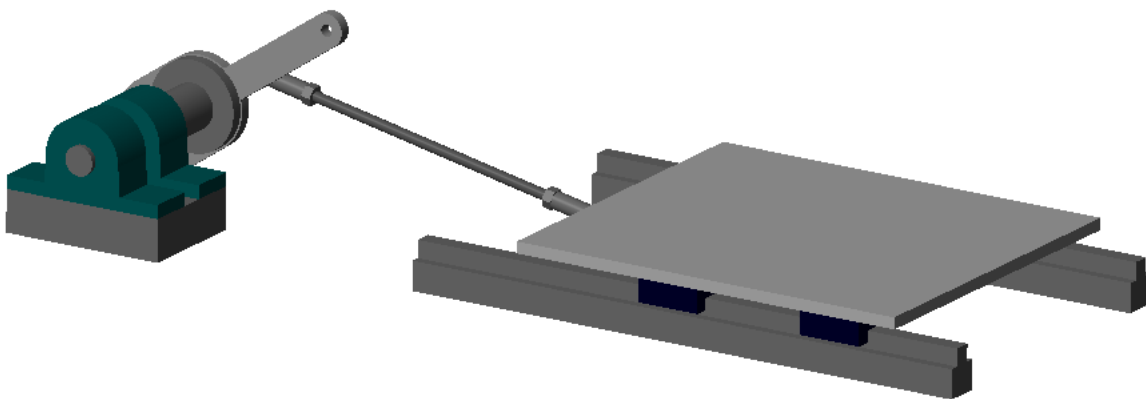


Figure 7.8: Horizontal slider-crankshaft mechanism

The ACSM1-04 can be operated locally from its control panel or externally via I/O connections; this was utilized for external velocity control by using a dSpace 1104.

The velocity control was executed together with the EKF algorithm and the PRBS generation in the dSpace module. The torque control was executed in the ACSM1-04. A diagram of the communication between the dSpace 1104 module and the drive control ACSM1-04 is depicted in Figure 7.9:

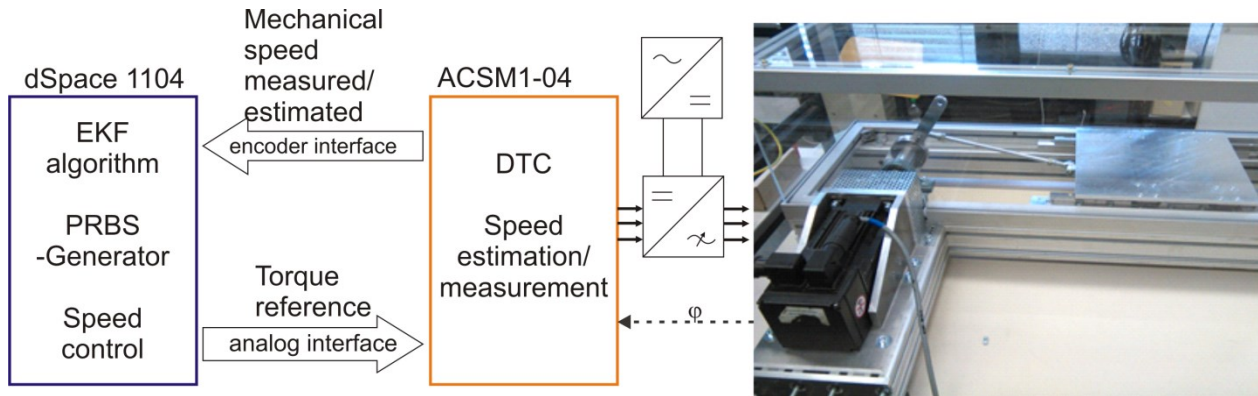


Figure 7.9: Experimental platform diagram

In a similar way as explained in [100] the kinetic energy analysis of the horizontal slider-crank mechanism was calculated by utilizing a dynamically equivalent model of mass particles as represented in Figure 7.10.

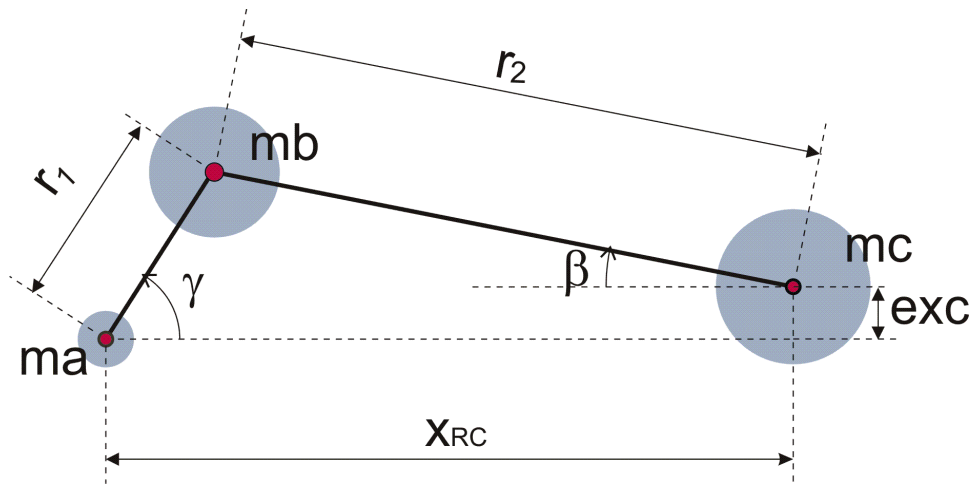


Figure 7.10: Dynamically equivalent mass model of the slider crank mechanism

The reduced moment of inertia is a function of the angular position of the crank:

$$J_{red}(\gamma) = J_{Motor} + m_b \cdot r_1^2 + m_c \cdot \left(\frac{dx(\gamma)}{d\gamma} \right)^2 \quad (7.1)$$

Equation (7.1) expressed in terms of the angular position results in the following equation:

$$J_{red}(\gamma) = J_{Motor} + mb \cdot r_1^2 + mc \cdot \left(r_1 \cdot \sin(\gamma) + \frac{r_1 \cdot \cos(\gamma) \cdot (e + r_1 \cdot \sin(\gamma))}{r_2 \cdot \sqrt{1 - \left(\frac{e + r_1 \cdot \sin(\gamma)}{r_2}\right)^2}} \right)^2 \quad (7.2)$$

The equation (7.2) was evaluated with the parameters given in the Appendix. This allows the graphical representation of the reduced moment of inertia shown in Figure 7.11.

By comparing the horizontal with the vertical configuration the equivalent moment of inertia of the whole mechanism was found to change in a similar way to the previous mechanism, with an apparent double frequency or the crank rotation, this is because in both cases the geometrical relation of the components is the same with respect to the crank.

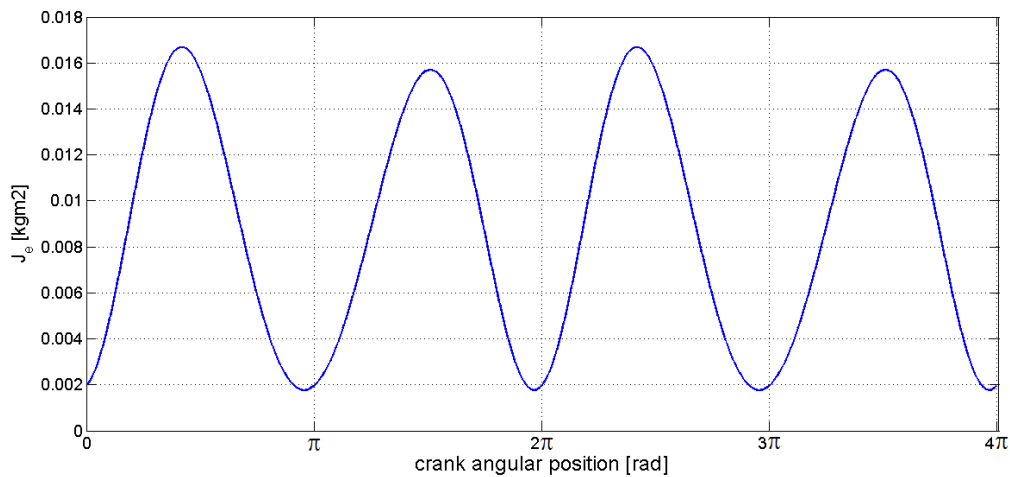


Figure 7.11: Equivalent moment of inertia of the crank-shaft as a function of the motor angular position

For the calculation of the theoretical load torque the procedure of the generalized force as utilized as described in [101] considering friction the only force that caused a significant effect as load. According to this, the load torque was found to be a function of the velocity, acceleration and mass of the slider and the angular position of the crank, where the friction generates the most significant load force.

7.1.2.2 Identification structure

The structure for the identification without encoder for the measurement of the shaft position is based on the one described in section 3.5. As mentioned in the description of the experimental platform II, the velocity and torque control were performed separately. The velocity control was executed within the program in the dSpace module. The EKF algorithm and the PRBS generation were executed in the dSpace board as well. The torque control and the motor velocity estimation were carried out within the ACSM1-04 drive control.

The encoderless control and identification scheme is described in the simplified diagram depicted in Figure 7.12.

Velocity estimation based on the model of the motor was utilized. For the velocity estimation it was used a technique that is commercially available within the control of several frequency converter brands.

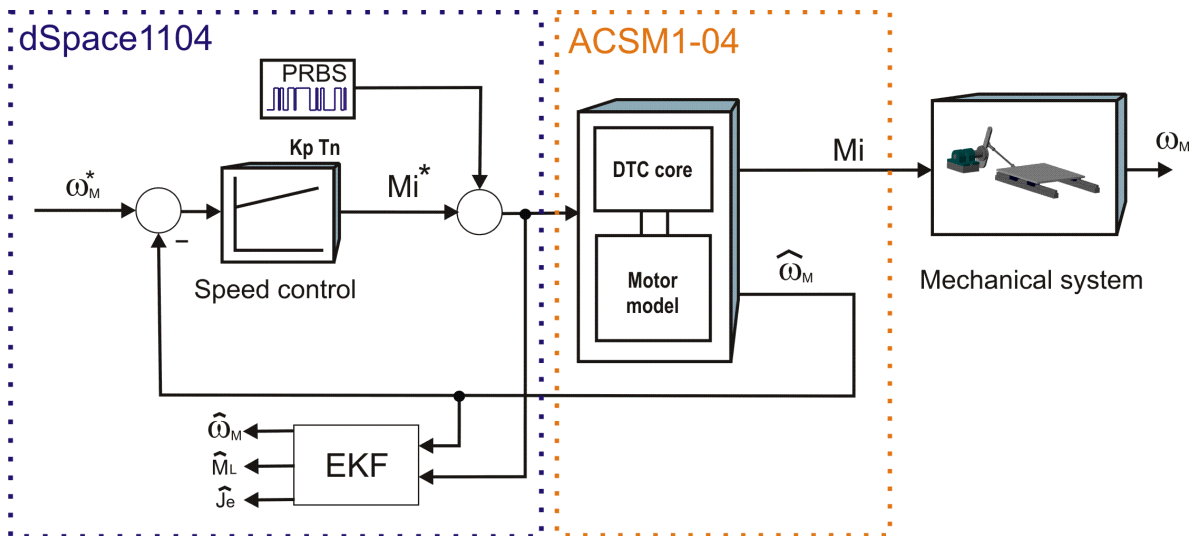


Figure 7.12: Simplified diagram of the velocity sensorless control and identification scheme

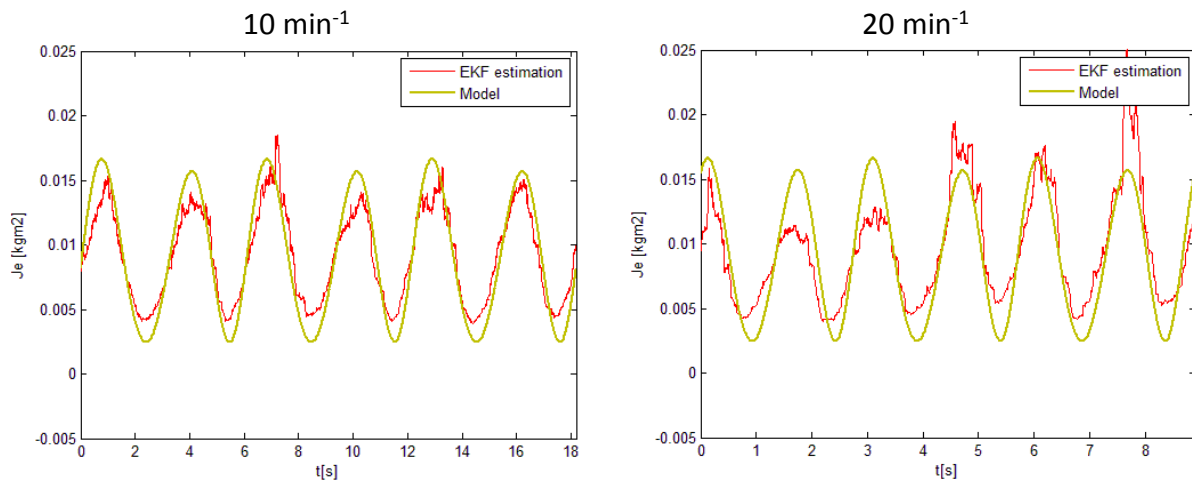
The ACSM1-04 is a motion drive controller from the company ABB that can be operated by utilizing the measurement of the encoder or the estimated velocity from the motor model as feedback to the control the frequency and phase of the output currents to the machine.

The module FEN-11 installed on the ACSM1 04 is an encoder interface which is capable of encoder emulation; a calculated position difference is transformed to a given number of TTL pulses to be sent through the TTL output. In this way the internal estimated velocity from ACSM1-04 can be then communicated to the encoder interface of the dSpace to be used as feedback to the control and input to the Extended Kalman Filter. The number of increments of the emulated TTL output can be chosen by setting the parameters in the ACSM1-04, for the experiment it was defined to emulate for 2^{12} increments per revolution of the motor shaft.

7.1.2.3 Influence of additional excitation and of the mechanical velocity

The procedure for the encoderless identification is similar to the one described in [100] , with the difference that a lower amplitude of the PRBS was required i.e. only 0.2 pu. Experimental test were carried out at different mechanical velocity of the motor, from 10 min^{-1} to 100 min^{-1} . The results obtained confirmed that better results are obtained at the lower velocity range.

The results of the identification of the reduced moment of inertia for different motor velocities are depicted in the following graphics and compared with the calculated results based on the model:



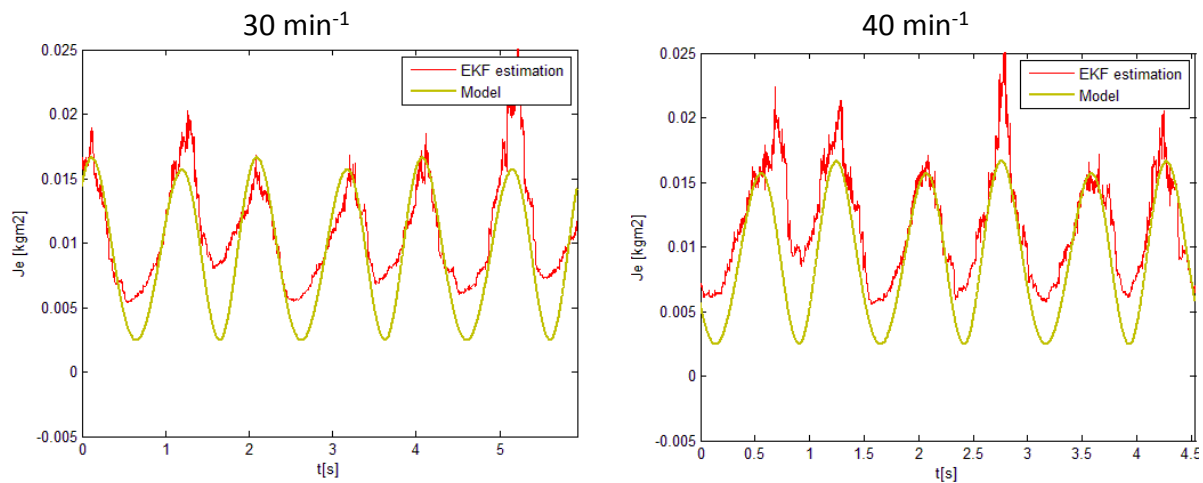


Figure 7.13: Experimental identification of the moment of inertia at different motor velocities under velocity sensorless control

7.1.2.4 Influence of the variation of the mass in the slider-crankshaft mechanism

The sensitivity of the identification of the reduced moment of inertia by using an EKF to the mass in the slider of the mechanism was also experimentally evaluated. For this purpose, defined masses were added to the slider of the mechanism. The test were carried out with defined masses of: 0.5 kg, 1 kg, 1.5 kg, 2 kg, 3 kg, 5 kg and 8 kg. For all the test the motor velocity was set to 10 min^{-1} .

The experimental results of the identification of the reduced moment of inertia of the slider-crankshaft are presented in Figure 7.14. It can be noticed that even though the velocity was the same for all the trials and only the mass changes, the EKF yields better results for the lighters slider mass when the mass changes.

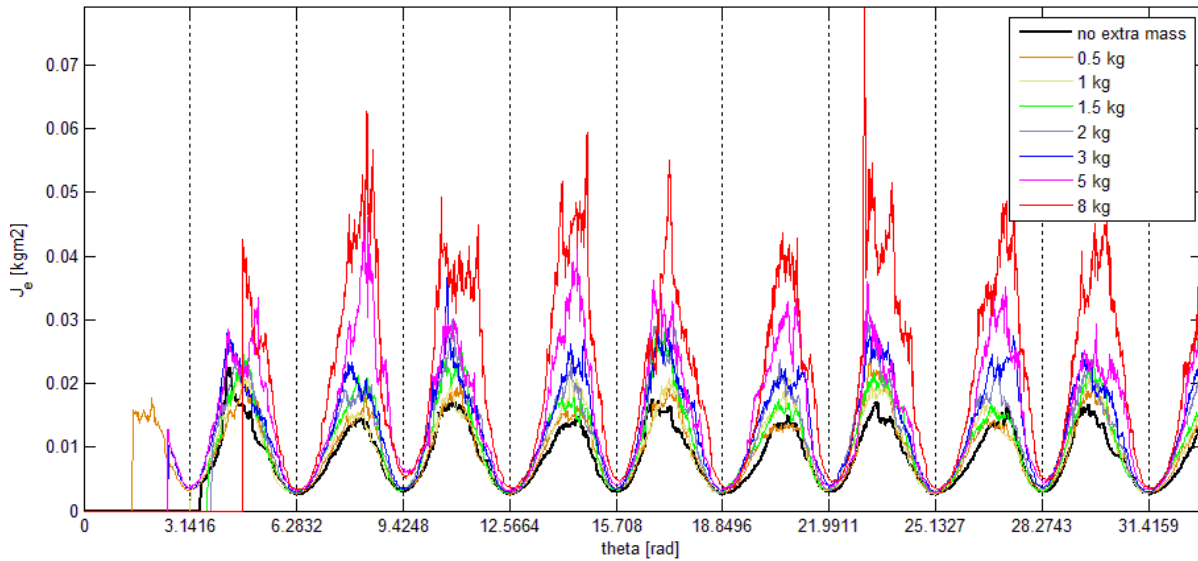


Figure 7.14: Estimation of the reduced moment of inertia at 10 min^{-1} by adding mass to the slider plate.

The additional mass increase the actual amplitude of the reduced moment of inertia and this represent a faster change in time, as well as with respect to the angular position. The variation of the slider mass affects the EKF estimation in a similar way like the variation of the motor velocity, in the sense that it represents a higher rate of change when it is increased. The model utilized in the EKF considers the reduced moment of inertia to be constant, therefore the results of the EKF estimation with higher rates of change in the reduced moment of inertia results are less accurate than those obtained when the changes of the reduced moment of inertia are slower.

7.2 Identification of the torque by means of a deterministic procedure

The deterministic identification method described in section 4 was also experimentally tested. The reference value of the motor torque can be approximated with Fourier series. By applying the defined working conditions described in section 4.3, the harmonics related to the varying reduced moment of inertia of the mechanism are indirectly identified by the coefficients of the Fourier series approximation.

Initially, the deterministic identification was carried out utilizing the measured velocity from an encoder. The identification structure utilized in this initial part of the experimentation was depicted in section 4.6.

The second part of the experimental test of the deterministic identification was achieved with a speed-sensorless control structure. In this test, the mechanical velocity was estimated without the use of an encoder.

All the experiments correspondent to the deterministic identification with Fourier series were performed on the experimental platform II that was described in section 7.1.2.1.

7.2.1 Deterministic identification using the measured mechanical velocity

The deterministic identification of the driving torque with Fourier series was experimentally tested at different velocities in order to find out the effect of the mechanical velocity on the Fourier coefficients that describe the torque. The test were carried out at motor velocities of 10 min^{-1} , 20 min^{-1} , 30 min^{-1} , 40 min^{-1} , 50 min^{-1} , 60 min^{-1} , 70 min^{-1} , 80 min^{-1} , 90 min^{-1} , and 100 min^{-1} .

As it was explained in section 4.5, the Fourier coefficients were calculated with a sliding window for the integration with respect to the angular position. The program developed for the Fourier coefficient calculations was executed during the operation, so the output was calculated in real time. The sliding window algorithm moves forward and yields new values after the crank has moved one defined increment of the angular position $\Delta\gamma$. Therefore, the calculated coefficient values deliver a correct value only after the mechanism completed one cycle of movement. Nevertheless, after the values had converged, there were small variations due to numerical round-off effect but also because of the nature of friction. Therefore after convergence of the calculation, the mean value of each Fourier coefficient over two periods of motion is considered to be the result of the deterministic identification.

The computed coefficients for different velocities are presented in Figure 7.15.

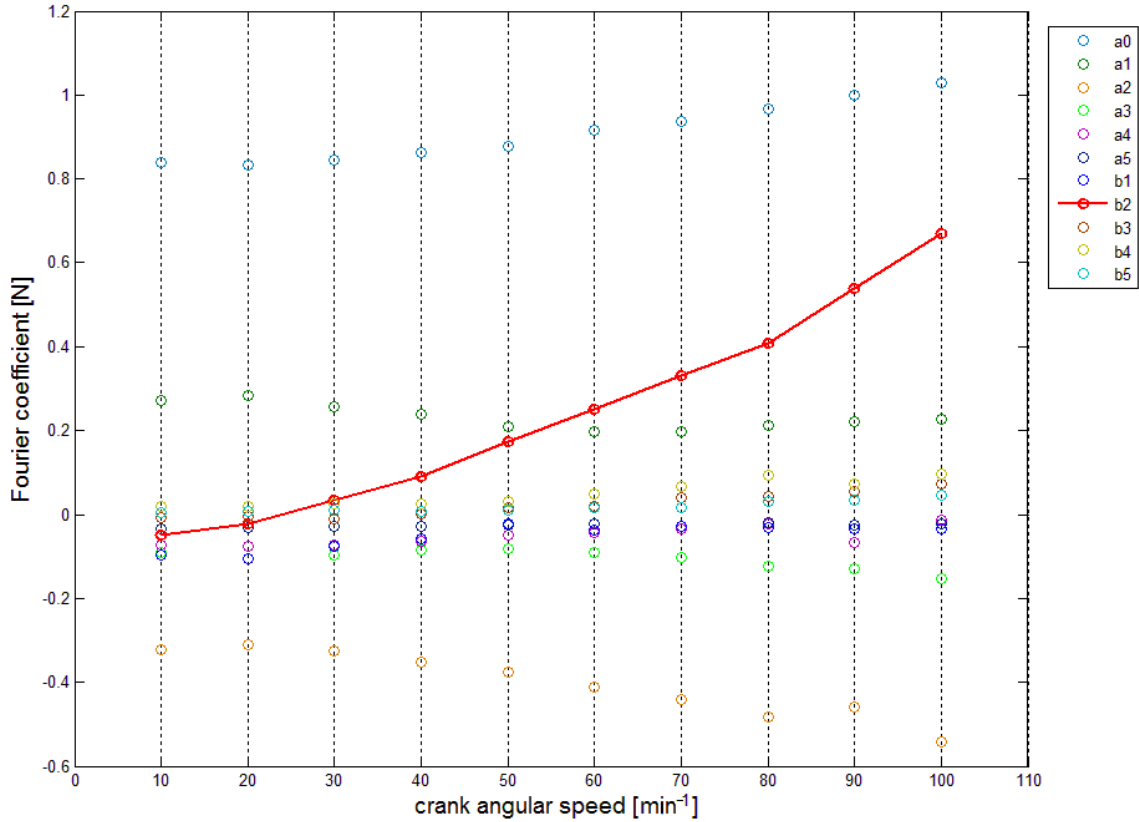


Figure 7.15: Fourier coefficients at several crank velocity of rotation

As it can be seen from Figure 7.15 the coefficient that presents a higher proportional relation to the rotational velocity is \mathbf{b}_2 . This was expected due to the rate of change of the reduced moment of inertia. Based on this obtained results and on the conditions defined on section 4.3, the torque reference signal can be characterized for a large range of angular velocities.

The proposed characterization is a function of the angular velocity and angular position of the crank, where the zero position corresponds to the same used for the calculation of the reduced moment of inertia i.e. the crank is in a horizontal position with the extended connecting rod. The angular position zero is depicted in Figure 7.16.



Figure 7.16: Crank in position $\gamma = 0^\circ$

The torque model is then defined by using this defined zero position. The model precision depends on the calculated Fourier coefficients and its accuracy is related to the accuracy of angular measurement, therefore it is important that the measured zero position actually match the position when the crank is placed horizontally.

After the characterization of the driving torque reference, the performance of the obtained model was compared to the actual driving torque reference for the whole velocity range from 10 min^{-1} to 100 min^{-1} . The results of this comparison at different velocities within this range are depicted in Figure 7.17 and Figure 7.18.

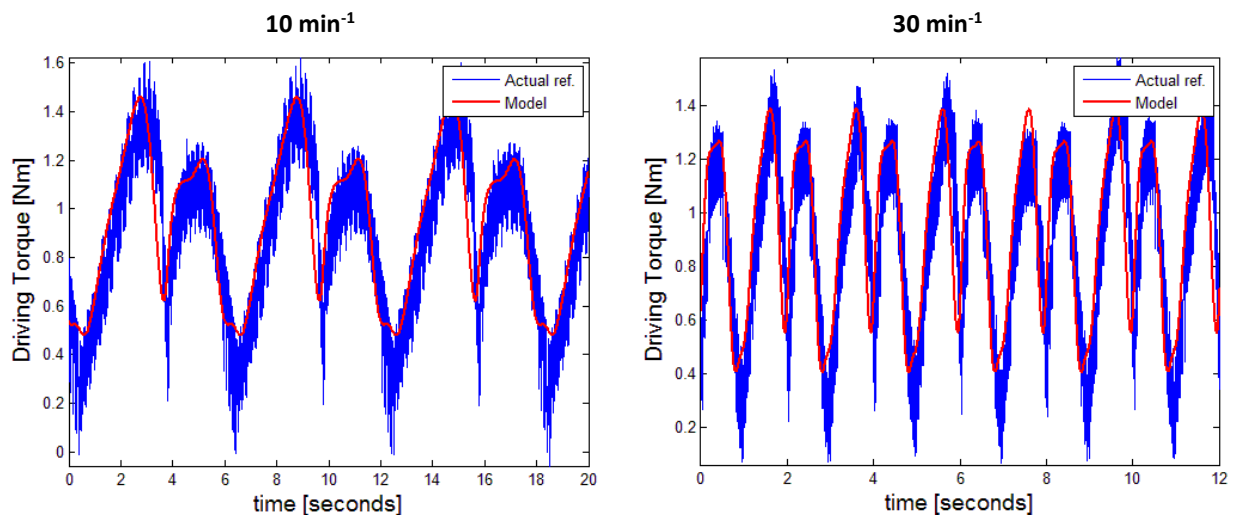


Figure 7.17: Model output compared to the driving torque reference at 10 min^{-1} and 30 min^{-1}

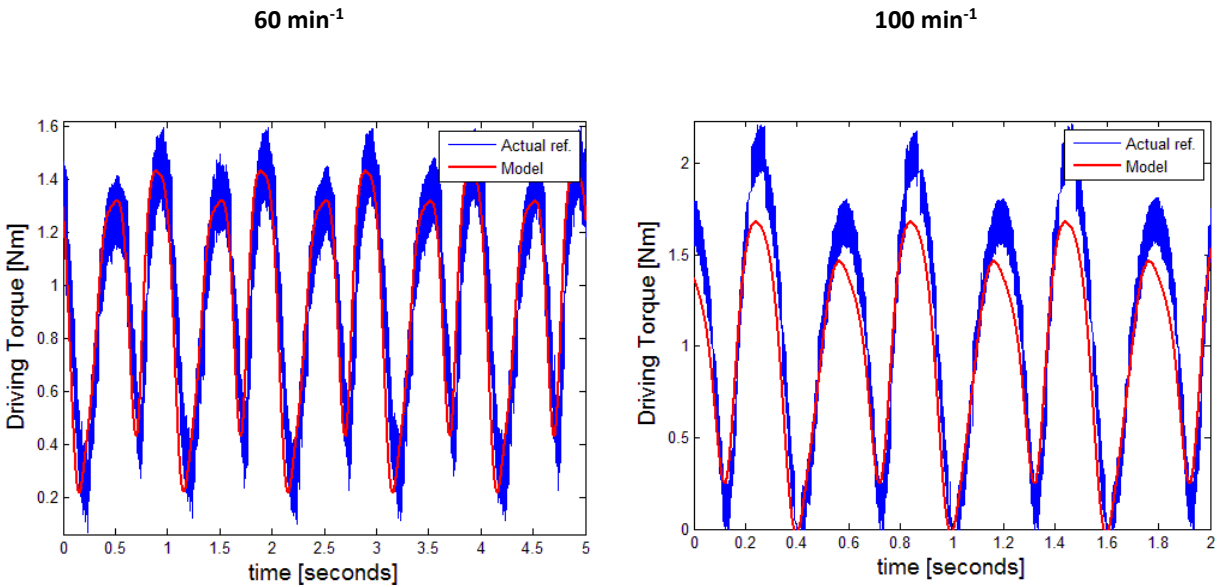


Figure 7.18: Model output compared to the driving torque reference at 60 min^{-1} and 100 min^{-1}

The results obtained with the identified model corresponds very well with the actual values obtained from the drive control, but it can be noticed that in the higher velocity range it starts to diverge. This is because the parameter \mathbf{b}_2 is interpolated for velocities within the range, but there are other harmonic components related to the mechanical velocity that are not included in the model and become more significant when the test approaches to the limits of the velocity range.

7.2.2 Deterministic identification in a system without encoder

The deterministic identification technique based on the Fourier approximation of the driving torque was also evaluated by using a drive with a speed-sensorless control scheme. As previously mentioned, an estimation of the mechanical velocity of the motor obtained from the drive control was utilized. The encoder module FEM-11 of the ACSM1-04 can deliver an emulated TTL signal

based on the internally estimated velocity. This signal was transmitted to the dSpace 1104 module through the TTL encoder interface.

The velocity control, and the deterministic identification algorithm were executed within the dSpace 1104 module. The reference torque value was transmitted to the ACSM1-04 through the same analog interphase as in the case of the test done with encoder feedback. The diagram of control and identification is depicted in Figure 7.19.

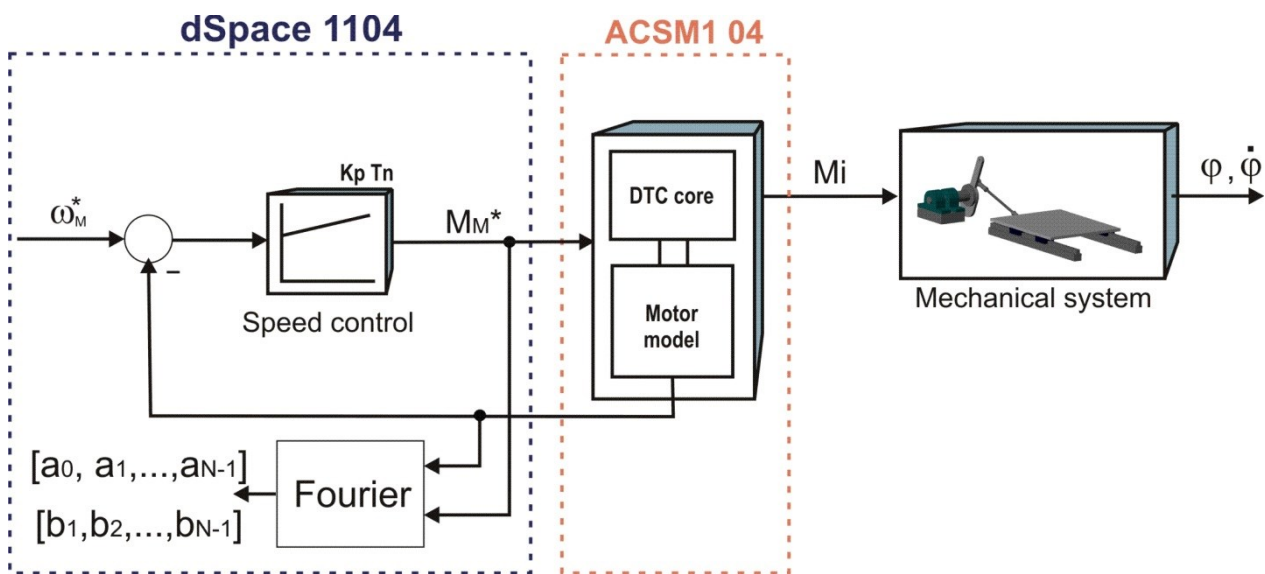


Figure 7.19: Velocity Control and Fourier sensorless identification diagram structure

Working under this sensorless control scheme, the online identification procedure was performed for the same velocity range with motor velocities of 10 min^{-1} , 20 min^{-1} , 30 min^{-1} , 40 min^{-1} , 50 min^{-1} , 60 min^{-1} , 70 min^{-1} , 80 min^{-1} , 90 min^{-1} and 100 min^{-1} . The calculated coefficients for these velocities are presented in Figure 7.20. The results nearly coincide with those obtained by using velocity and position feedback from the encoder because the coefficient b_2 presented a significant proportional relation with the angular velocity. As explained in section 4.3 the effect of the variable reduced moment of inertia is expected to be represented in term b_2 . The term a_0 presents also a proportional relation with the velocity in the experimentation without encoder which is the constant component of the driving torque.

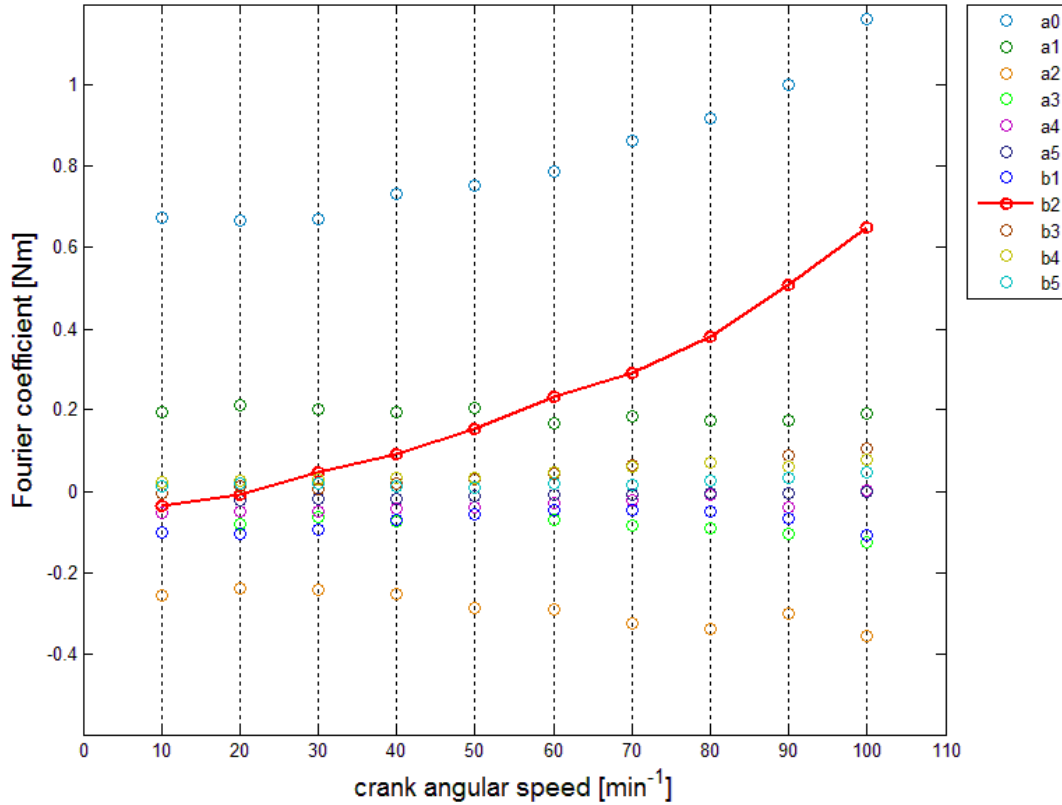


Figure 7.20: Fourier coefficients at several crank velocity of rotation under a sensorless control scheme

7.3 Feed-forward compensation

The feed-forward compensation with PI velocity control as explained in section 5 was also experimentally tested. The model utilized to compute the signal to be added to the output of the velocity as feed-forward control is based on the deterministic identification with the Fourier series. In section 5.2 it is explained how the output of the speed control contains information about the load torque and the variable inertia effects.

The results of the Fourier characterization of the driving torque reference were used for the calculation of the model as it is explained in section 7.2.1.

The structure that combines feed-forward compensation with the classical PI velocity control was explained in section 5.1. This structure was initially tested utilizing the encoder feedback as input

to the model and to the velocity control. In a further step, an estimate of the mechanical velocity of the motor was utilized to evaluate this structure of velocity control.

The experimental evaluation of this control scheme was focused on the velocity response of the system. The tests addressed 3 instances of experimentation:

- Velocity response in steady state
- Velocity response to a step function as reference
- Velocity response to a ramp function as reference

As the model utilized for the feed-forward compensation is valid only within certain velocity range, the tests were carried out with motor velocity from 10 min^{-1} up to 100 min^{-1} .

7.3.1 Feed-forward compensation with encoder feedback

The identified driving torque can be added at the output of the PI velocity control to reduce the control effort. By doing this, a feed-forward compensation of the torque fluctuation can be achieved. The advantage is that the motor velocity can be better controlled and the response in the motor velocity can better follow its reference value because disturbances due to the mechanism are compensated.

The velocity response in steady state is depicted in the graphics of Figure 7.21. The proper nature of the slider-crankshaft movement create oscillations because of the change of motion direction in the slider. Therefore, the motor velocity cannot be kept constant even if the velocity reference to the control is a constant signal. However, if feed-forward compensation together with classical PI control is utilized the motor velocity can track the reference signal more precisely.

Figure 7.21 shows a comparison between the system response with and without feed-forward compensation. The velocity reference is depicted as well.

The test were executed within the range of 10 min^{-1} up to 100 min^{-1} . The amplitude of the oscillations is larger for higher motor velocities because the acceleration change of the slider at the stroke end is larger in those cases.

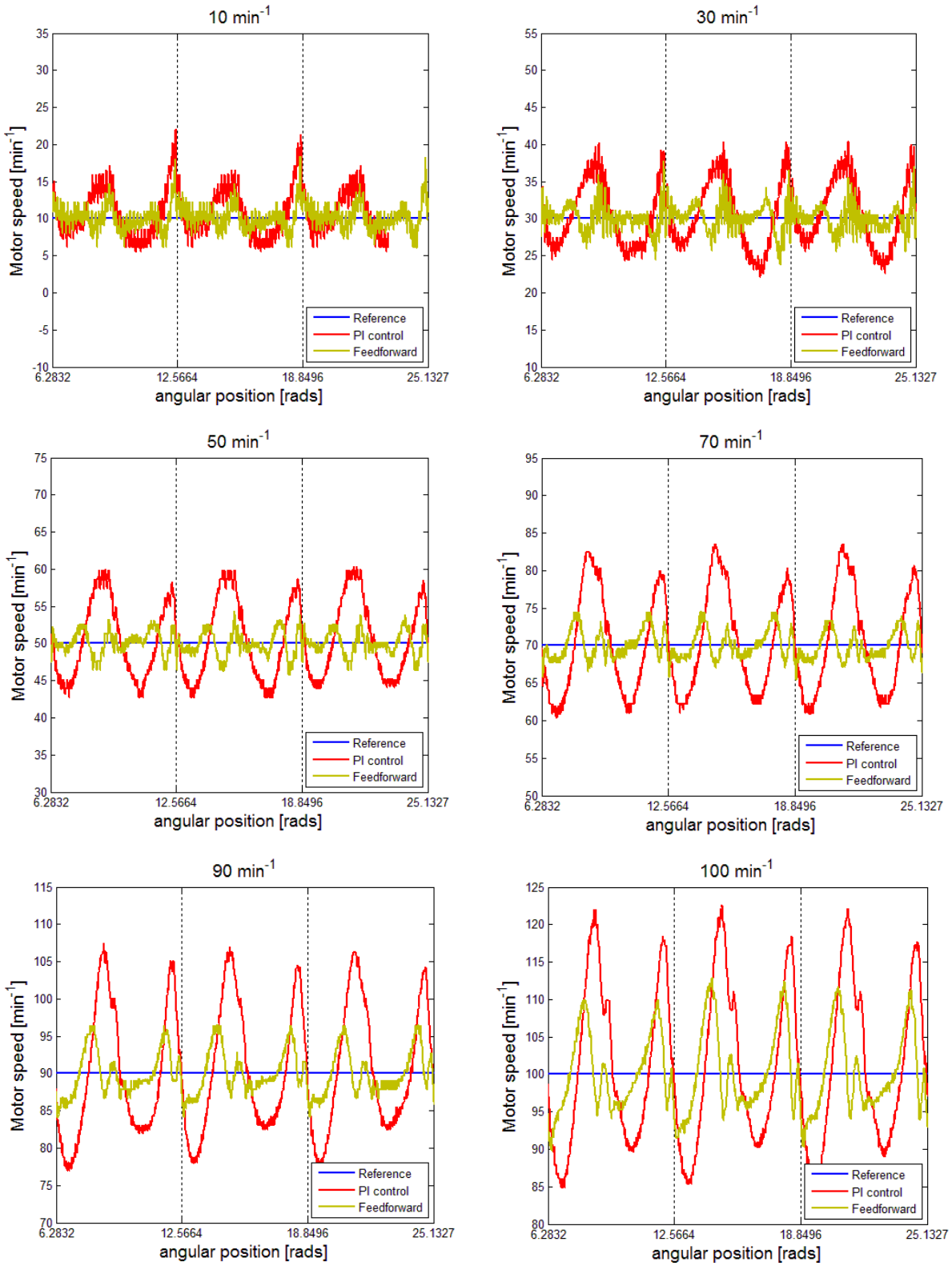
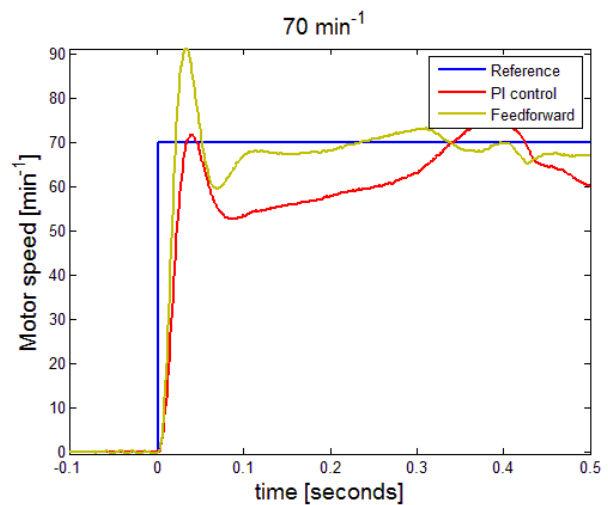
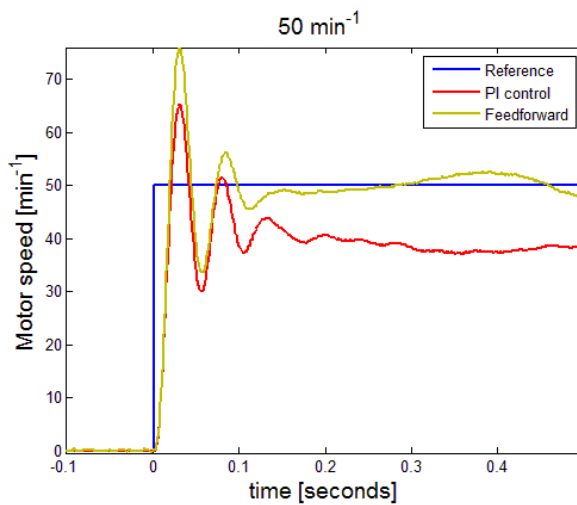
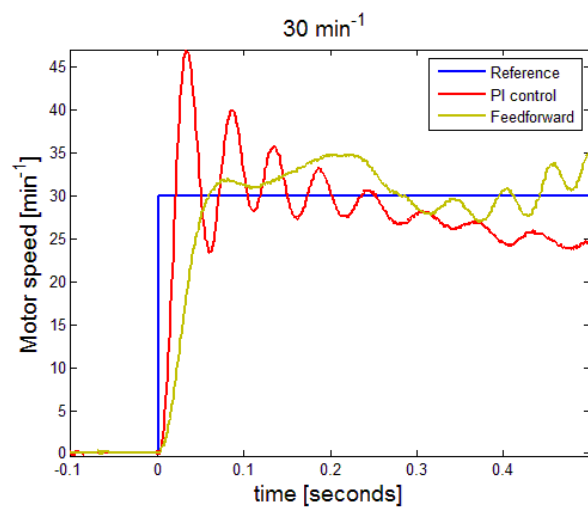
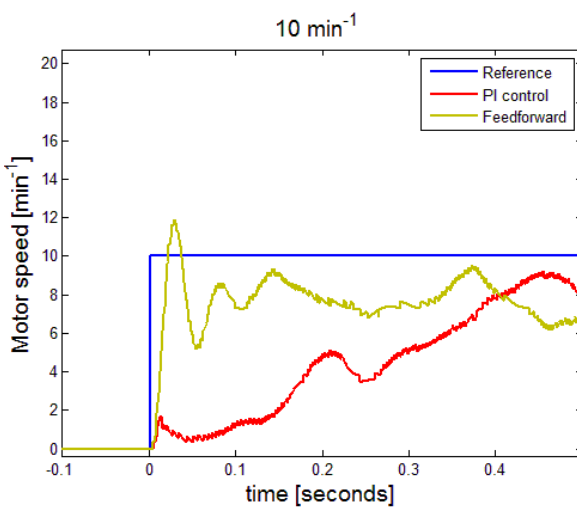


Figure 7.21: Motor velocity comparison with and without feed-forward compensation at steady state

It can be noticed, that the oscillations are reduced when feed-forward compensation is applied, which represent an improvement of the system response when compared with that obtained with single PI velocity control.

The step response is also faster with feed-forward compensation. The settling time reduces as it shown in the graphics below. Measurements were taken utilizing several velocity steps, from 0 to 10 min^{-1} and steps up to 100 min^{-1} .



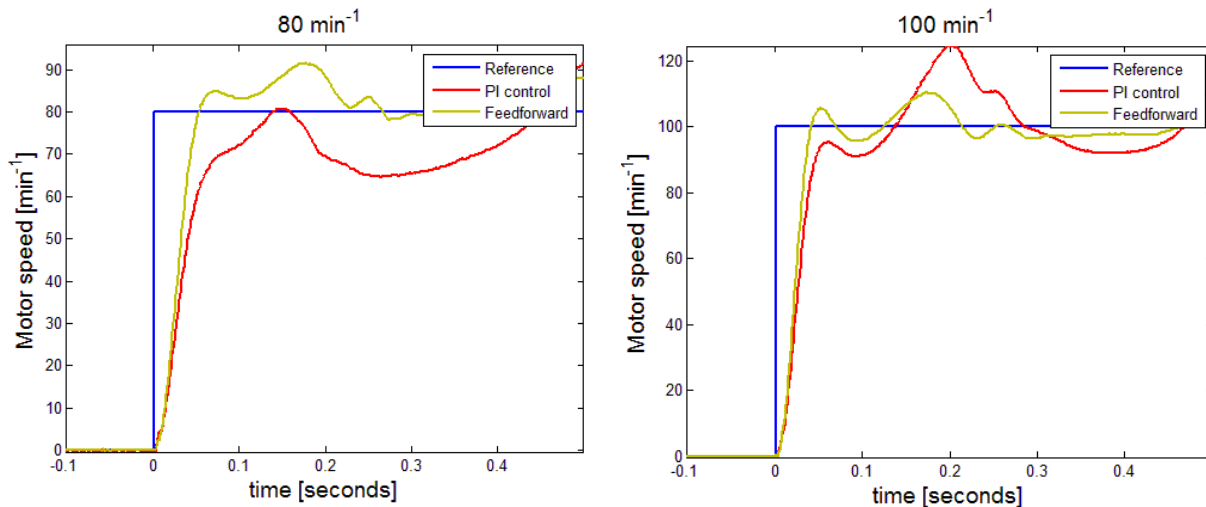


Figure 7.22: Step response comparison with and without feed-forward compensation

In motion control applications, a high dynamical response is usually desired. From the graphical comparison it can be noticed that a shorter settling time is achieved when feed-forward is used to save effort of the PI velocity control, especially at the lower speed range. The initial position of the mechanism has also an influence on the settling time of the step response of the system therefore all the measurements were taken with the mechanism starting at the position zero of the crank.

Finally, the system response with feed-forward control was tested with a ramp function as reference signal for the velocity. The experimental test were carried out with different acceleration times from 0.01 s up to 3 s. The mechanism was started for this test at the position zero of the crank, like in the previous experiments.

The following graphics depict a comparison of the system response to the ramp function when feed-forward control is used and with single PI velocity feedback control. The dynamic of the velocity response improves with the feed-forward compensation allowing the system to track the velocity reference more precisely.

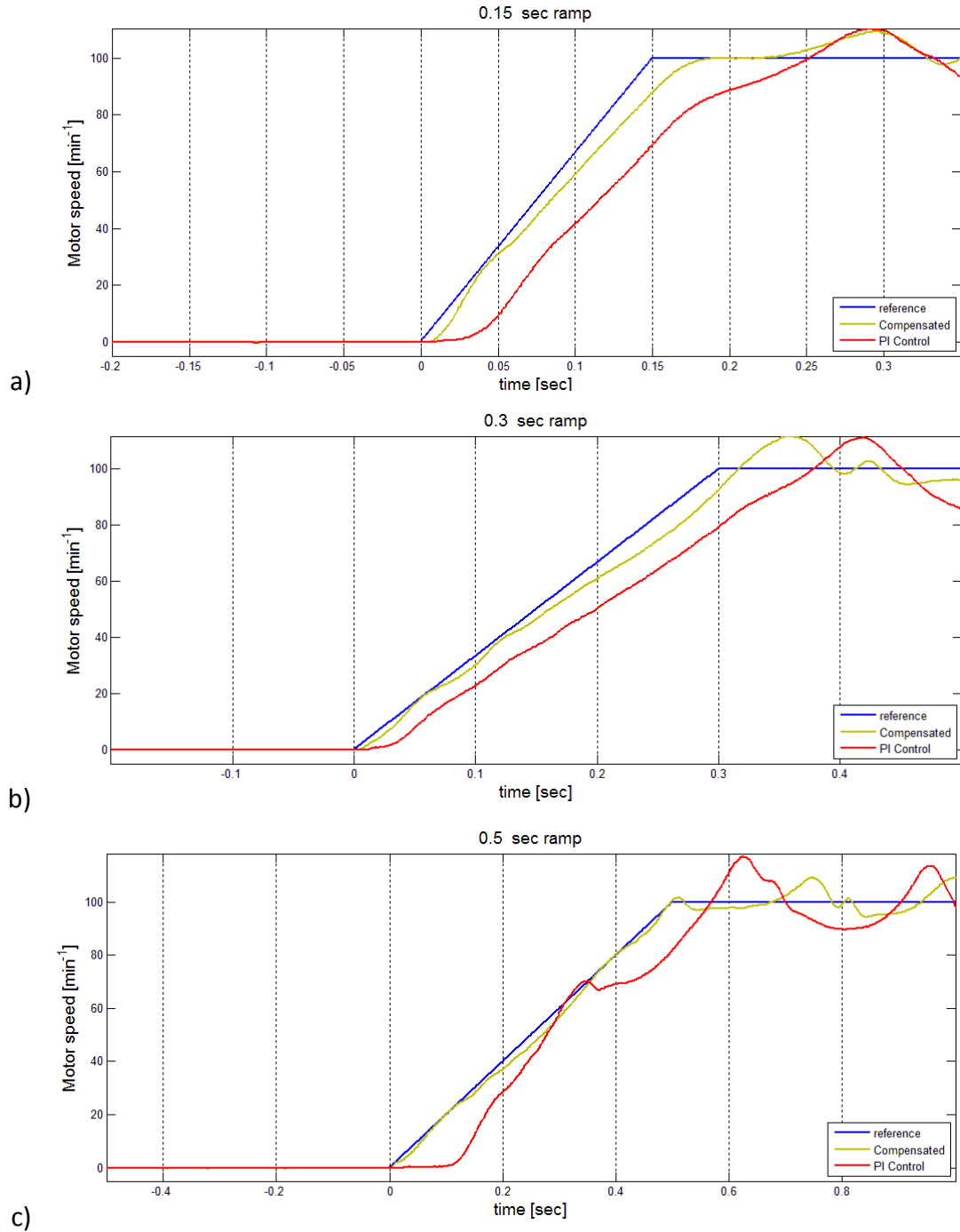


Figure 7.23: Model output compared to the drive torque reference with and without feed-forward compensation a) 0.15 s b) 0.30 s c) 0.50 s ramp

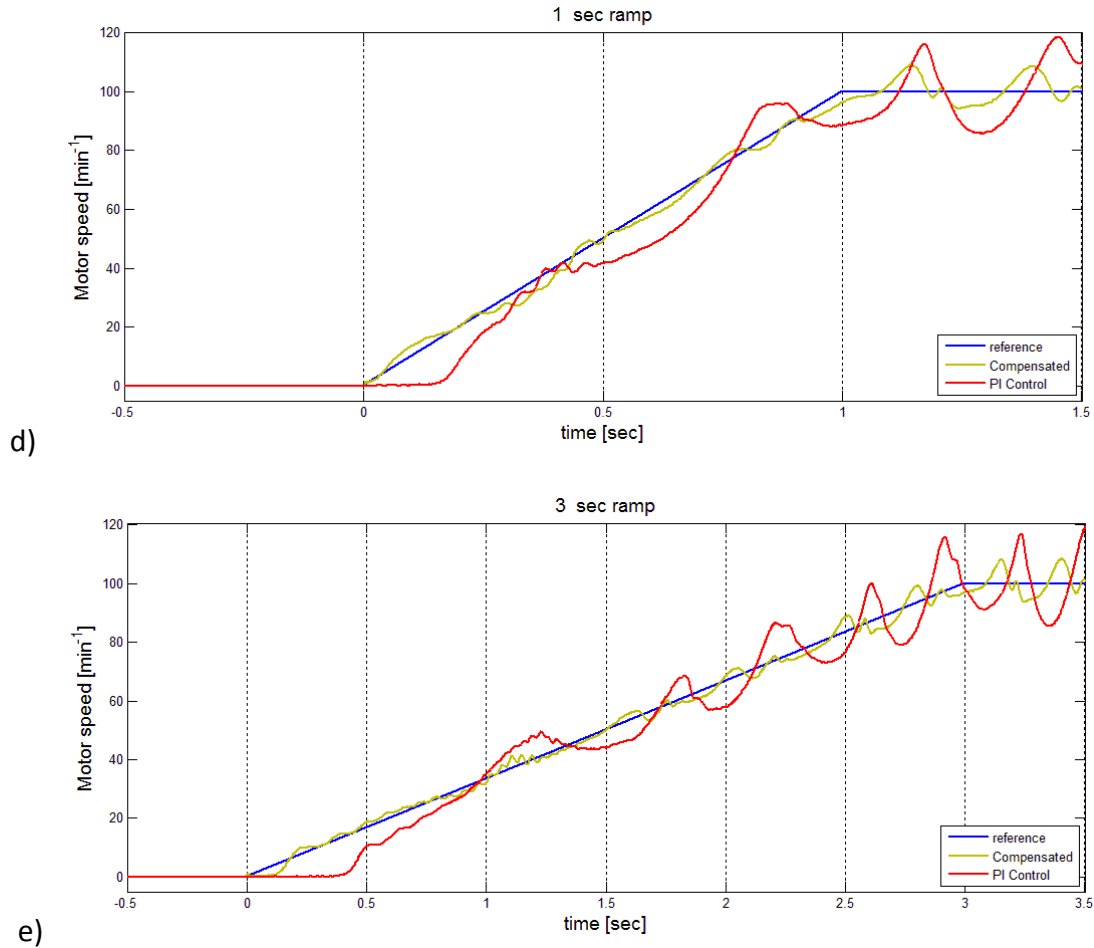


Figure 7.23: Model output compared to the drive torque reference with and without feed-forward compensation d) 1 s e) 3 s ramp

7.3.2 Feed-forward compensation in encoderless control scheme

In the same velocity range, from 10 min^{-1} to 100 min^{-1} several tests were performed by utilizing feed-forward compensation and motor-drive with a speed-sensorless control scheme. The velocity of the motor is estimated by the motor drive that uses a model of the machine and a direct torque control (DTC in the ABB-ACSM1-04-Drive).

Figure 7.24 shows a comparison between the estimated motor velocity when utilizing feed-forward compensation and a conventional PI velocity control without a compensation.

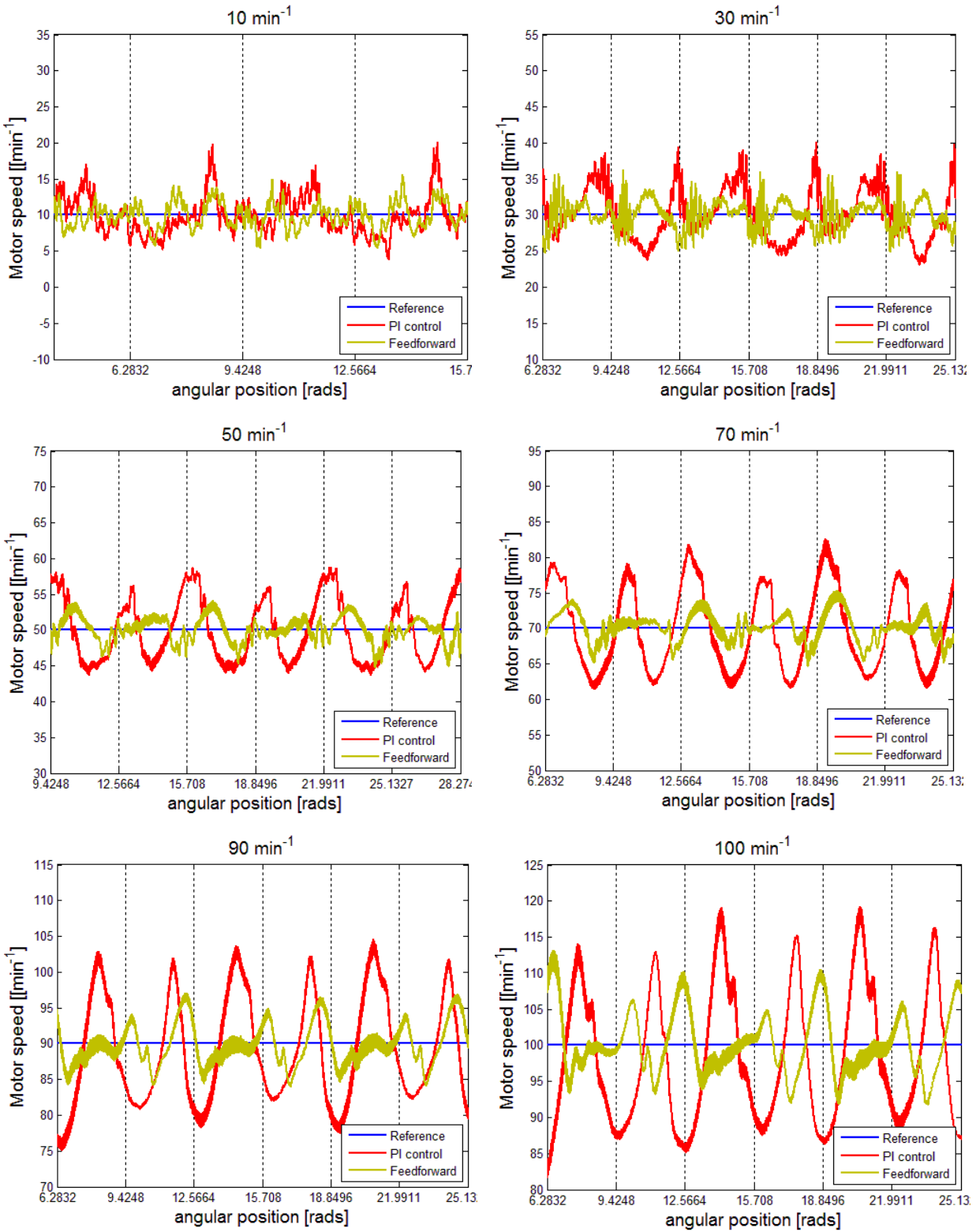


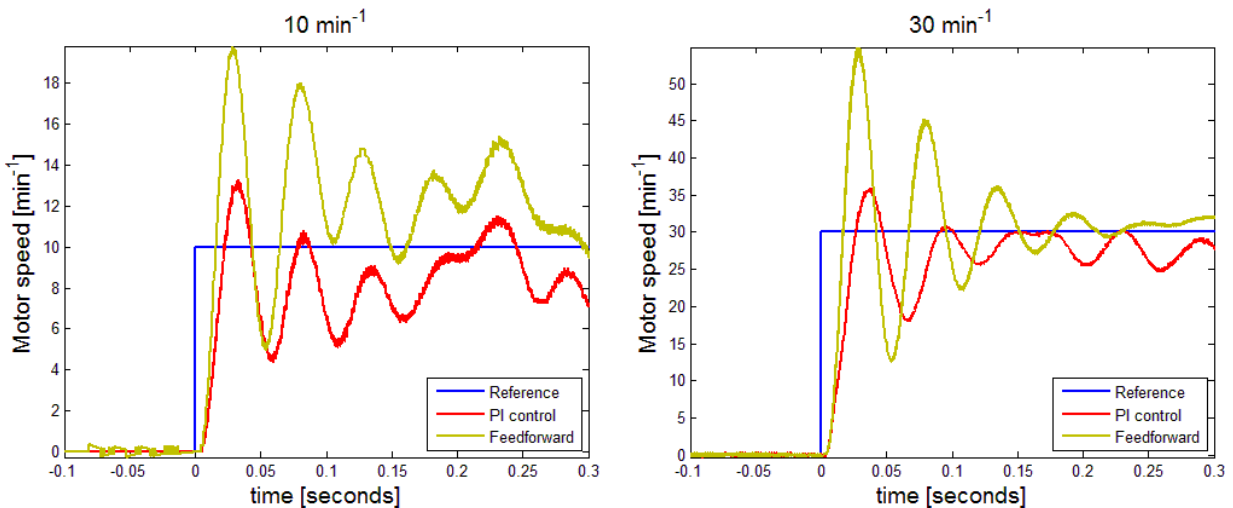
Figure 7.24: Motor velocity comparison with and without feed-forward compensation at steady state

The system response is improved even when the compensation algorithm and identification are based on the estimated values of the velocity and of the position of the motor instead of the measured ones. As it can be seen in the present results, the oscillation of the motor velocity in steady state is reduced.

The system step response with feed-forward compensation under sensorless control schemes was tested as well. The response of the system was tested with different step signals as reference to the velocity control. The steps utilized were from 10 min^{-1} up to 100 min^{-1} . The system response with feed-forward compensation together with PI control is depicted in the graphics of Figure 7.25. These are compared with the responses obtained with single PI velocity control under the same conditions.

Although at some velocities the settling time reduces with feed-forward compensation at most of the tests, the settling time remain the same with feed-forward compensation.

The improvement of the velocity step response with feed-forward compensation is just perceptible at the low velocity range up to 50 min^{-1} . This could be due to the signal injection that was utilized for the speed-sensorless DTC control stabilization in the ACSM1-04.



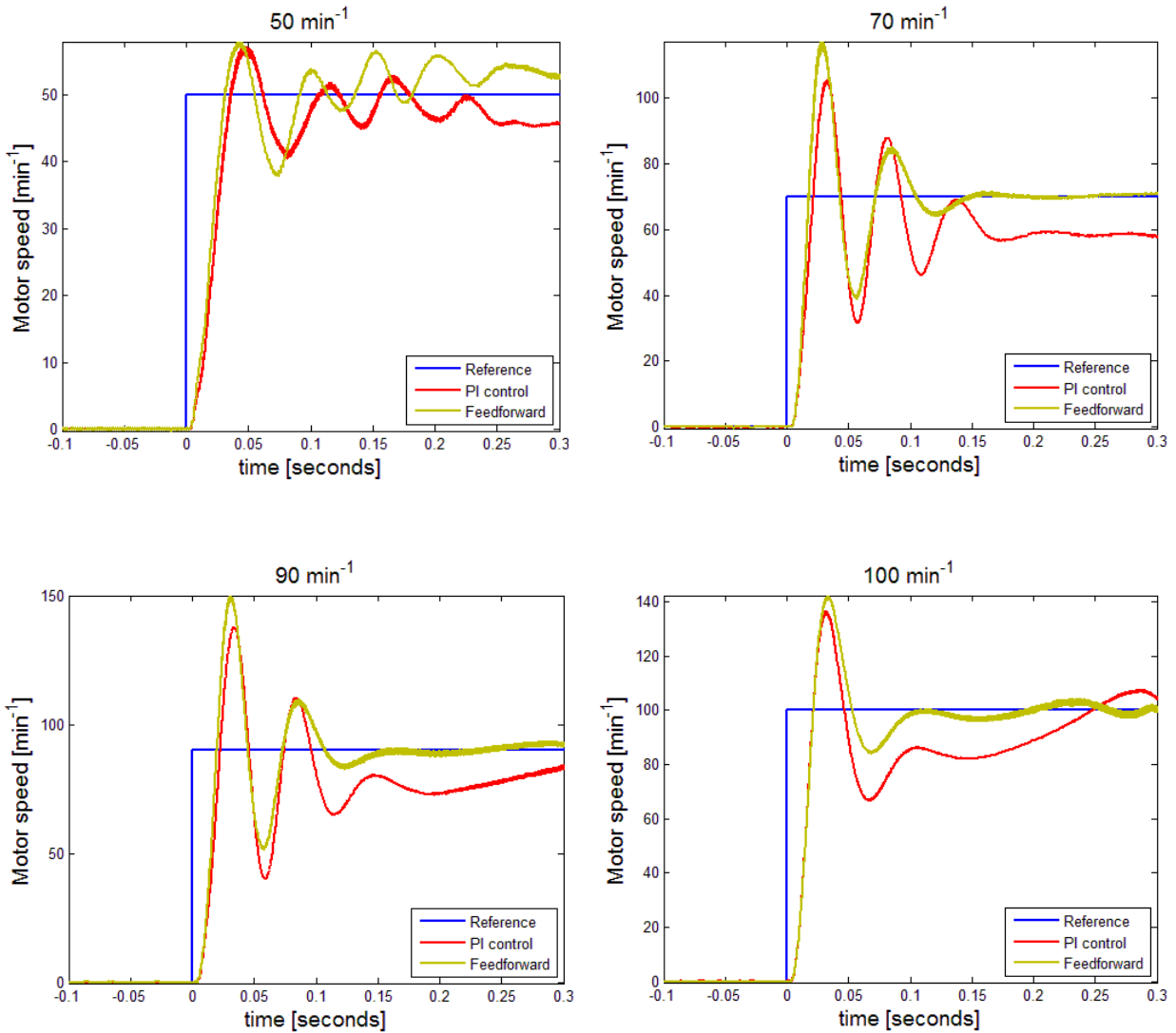


Figure 7.25: Step response comparison with and without feed-forward compensation

The last part of the experimentation of this control, correspond to the ramp response. The ramp signals utilized as velocity reference had acceleration times of 0.01 s, 0.15 s, 0.3 s, 0.5 s, 1 s and 3s.

The test results are shown in Figure 7.26. The ramp response of the system improves when feed-forward compensation is utilized also under sensorless control schemes.

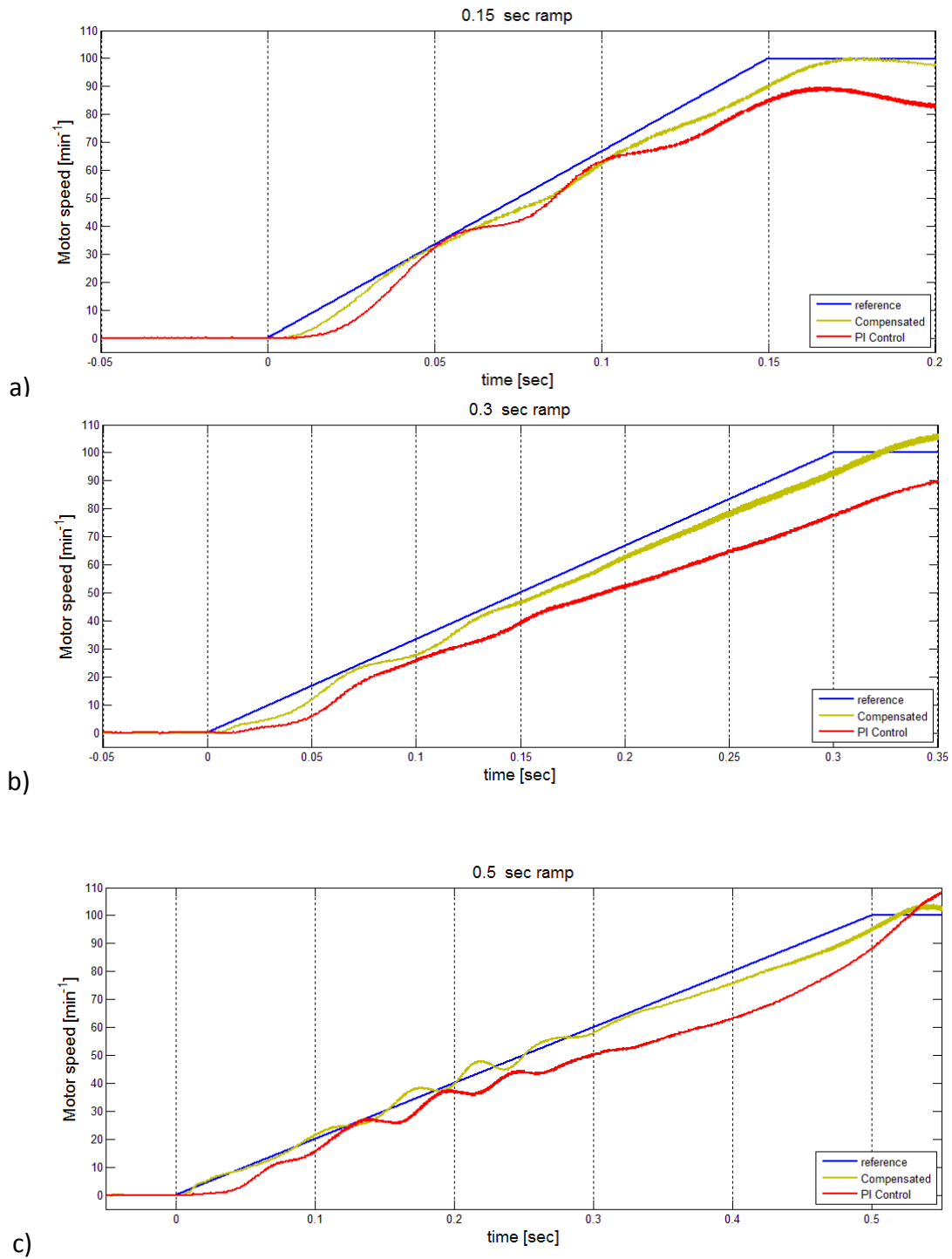


Figure 7.26: Velocity ramp response comparison with and without feed-forward compensation a)0.15 s
b)0.30 s c)0.50 s ramp

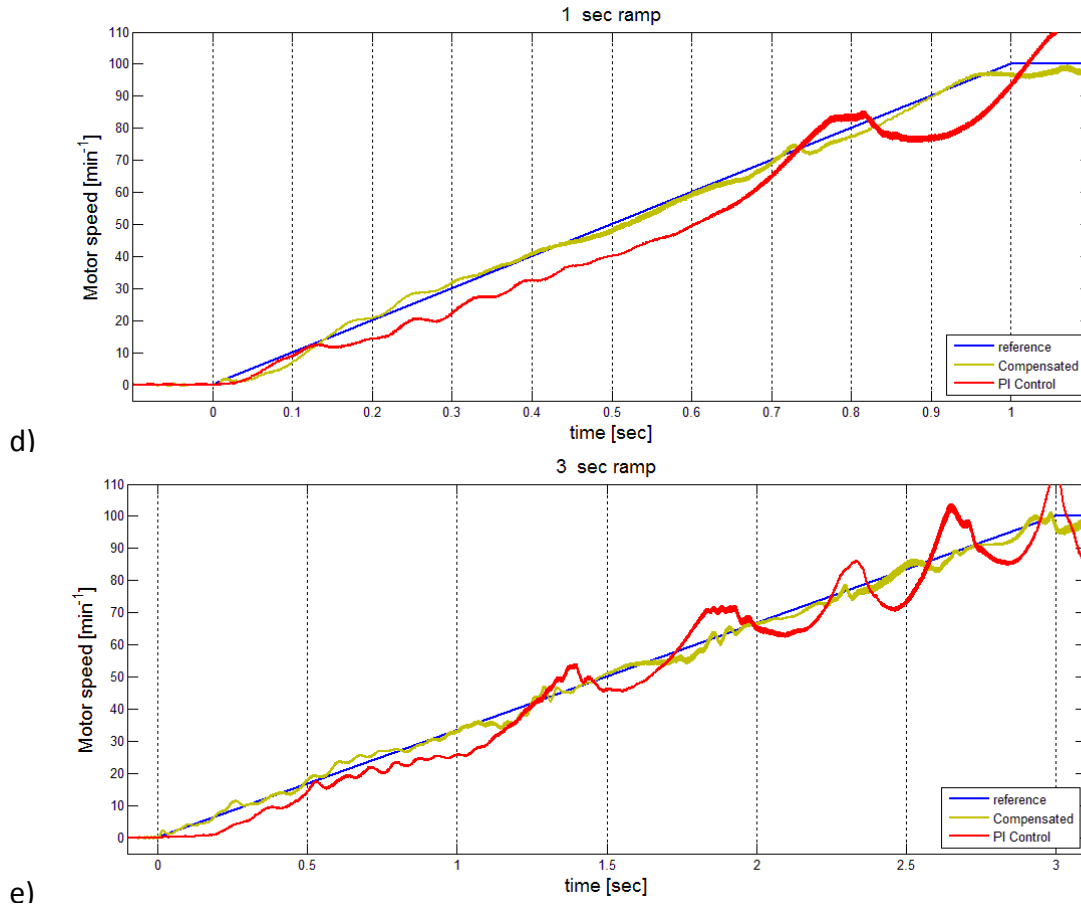


Figure 7.26: Velocity ramp response comparison with and without feed-forward compensation d) 1s e) 3s ramp

The velocity ramp reference is better tracked by the motor velocity also with feed-forward compensation and PI control even when the estimated motor velocity is used instead of encoder measurements. The feed-forward model successfully compensates the oscillations produced by the non-linear load at the slide i.e. friction and the variable reduced moment of inertia of the mechanism.

7.4 Diagnostics

The last part of the experimentation corresponds to the diagnostics of faults in rolling bearings located between the motor and the mechanism that performs a periodical motion such as the

slider-crankshaft. The detection of bearing faults was focused on the classification described in section 6.2:

- Generalized rough
- Single point faults

For the experimental diagnosis, the motor torque reference signal was monitored as explained in section 6.5.

When single point faults are not severe, they can produce a similar effect in the motor torque reference as generalized rough produce. Therefore the effect of severe single point failures was separately experimented. The tests were carried out in the experimental platform II as described in section 7.1.2.1.

7.4.1 Single point bearing damage

In order to simulate the damage, a piece of metal was cut from the external ring of a ball bearing located between the motor shaft and the mechanism. The location of the damaged bearing is depicted in Figure 7.27.

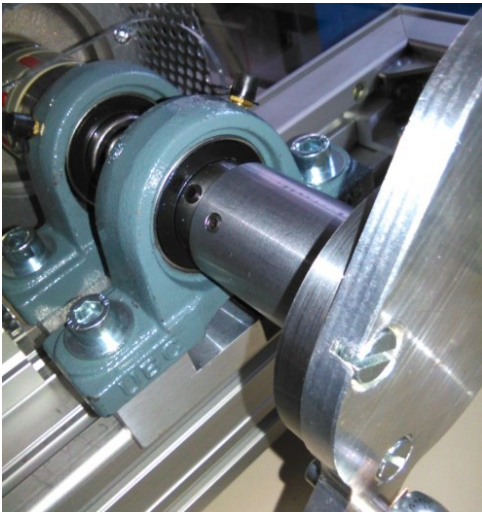


Figure 7.27: Location of the damaged bearing



Figure 7.28: Fault at the damaged bearing

The fault was located facing the lower hollow part of the pillow bearing where the higher static load is exerted on the bearing. The single point fault, as shown in Figure 7.28, was tested for

diagnosis by monitoring the motor torque reference with motor velocities between 10 min^{-1} and 100 min^{-1} .

First, the motor torque reference was recorded with a healthy bearing. Then the healthy bearing was substituted with the damaged bearing and the motor torque was recorded again. By comparing both the measurements the fault could be detected. The measurements taken with healthy and damaged bearings are compared in the Figure 7.29.

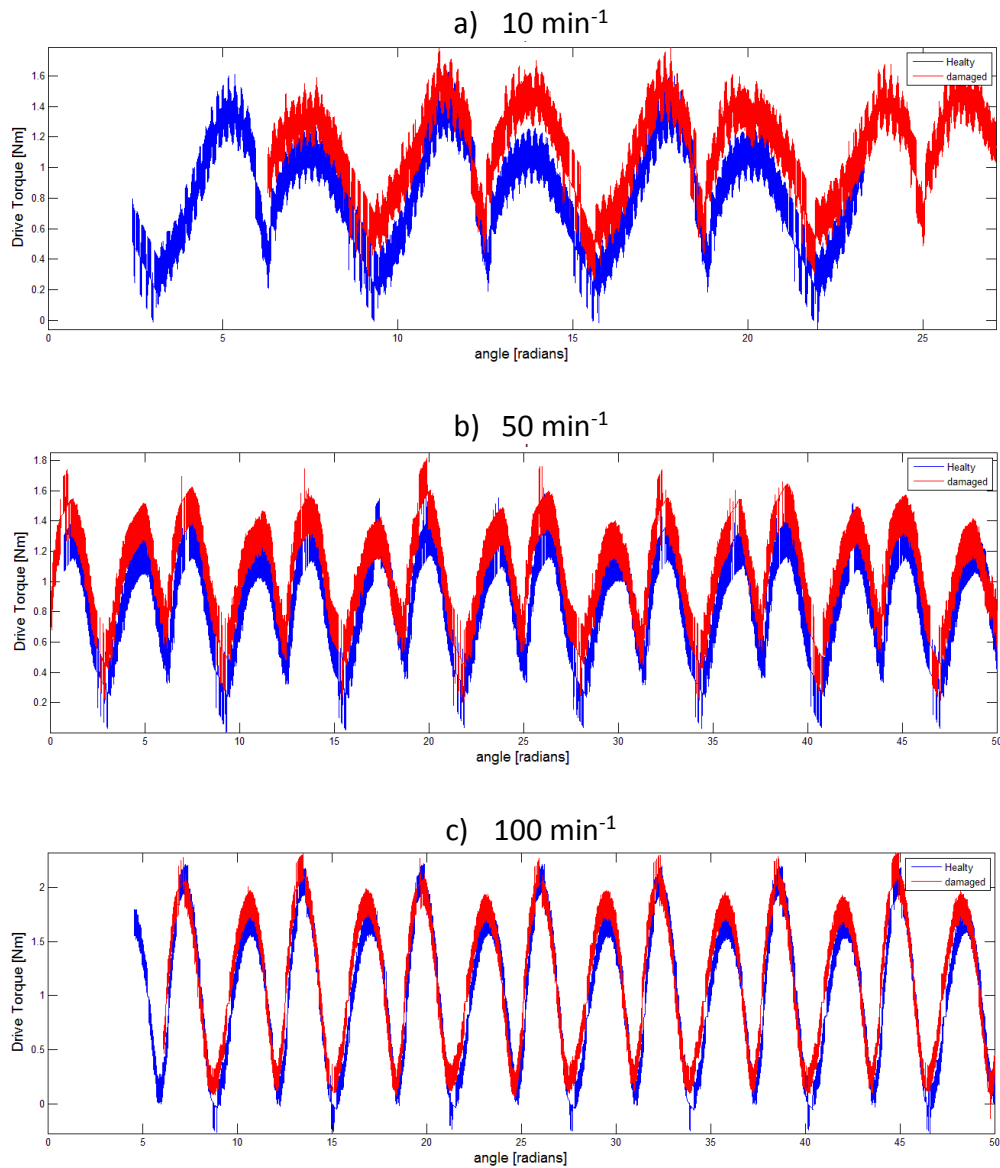


Figure 7.29: Comparison of the motor torque reference with single point bearing damage

The results only showed an increment of constant friction, similar at that produced by generalized rough damage. This resulted on the addition of an offset or constant to the load torque in comparison to the measurements with a healthy bearing.

The recorded data of the motor torque reference was aligned by correlation, in order to detect possible pulsations of the signal taken with the damaged bearing. However, the load torque created by the bearing ball when trying to leave the hole of the fault was not so significant when compared whit that demanded by the mechanism. This fact together with the oscillations due to the slider change of motion direction caused that a pulsation related to the bearing fault could not be detected.

7.4.2 Severe single point fault on bearings

To simulate a more severe fault, a thread was introduced into the cut on the external ring of the bearing to insert a bolt in the path of the rolling balls. In this way, the load torque rises at that single point causing pulsations that are present in the driving torque reference at the output of the velocity control.

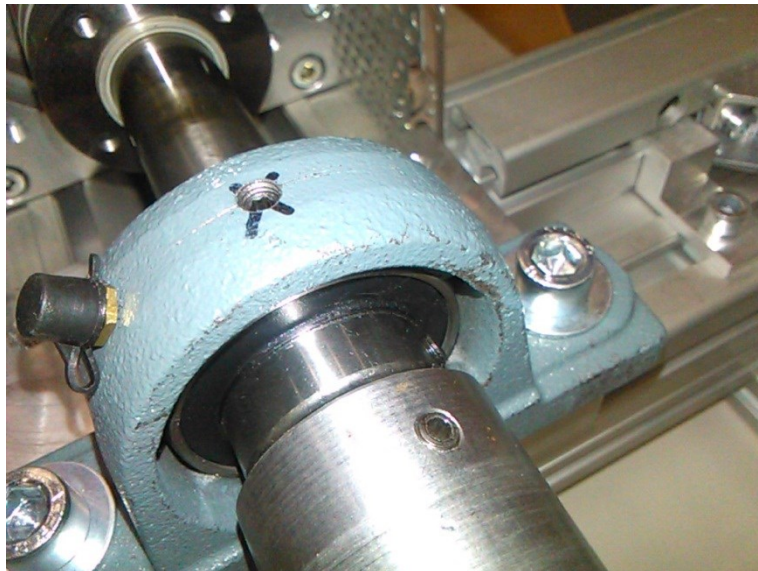


Figure 7.30: Location of the damaged bearing with inserted bolt

The motor torque reference signal was recorded for different tests within the same velocity range as in the previous experiment described in section 7.4.1. This data was compared with the recorded data of the healthy bearing. By utilizing correlation the two signals were aligned to be represented with respect to the angular position. The aligned signals are depicted in the Figure 7.31.

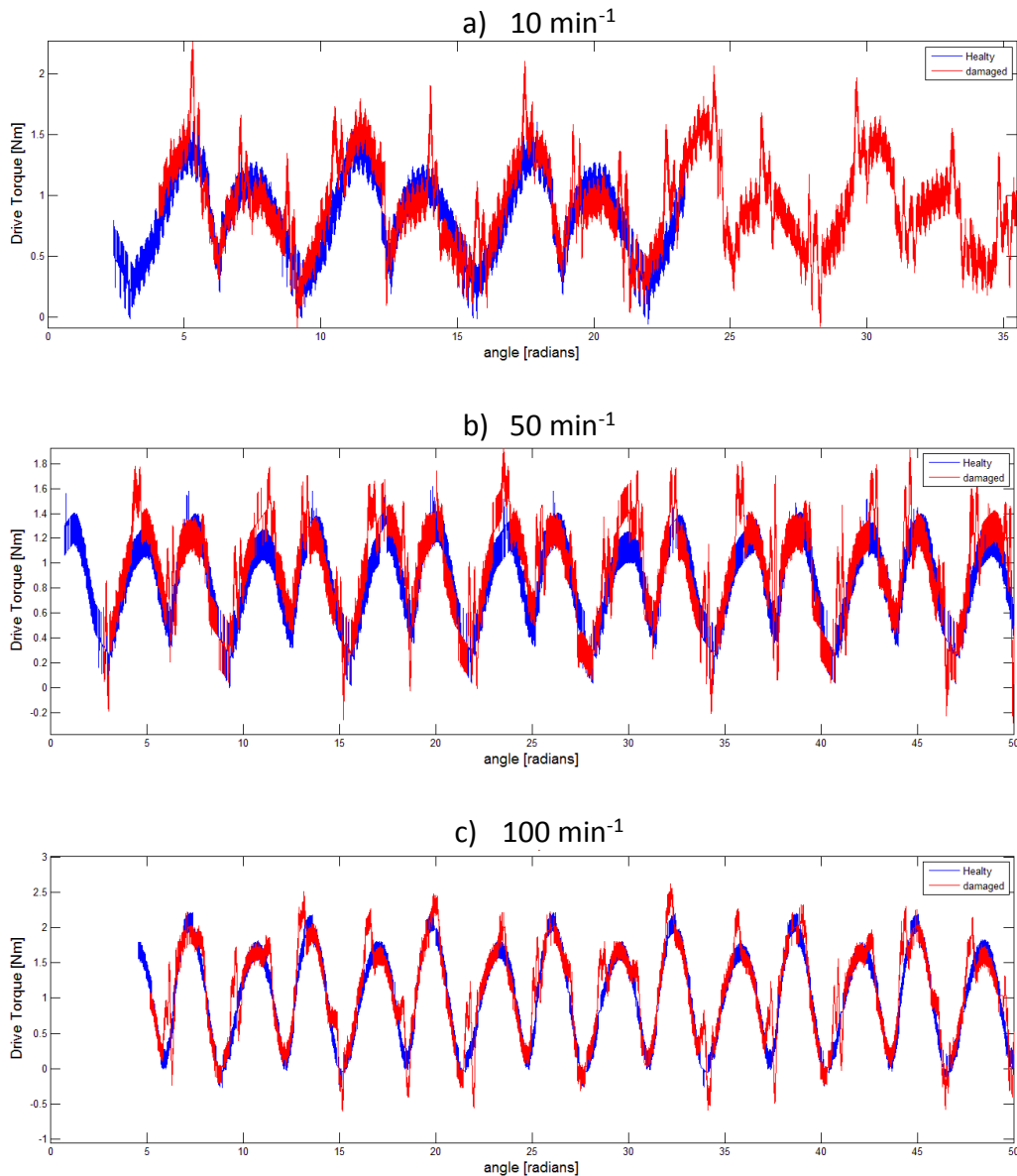


Figure 7.31: Comparison of the motor torque reference with severe single point bearing damage

By this graphical comparison of the motor torque reference taken with healthy and damaged bearing, the pulsation of the motor torque due to severe punctual faults can be detected. On an

expanded view of the comparison taken at 10 min^{-1} , the pulsations can be clearly perceived. This is depicted on Figure 7.32.

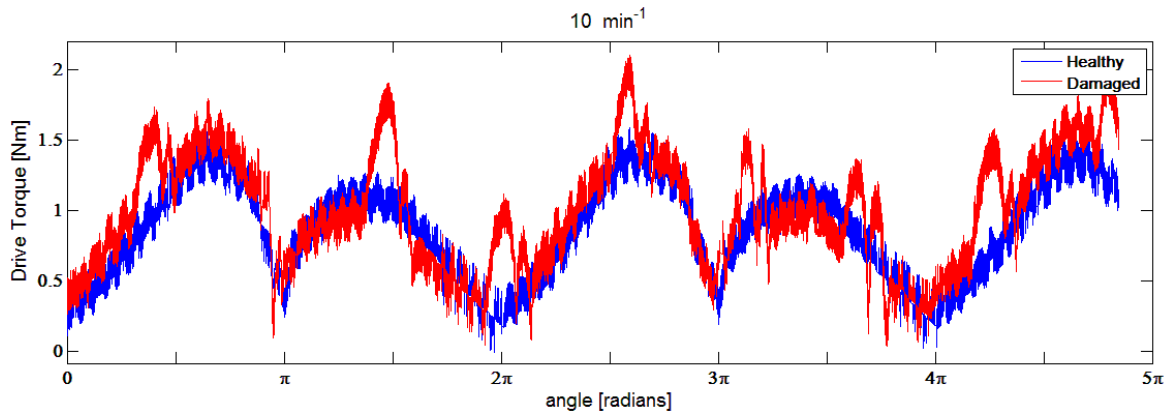


Figure 7.32: Comparison of the motor torque reference at 10 min^{-1} . Expanded view.

By calculating the difference between the motor torque reference taken with the healthy and severe damaged bearing at 10 min^{-1} , the pulsations are still not graphically visible, because of the measurement noise present on both data. However, by filtering the difference between the data of healthy and damaged bearing, the pulsation can be better detected. The difference between measurements was filtered by applying a Butterworth filter of 2nd order and cutoff frequency of 0.01 rad/sample. This filtered difference is depicted on Figure 7.33.

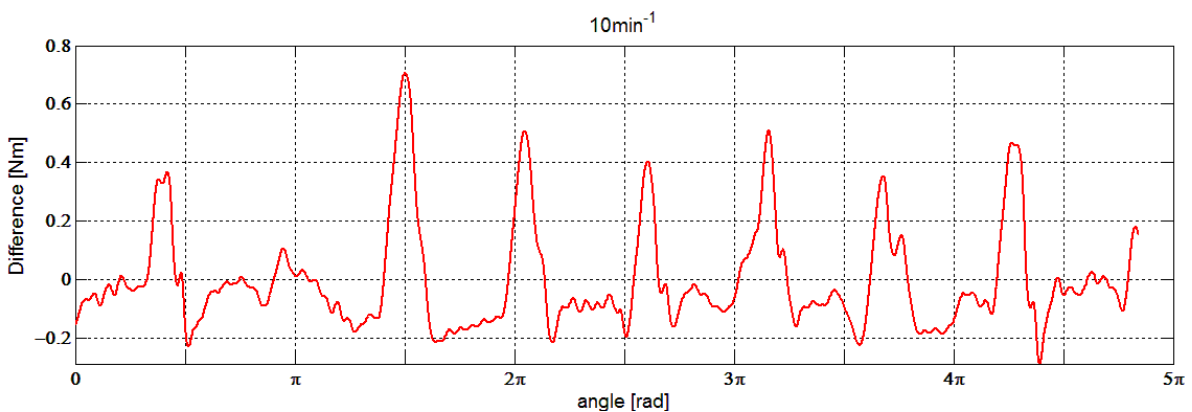


Figure 7.33: Filtered difference on motor torque reference at 10 min^{-1} .

7.5 Summary of the chapter

This chapter presents the results obtained for the experimental verification of the identification, feed-forward control and diagnostic procedures proposed in this work. Two experimental platforms were utilized for the test.

The first part of the chapter is dedicated to the stochastic identification technique with extended Kalman filters. The sensitivity analysis of the EKF to different factors was carried out. The experimental results pointed that the additional excitation and the rate of change of state values were the more important factors.

The Identification of the variable reduced moment of inertia with EKF under a speed sensorless control scheme was achieved. Similar results as those obtained with velocity measurement were obtained, such as higher quality of estimation at lower velocity range and the requirement of large additional excitation to obtain a satisfactory accuracy in the estimated parameters.

The second section the chapter corresponds to the experimental results obtained with the deterministic identification of the drive torque by Fourier series coefficients. The motor torque can be described as a function of the motor position. Sensorless identification by utilizing the Fourier series was also achieved obtaining similar results. These results were used to calculate a mathematical model to emulate the dynamical behavior of the system and its disturbances. The output of the mathematical model of the drive torque was compared to the drive torque reference and both presented a similar behavior.

The third section of this chapter describes the practical implementation of the feed-forward compensation applied together with the classical PI feedback velocity control. By utilizing the mathematical model obtained from the deterministic identification results, the disturbances to the system can be compensated and the velocity response of the system improves. This control was tested to evaluate the steady state, the step response and the ramp response of the system.

The fourth part of the experimental results corresponds to diagnostics. Initially a damage bearing with a fissure in the external ring was utilized. In this initial test, just an increment of friction as an additional constant torque could be detected. A more severe single point fault was simulated

by inserting a physical obstacle to the rolling elements of the bearing. The more severe single point fault caused a periodical pulsation that could be detected when the driving torque reference was measured and compared to the measurements correspondent to the healthy bearing.

8. Conclusions

In the first part of the present dissertation, two velocity-sensorless methods for identification in time domain were presented. The configuration of the mechanical system with repetitive production cycles are frequently found in industrial applications. From the point of view of the drive control a composed mechanism can be represented by its variable reduced moment of inertia and its identification can be used to optimize the controller or to calculate a mathematical model of the system.

First a stochastic identification method was analyzed. This method is of advantage when both load torque and moment of inertia of the mechanical part are unknown. At the present time, this identification method has never been applied to identify a varying moment of inertia under velocity-sensorless control schemes. An EKF sensorless identification structure for the estimation of a variable moment of inertia and variable load torque in motor drives was designed and has been experimentally validated. The noise covariance matrixes of measurements and process model are of prime importance to the accurate estimation and convergence of the estimation to the actual values of the parameters, so any a priori information about the systems is valuable. Additional excitation is of prime importance for the estimation; the model utilized within the EKF assumes a constant load torque and constant moment of inertia, therefore a large amplitude in the additional excitation signal is required to put more weight in the measurements and compensate the modeling errors. The number of shift registers of the PRBS does not perceptibly exert a significant influence on the identification in time domain, this factor was analyzed because on frequency domain methods it has an effect on the identification. The better identification results were achieved at lower velocities ranges, this is also related to the utilized model of constant moment of inertia and constant load torque, as the model calculates each step a constant value, the measurement cannot correct the estimation fast enough if the parameters or variables changes too fast.

In another approach, a novel deterministic method for the identification time domain of a composed mechanism dynamics system based on the approximation of the drive torque reference with Fourier series was developed. Here the velocity control is used as estimator, as

the driving torque must compensate the disturbance to the system, and the changing dynamics of the system due to the varying reduced moment of inertia during operation, so the drive torque reference contains the necessary information to reproduce these factors. By measuring the drive torque at a certain velocity of operation, the Fourier series can be used to obtain an approximation of the dynamics of the system as a function of the position for a given motor velocity.

In the second part of this dissertation, Feed-forward control was utilized for the improvement of the system response. By performing several measurements at different velocity within a range, the Fourier coefficients presenting a direct proportional relation to velocity, can be identified the harmonics related to the variable reduced moment of inertia. The parameters of the model of the mechanical load used for feed-forward compensation were calculated by interpolation. The calculated mathematical model of the system was valid within a range of mechanical velocities from 10 min^{-1} to 100 min^{-1} . Experimental test proved a significant improvement of the velocity response of the system, however the limitations of the model were more evident with the higher velocities of the range. The model could be improved if the effect of viscous friction at higher speeds was included.

In the third part of this dissertation, an outline for the diagnosis on rolling bar bearings in composed mechanism was presented. Two main categories of faults were considered: Generalized rough and single point faults. Because of the changing dynamics of the system and non linearities in the load, oscillations are present in composed mechanism what makes especially difficult to detect the effect of damaged rolling bearings. If the bearing fault is generalized rough, the effect will be the increment of the friction torque in the bearings. In the other hand, large single point faults produces pulsation in the load torque which can be detected as the drive torque reference pulsations. By comparing actual measurements of the drive torque reference to those taken at the commissioning of the drive, pulsations or apparent offset of the signals can be used as indicators of rolling bearing failures.

Future work in the context of identification would be to design modifications to the mechanical model utilized by the EKF algorithm of identification to consider the variation of the reduced moment of inertia and load torque values. This would be a potential improvement for the

estimation of variable mechanical parameters at larger velocity range. Also the amplitude of the additional excitation signal could be reduced and the accuracy of estimation could increase. Then the development of condition monitor strategies in base on the EKF identification could be considered. Comparing the identified mechanical parameters with those obtained at the commissioning of the system can offer an instance for fault detection.

In the context of diagnosis, the deterministic identification with Fourier coefficients could also be utilized to automatically detect drive torque reference changes by comparing actual measurements with criteria defined at the commissioning of the drive.

9. Appendix

9.1 Characterization of the crank slider mechanism for the mass particles model

A multibody system composed by rigid components as a crank slider mechanism can be dynamically represented as a model of mass particles [98] [80]. The mass of the rigid components is distributed on mass particles located at joint of the linkers. The proportion of mass represented by each mass particle is given by the distance of the joint at where the particle is located, to the center of mass of the component.

The geometry of the crank could be described as an extruded prism, so that the distance between the joints and center of mass is determined by the area of the top face. The dimensions of the top face of the crank and distances between joints and center of mass are depicted on Figure 9.1.

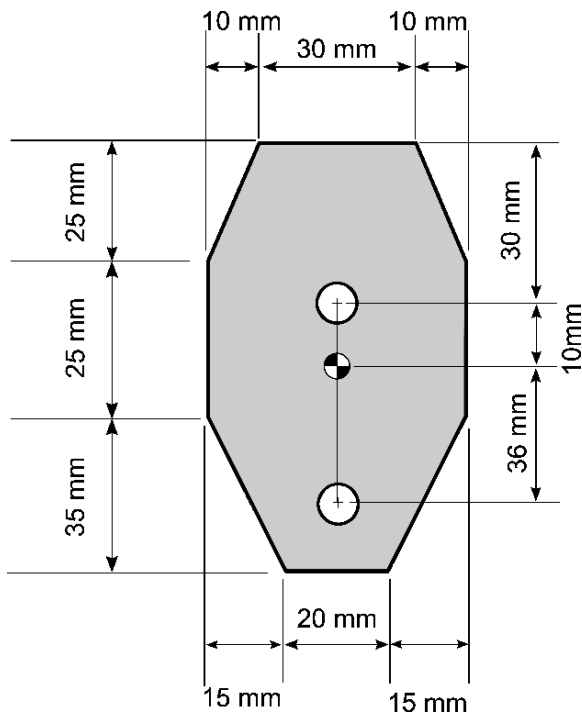


Figure 9.1: Dimensions of the top face of the crank and distance between joints and mass center

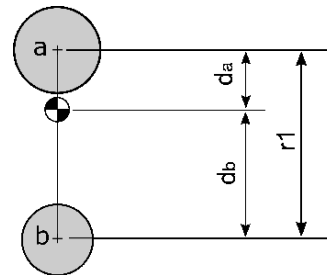


Figure 9.2: Equivalent model of mass particles

The mass particles are given by the expressions:

$$m_{a_crank} = m_{crank} \frac{d_b}{r1} \quad (9.1)$$

$$m_{b_crank} = m_{crank} \frac{d_a}{r1} \quad (9.2)$$

By substituting the dimensions, the values of the mass particles correspondent to the crank were calculated:

$$m_{a_crank} = m_{crank} \frac{36mm}{46mm} \cong m_{crank} \frac{4}{5} \quad (9.3)$$

$$m_{b_crank} = m_{crank} \frac{10}{46} \cong m_{crank} \frac{1}{5} \quad (9.4)$$

As the geometry of the connecting rod is a regular cylinder the mass center is located exactly at the middle of the distance between joints. The slider has only one joint to the connecting rode, therefore the total mass is located at that joint. This can be expressed as:

$$m_{b_connecting_rod} = m_{connecting_rod} \frac{1}{2} \quad (9.5)$$

$$m_{c_connecting_rod} = m_{connecting_rod} \frac{1}{2} \quad (9.6)$$

$$m_{c_slider} = m_{slider} \quad (9.5)$$

The total mass particle at every joint is the total sum of the correspondent mass particles of every element that is located at that joint:

$$m_a = m_{a_crank} \quad (9.7)$$

$$m_b = m_{b_crank} + m_{b_connecting_rod} \quad (9.8)$$

$$m_c = m_{c_connecting_rod} + m_{c_slider} \quad (9.9)$$

By substitution the final expressions for the calculation of the mass particles are:

$$m_a = \frac{4}{5} m_{crank} \quad (9.10)$$

$$m_b = \frac{1}{5} m_{crank} + \frac{1}{2} m_{connecting_rod} \quad (9.11)$$

$$m_c = \frac{1}{2} m_{connecting_rod} + m_{slider} \quad (9.12)$$

9.2 Experimental Platform I

Mass particles model parameter	
$ma=0.30\text{kg}$	$r1=0.07\text{ m}$
$mb=0.9\text{ kg}$	$r2=0.31\text{ m}$
$mc=6.5\text{ kg}$	$exc=0.02\text{ m}$

Moment of inertia	
$J_{motor} = 0.00012\text{ kgm}^2$	$J_{coupling} = 0.001\text{ kgm}^2$

PM Synchronous Motor: Lenze MDKS 056-23	
$M_N = 2.8\text{ Nm}$	
$I_N = 2.3\text{ A}$	

$n_N = 3800 \text{ min}^{-1}$
$P_N = 1.1 \text{ kW}$
<i>pair of poles = 3</i>
$J_M = 1.2 \text{ kg} \cdot \text{cm}^2$

Frequency converter and control: LENZE Servo-drive L-9400

9.3 Experimental Platform II

Mass particles model parameter	
$ma=0.3\text{kg}$	$r1=0.05 \text{ m}$
$mb=0.63 \text{ kg}$	$r2=0.33 \text{ m}$
$mc=5.06 \text{ kg}$	$exc=0.03\text{m}$

Moment of inertia	
$J_{motor} = 0.0006 \text{ kgm}^2$	$J_{coupling} = 0.001 \text{ kgm}^2$

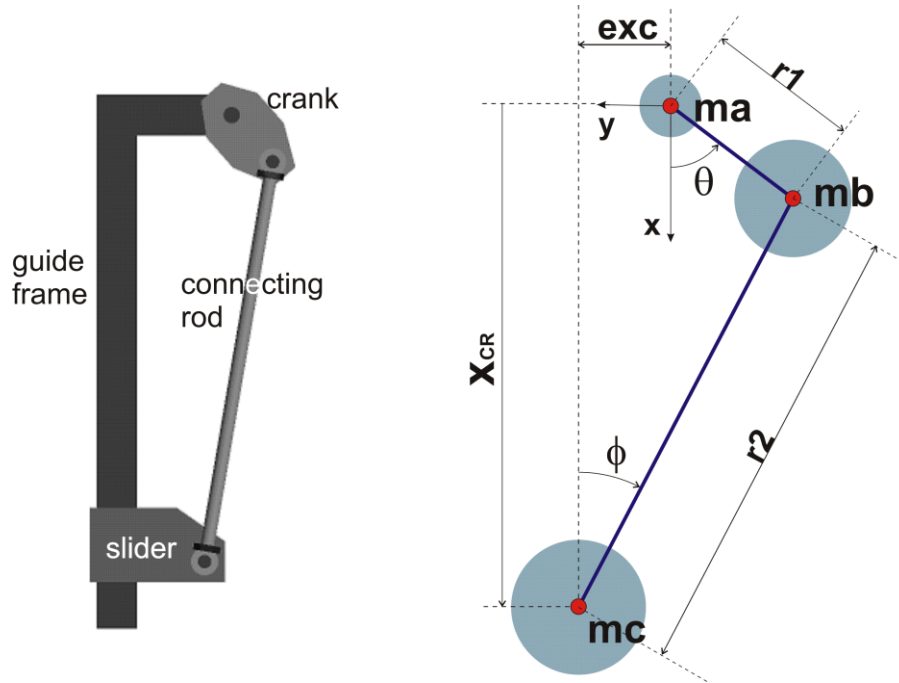
PM Synchronous Motor: <i>ABB Synchronous-Servomotor SDM 101-005N8-115</i>
$M_N = 4.9 \text{ Nm}$
$I_N = 3.3 \text{ A}$
$n_N = 3000 \text{ min}^{-1}$
$P_N = 1.54 \text{ kW}$
<i>pair of poles = 3</i>
$J_M = 6 \text{ kg} \cdot \text{cm}^2$

Frequency converter and control: ABB ACSM1-04 drive Module 0.75-45 kW

9.4 Kinetic energy analysis

The reduced moment of inertia of the slider-crank is obtained from the kinetic energy analysis as explained in section 2.1.3. In the following lines the kinetic energy analysis is calculated

The slider-crank mechanism is composed by 4 elements: slider, crank, connecting rod and guide frame. Each element is a rigid body, and can be approximated as a massless rod connecting two mass particles.



The mass particles utilized in the dynamical models depends on the mass of the elements and the distance between the joint and the center of mass of each element. A detailed procedure for this calculations can be found in the literature [80]

$$m_a = \frac{4}{5} m_{crank} \quad (9.13)$$

$$m_b = \frac{1}{5} m_{crank} + \frac{1}{2} m_{CR} \quad (9.14)$$

$$m_c = \frac{1}{2} m_{CR} + m_{slider} \quad (9.15)$$

The total kinetic energy is:

$$E_k = \frac{1}{2} m_b (r_1 \dot{\theta})^2 + \frac{1}{2} m_c (\dot{x}^2 + \dot{y}^2) \quad (9.16)$$

The closure equations of the mechanism are:

$$x = r_1 \cos \theta + r_2 \cos \phi \quad (9.17)$$

$$exc + r_1 \sin \theta = r_2 \sin \phi \quad (9.18)$$

An expression for ϕ as function of θ can be obtained solving the equation (9.18):

$$\phi = \arcsin \left(\frac{exc + r_1 \sin \theta}{r_2} \right) \quad (9.19)$$

Derivation the equations (9.17) and (9.19) yields:

$$\dot{x} = r_1 \dot{\theta} (-\sin \theta) + r_2 \dot{\phi} (-\sin \phi) \quad (9.20)$$

$$\dot{\phi} = \frac{1}{\sqrt{1 - \left(\frac{exc + r_1 \sin \theta}{r_2} \right)^2}} \cdot \frac{r_1}{r_2} \dot{\theta} \cos \theta \quad (9.21)$$

Substituting equation (9.21) and in (9.17) yields an expression of \dot{x} in terms of θ :

$$\dot{x} = -r_1 \dot{\theta} \sin \theta - r_2 \frac{\frac{r_1}{r_2} \dot{\theta} \cos \theta}{\sqrt{1 - \left(\frac{exc + r_1 \sin \theta}{r_2} \right)^2}} \cdot \frac{exc + r_1 \sin \theta}{r_2} \quad (9.22)$$

Only vertical movement is possible for the slider, therefore:

$$\dot{y} = 0 \quad (9.23)$$

The total kinetic energy, with equation (9.22) and (9.23) results in:

$$E_k = \frac{1}{2} mb(r_1\dot{\theta})^2 + \frac{1}{2} mc \left[-r_1\dot{\theta}\sin\theta - r_2 \frac{\frac{r_1}{r_2}\dot{\theta}\cos\theta}{\sqrt{1 - \left(\frac{exc + r_1\sin\theta}{r_2}\right)^2}} \cdot \frac{exc + r_1\sin\theta}{r_2} \right]^2 \quad (9.24)$$

The equation can be expressed as:

$$E_k = \frac{1}{2} \left\{ mb(r_1)^2 + mc \left[r_1\sin\theta + \frac{\frac{r_1}{r_2}\cos\theta}{\sqrt{1 - \left(\frac{exc + r_1\sin\theta}{r_2}\right)^2}} \cdot (exc + r_1\sin\theta) \right]^2 \right\} \dot{\theta}^2 \quad (9.25)$$

$$= \frac{1}{2} J_e \dot{\theta}^2$$

From this expression of the kinetic energy the reduced moment of inertia can be obtained. The reduced or equivalent moment of inertia of the vertical slider-crank with respect to the crank rotation axis is:

$$J_e = mb(r_1)^2 + mc \left[r_1\sin\theta + \frac{\frac{r_1}{r_2}\cos\theta}{\sqrt{1 - \left(\frac{exc + r_1\sin\theta}{r_2}\right)^2}} \cdot (exc + r_1\sin\theta) \right]^2 \quad (9.26)$$

List of Figures

Figure 1.1 Classification of feed-forward adaptive controllers.....	17
Figure 2.1 Rotary movement scheme	25
Figure 2.2 Block representation of one mass system	26
Figure 2.3 Two mass system scheme	26
Figure 2.4 Three mass system scheme with two examples of possible causes of non-linearities.....	27
Figure 2.5 Cascade control structure	29
Figure 2.6 Diagram of Field Oriented Control with PI velocity control.	30
Figure 2.7 Diagram of Direct Torque control	31
Figure 2.8 Typical cascade control configuration for electrical drives.....	32
Figure 3.1 Extended Kalman Filter structure.....	36
Figure 3.2 PRBS sequence generator	42
Figure 3.3 Time behavior of a PRBS.....	43
Figure 3.4 Possible feedback combinations for PRBS generators with different registers.....	44
Figure 3.5 Control and identification structure.....	46
Figure 3.6 Speed-sensorless identification structure.....	47
Figure 3.7 Mass particle model of the crank shaft.....	49
Figure 3.8 Load torque and equivalent moment of inertia as function of the position	51
Figure 3.9: Simulation results without additional excitation to the system	52
Figure 3.10: Simulation results of the EKF identification with PRBS of 0.4 pu as additional excitation	53
Figure 4.1 Sliding window	62
Figure 4.2 Summation elements within the sliding window for integration	63
Figure 4.3 Velocity control and Fourier identification diagram	64
Figure 5.1 Basic structure of digital feed-forward control.....	67
Figure 5.2 Crank-shaft slider mechanism	68
Figure 5.3 Feed-forward compensation structure	69
Figure 5.4 Reduced moment of inertia representation with respect to the crank angular position.....	70
Figure 6.1 Mechanical construction of a radial ball rolling bearing	74
Figure 6.2 Comparison between measurements of the drive torque reference with healthy and damaged bearing with severe single point failure.....	79
Figure 6.3 Comparison between measurements of the drive torque reference with healthy and damaged bearing with slight single point failure or generalized rough.	80
Figure 7.1 Front view of the mechanical experimental setup.....	84
Figure 7.2 Communication diagram between control and identification board	85
Figure 7.3: Estimation results without additional excitation to the system	86
Figure 7.4: Estimation results when using PRBS with amplitude of 0.48A – 0.1 pu.	87
Figure 7.5: Estimation results when using PRBS with an amplitude of 1.2A - 0.52pu.	88
Figure 7.6: Experimental results at: c)15 min ⁻¹ d)20 min ⁻¹ d)25 min ⁻¹ f)30 min ⁻¹	91
Figure 7.7: Estimation of the reduced moment of inertia at different velocities and model as function of the crank position.....	92
Figure 7.8: Horizontal slider-crankshaft mechanism.....	93
Figure 7.9: Experimental platform diagram	94

Figure 7.10: Dynamically equivalent mass model of the slider crank mechanism	94
Figure 7.11: Equivalent moment of inertia of the crank-shaft as a function of the motor angular position	95
Figure 7.12: Simplified diagram of the velocity sensorless control and identification scheme.....	96
Figure 7.13: Experimental identification of the moment of inertia at different motor velocities under velocity sensorless control	98
Figure 7.14: Estimation of the reduced moment of inertia at 10 min^{-1} by adding mass to the slider plate.	99
Figure 7.15: Fourier coefficients at several crank velocity of rotation	101
Figure 7.16: Crank in position $\gamma = 0^\circ$	102
Figure 7.17: Model output compared to the driving torque reference at 10 min^{-1} and 30 min^{-1}	103
Figure 7.18: Model output compared to the driving torque reference at 60 min^{-1} and 100 min^{-1}	103
Figure 7.19: Velocity Control and Fourier sensorless identification diagram structure	104
Figure 7.20: Fourier coefficients at several crank velocity of rotation under a sensorless control scheme	105
Figure 7.21: Motor velocity comparison with and without feed-forward compensation at steady state	107
Figure 7.22: Step response comparison with and without feed-forward compensation	109
Figure 7.23: Model output compared to the drive torque reference with and without feed-forward compensation d) 1 s e) 3 s ramp	111
Figure 7.24: Motor velocity comparison with and without feed-forward compensation at steady state	112
Figure 7.25: Step response comparison with and without feed-forward compensation	114
Figure 7.26: Velocity ramp response comparison with and without feed-forward compensation d) 1s e) 3s ramp.....	116
Figure 7.27: Location of the damaged bearing	117
Figure 7.28: Fault at the damaged bearing	117
Figure 7.29: Comparison of the motor torque reference with single point bearing damage	118
Figure 7.30: Location of the damaged bearing with inserted bolt	119
Figure 7.31: Comparison of the motor torque reference with severe single point bearing damage	120
Figure 7.32: Comparison of the motor torque reference at 10 min^{-1} . Expanded view.....	121
Figure 7.33: Filtered difference on motor torque reference at 10 min^{-1}	121
Figure 9.1: Dimensions of the top face of the crank and distance between joints and mass center	127
Figure 9.2: Equivalent model of mass particles.....	127

10. References

- [1] C. Schauder, "Adaptive Speed Identification for Vector Control of Induction Motors without Rotational Transducers," *IEEE Transactions on Industry Applications Vol. 28*, p. 1054, October 1992.
- [2] J. W. Finch and D. Giaouris, "Controlled AC Electrical Drives," *IEEE Transactions on industrial electronics Vol. 55 No. 2*, p. 481, February 2008.
- [3] H. Zoubek and M. Pacas, "An Identification Method for Multi-Mass-System in Speed-Sensorless Operation," *IEEE International Symposium on Industrial Electronics*, p. 1895, 27-30 June 2011.
- [4] H. Zoubek and M. Pacas, "Two steps towards speed estimation and encoderless identification of two mass-systems with extended speed adaptive observer structure," *IECON-37th Annual Conference on IEEE Industrial Electronics Society*, p. 1553, 7-10 November 2011.
- [5] S. Saarakkala, T. Leppinen, M. Hinkkanen and J. Luomi, "Parameter estimation of two-mass mechanical loads in electric drives," in *IEEE International Workshop on Advanced Motion Control*, Sarajevo, 2012.
- [6] S. Saarakkala and M. Hinkkanen, "Identification of two-mass mechanical systems in closed-loop speed control," in *Annual Conference of the IEEE Industrial Electronics Society*, Viena, 2013.
- [7] S. E. Saarakkala and M. Hinkkanen, "Identification of two-mass mechanical systems using torque excitation: Design and experimental evaluation," in *International Power Electronics Conference (IPEC-Hiroshima 2014 - ECCE-ASIA)*, Hiroshima, 2014.
- [8] F. Andoh, "Moment of inertia identification usgin the time average of the product of torque reference input and motor position," *IEEE Transactions on power electronics*, p. 2534, November 2007.
- [9] F. Andoh, "Inertia identification of mechatronic servo systems with infinitesimal motions," in *Proceedings of the 3rd Annual Conference on Automation Science and Engineering*, Scottsdale, 2007.
- [10] Y. Guo, "Research on inertia identification and auto-tuning of speed controller for AC servo system," in *IEEE Proceedings of the Power Conversion Conference*, Osaka, 2002.
- [11] Y. Toyozawa, N. Sonoda, H. Harada and H. Kashiwagi, "A method for on-line identification of mechanical system by use of M-sequence," in *IEEE Proceedings of SICE Annual Conference2010*, Taiwan, 2010.

-
- [12] I. Pletschen, S. Rohr, G. Herrman and R. Kennel, "Online parameter-estimation of feedforward gains in cascaded control structures for servo drives," in *IEEE Proceedings of the Power Electronics and Applications European Conference*, Birmingham , 2011.
- [13] I. Pletschen, S. Rohr and R. Kennel, "Inertia estimation of servo drives with elastically attached masses," in *IET International Conference on Power Electronics, Machines and Drives*, Bristol , 2012.
- [14] K. Szabat and T. Orłowska-Kowalska, "Application of the extended Kalman filter in advanced control structure of a drive system with elastic joint," in *IEEE International Conference on Industrial Technology, ICIT 2008.*, Chengdu, 2008.
- [15] L. Harnefors, S. Saarakkala and M. Hinkkanen, "Speed Control of Electrical Drives Using Classical Control Methods," *IEEE Transactions on Industry Applications*, pp. 889-898, March-April 2013.
- [16] C. De Angelo, G. Bossio, J. Solsona, G. O. García and M. I. Valla, "Mechanical Sensorless Speed Control of Permanent-Magnet AC Motors Driving an Unknown Load," *IEEE Transactions on Industrial Electronics*, pp. 406-414, April 2006.
- [17] D. Janiszewski, "Load torque estimation in sensorless PMSM drive using Unscented Kalmana Filter," in *IEEE International Symposium on Industrial Electronics*, Gdansk, 2011.
- [18] D. Janiszewski, "Load Torque Estimation for sensorless PMSM drive with output filter fed by PWM converter," in *39th Annual Conference Industrial Electronics Society*, Vienna, 2013.
- [19] K. Szabat and T. Orłowska-Kowalska, "Vibration Suppression in a Two-Mass Drive System Using PI Speed Controller and Additional Feedbacks—Comparative Study," *IEEE Transactions on Industrial Electronics* , pp. 1193-1206, April 2007.
- [20] K. Szabat and T. Orłowska-Kowalska, "Damping of the Torsional Vibration in Two-Mass Drive System Using Forced Dynamic Control," in *The international Conference on Computer as a Tool, EUROCON 2007*, Warsaw, 2007.
- [21] K. Szabat, T. Orłowska-Kowalska and M. Dybkowski, "Indirect Adaptive Control of Induction Motor Drive System With an Elastic Coupling," *IEEE Transactions on Industrial Electronics*, pp. 4098-4042, October 2009.
- [22] M. Cychowski, K. Szabat and T. Orłowska-Kowalska, "Constrained Model Predictive Control of the Drive System With Mechanical Elasticity," *IEEE Transactions on Industrial Electronics*, vol. 56, no. 6, pp. 1963-1973, 2009.
- [23] K. Szabat, P. Serkies, T. Orłowska-Kowalska and M. Cychowski, "Robust torque constraints handling in drive systems with elastic transmission," in *IEEE International Conference on Industrial Technology ICIT*, Viña del Mar, 2010.

-
- [24] I. Herman and P. Vaclavek, "Load torque and moment of inertia observability analysis for alternating current drive sensorless control," in *38th Annual Conference on IEEE Industrial Electronics Society*, QC, 2012.
- [25] Y. Zhou, X. Mei, D. Liu, J. Gedong and S. N., "Sensorless rapid on-line evaluation for slide level," in *International Asia conference on informatics in control, automation and robotics*, Bangkok, 2009.
- [26] S. Villwock, *Identifikationsmethoden für die automatisierte Inbetriebnahme und Zustandsüberwachung elektrischer Antriebe*, Siegen: Universität Siegen, 2007.
- [27] H. Zoubeck and M. Pacas, "Two steps towards speed estimation and encoderless identification of two-mass-systems with extended speed adaptive observer structure," in *37th Annual Conference on IEEE Industrial Electronics Society*, Melbourne, VIC, 2011.
- [28] H. Zoubeck and M. Pacas, "A Method for Speed-Sensorless Identification of Two-Mass-Systems," Siegen, 2010.
- [29] I. Mareels and J. W. Polderman, *Adaptive systems, an introduction*, Boston: Birkhäuser, 1996.
- [30] R. Isermann, K.-H. Lachmann and D. Matko, *Adaptive Control Systems*, UK: Prentice Hall, 1992.
- [31] H. Unbehauen, "Adaptive dual control systems: a survey," in *Adaptive Systems for Signal Processing, Communications and Control Symposium AS-SPPC IEEE*, Lake Louise, Alta, 2000.
- [32] "Report of Large Motor Reliability Survey of Industrial and Commercial Installations, Part I," *IEEE Transactions on Industry Applications*, Vols. IA-21, no. 4, pp. 853-864, 1985.
- [33] P. F. Albrecht, J. C. Appiaris, R. M. McCoy, E. Owen and D. K. Sharma, "Assessment of the Reliability of Motors in Utility Applications - Updated," *IEEE Transactions on Energy Conversion*, Vols. EC-1, no. 1, pp. 39 - 46, 1986.
- [34] P. Vas, *Parameter Estimation, Condition Monitoring and Diagnosis of Electrical Machines*, Oxford, UK: Clarendon Press, 1993.
- [35] P. Zhang and Y. Du, "A Survey of Condition Monitoring and Protection Methods for Medium-Voltage Induction Motors," *IEEE Transactions on Industry Applications*, vol. 47, no. 1, pp. 34 - 46, 2011.
- [36] J. Stack, T. Habetler and R. Harley, "Fault signature modeling and detection of inner race bearing faults," in *IEEE International Conference on Machines and Drives*, San Antonio, TX, 2005.
- [37] J. Stack, R. Harley and T. Habetler, "An amplitude Modulation detector for fault diagnosis in rolling element bearings," *IEEE Transactions on Industrial Electronics*, vol. 51, no. 5, pp. 1097 - 1102, 2004.

-
- [38] L. Shuang and L. Meng, "Bearing Fault Diagnosis Based on PCA and SVM," in *IEEE International Conference on Mechatronics and Automation*, Harbin, 2007.
- [39] S. McInerney and Y. Dai, "Basic vibration signal processing for bearing fault detection," *IEEE Transactions on Education*, vol. 46, no. 1, pp. 149 - 156, 2003.
- [40] U. Klein, *Schwingungsdiagnostische Beurteilung von Maschinen und Anlagen*, Germany: Stahleisen Verlag, 2003.
- [41] J. Kolerus and J. Wassermann, *Zustandsüberwachung von Maschinen*, Germany: expert verlag, 2009.
- [42] I. Onel and M. El Hachemi Benbouzid, "Induction Motor Bearing Failure Detection and Diagnosis: Park and Concordia Transform Approaches Comparative Study," *IEEE/ASME Transactions on Mechatronics*, vol. 13, no. 2, pp. 257-262, 2008.
- [43] J. Stack, T. Habetler and R. Harley, "Bearing fault detection via autoregressive stator current modeling," in *IAS Annual Meeting. Conference Record of the Applications Conference*, Salt Lake City, 2003.
- [44] M. Pineda-Sanchez, R. Puche-Panadero, M. Riera-Guasp, J. Perez-Cruz, J. Roger-Folch, J. Pons-Llinares, V. Climente-Alarcon and J. Antonino-Daviu, "Application of the Teager-Kaiser Energy Operator to the Fault Diagnosis of Induction Motors," *IEEE Transactions on Energy Conversion*, vol. 28, no. 4, pp. 1036-1044, 2013.
- [45] A. Bellini, F. Immovilli, R. Rubini and C. Tassoni, "Diagnosis of bearing faults in induction machines by vibration or current signals: a critical comparison," in *IEEE Industry Applications Society Annual Meeting*, Edmonton, Alta, 2008.
- [46] Z. Wei, T. Habetler and R. Harley, "Bearing Fault Detection Via Stator Current Noise Cancellation and Statistical Control," *IEEE Transactions on Industrial Electronics*, vol. 55, no. 12, pp. 4260 - 4269, 2008.
- [47] M. Blodt, P. Granjon, B. Raison and G. Rostaing, "Models for bearing damage detection in induction motors using stator current monitoring," in *IEEE International Symposium on Industrial Electronics*, Ajaccio, 2004.
- [48] M. Blödt, D. Bonacci, J. Regnier and M. Chabert, "Diagnosis of Bearing Faults of Induction Machines by Vibration or Current Signals: A Critical Comparison," *IEEE Transactions on Industrial Electronics*, vol. 55, no. 2, pp. 522-533, October 2008.

-
- [49] S. Villwock, M. Pacas and T. Eutebach, "Application of the Welch-method for the automatic parameter identification of electrical drives," in *31st Annual Conference of IEEE Industrial Electronics Society IECON*, 2005.
- [50] M. Pacas, S. Villwock and T. Eutebach, "Identification of the mechanical system of a drive in the frequency domain," in *Annual Conference of IEEE Industrial Electronics Society*, 2004.
- [51] S. Villwock, H. Zoubek and M. Pacas, "Rolling Bearing Condition Monitoring Based on Frequency Response Analysis," in *IEEE International Diagnostics for Electric Machines, Power Electronics and Drives SDEMPED*, Cracow, 2007.
- [52] H. Zoubek, S. Villwock and M. Pacas, "Automated diagnosis of rolling bearing faults in electrical drives," in *7th International Conference on Power Electronics, ICPE*, Daegu, 2007.
- [53] H. Zoubek, S. Villwock and M. Pacas, "Frequency Response Analysis for Rolling-Bearing Damage Diagnosis," *IEEE Transactions on Industrial Electronics*, vol. 55, no. 12, pp. 4270 - 4276, 2008.
- [54] S. Villwock and M. Pacas, "Deterministic Method for the Identification of Backlash in the Time Domain," in *IEEE International Symposium on Industrial Electronics*, Montreal, Que., 2006.
- [55] S. Villwock and M. Pacas, "Time-Domain Identification Method for Detecting Mechanical Backlash in Electrical Drives," in *IEEE Transactions on Industrial Electronics*, Vol. 56, No.2, Siegen, 2009.
- [56] M. Pacas and S. Villwock, "Development of an expert system for identification, commissioning and monitoring of drives," in *Power Electronics and Motion Control Conference, 13th EPE-PEMC*, Poznan, 2008.
- [57] R. Isermann, *Mechatronische Systeme*, Berlin: Springer, 2008.
- [58] L. Ljung, *System identification*, USA: Prentice Hall, 1999.
- [59] S. Villwock and M. Pacas, "Application of the Welch-Method for the Identification of Two- and Three-Mass-Systems," *IEEE Transactions on Industrial Electronics*, vol. 55, no. 1, pp. 457-466, 2008.
- [60] S. Tøffner-Clausen, *System Identification and Robust Control*, London: Springer, 1996.
- [61] L. Litz, "Reduktion der Ordnung linearer Zustandsraummodelle mittels modaler Verfahren," Dissertation, Univ. Karlsruhe, 1979.
- [62] D. Schröder, *Elektrische Antriebe Regelung von Antriebssystemen*, Berlin: Springer, 2009.
- [63] K. Hoffer, *Sensorlose Antriebsregelungen*, Düsseldorf: VDI, 1990.

- [64] W. Leonhard, *Control of Electrical Drives*, Berlin: Springer-Verlag, 2001.
- [65] K. Haase, "Zum dynamischen Verhalten der Asynchronmaschine bei Betrieb mit variabler Ständerfrequenz und Ständerspannung," *Elektrotechnische Zeitschrift*, vol. 89, no. A, pp. 387-391, 1968.
- [66] F. Blaschke, "The principle of field orientation applied to the new trans-vector closed-loop control system for rotating field machines," *Siemens-Review*, vol. 39, p. 217-220, 1972.
- [67] M. Depenbrock, "Direct self-control (DSC) of inverter-fed induction machine," *IEEE Transactions on Power Electronics*, vol. 3, no. 4, pp. 420 - 429, Oct 1988.
- [68] I. Takahashi and T. Noguchi, "A New Quick-Response and High-Efficiency Control Strategy of an Induction Motor," *IEEE Transactions on Industry Applications*, Vols. IA-22, no. 5, pp. 820 - 827, 1986.
- [69] J. Holtz and Q. Juntao, "Sensorless vector control of induction motors at very low speed using a nonlinear inverter model and parameter identification," *IEEE Transactions on Industry Applications*, vol. 38, no. 4, pp. 1087 - 1095, 2002.
- [70] J. Solsana, M. Valla and C. Muravchik, "A nonlinear reduced order observer for permanent synchronous motors," *IEEE Transactions Industrial Applications*, vol. 43, no. 4, pp. 492-497, 1996.
- [71] T. Takeshita, A. Usui and N. Matsui, "Sensorless salientpole PM synchronous motor drive in all speed ranges," *Electrical Engineering in Japan*, Vols. 120-D, no. 2, pp. 240-247, 2001.
- [72] R. Isermann, *Identifikation dynamischer Systeme I*, vol. I and II, Berlin: Springer-Verlag, 1988.
- [73] R. E. Kalman, "A New Approach to Linear Filtering and Prediction Problems," *Transaction of the ASME*, pp. 35 - 45, March 1960.
- [74] P. Maybeck, *Stochastic Models, Estimation and Control*, USA: Academic Press, Inc., 1979.
- [75] R. Isermann, *Digitale Regelsysteme*, Vol. 2, Berlin: Springer Verlag, 1991.
- [76] R. G. Brown and P. Hwang, *Introduction to Random Signals and Applied Kalman Filtering*, USA: Wiley, 2012.
- [77] D. Simon, *Optimal State Estimation*, USA: Wiley, 2006.
- [78] M. Werner, "Digitale Signalverarbeitung mit MATLAB," Vieweg+Teubner, Berlin, 2001.
- [79] H. Strobel, "Experimentelle Systemanalyse," Akademie-Verlag, Berlin, 1975.

- [80] A. Ghosh and A. Kumar Mallik, Theory of Mechanisms and Machines, New Delhi, India: Affiliated East-West Press , 1988.
- [81] J. G. Proakis and D. G. Manolakis, Digital Signal Processing, New Jersey: Prentice-Hall, 1996.
- [82] H. Kerle, B. Corves and M. Hüsing, Getriebetechnik, Wiesbaden: Vieweg+Teubner, 2011.
- [83] P. Vas, Vector Control of AC Machines, Great Britain: Oxford Science Publications, 1990.
- [84] R. Stevens B., Handbook of mathematical tables and formulas, USA: McGraw-Hill, 1972.
- [85] S. Dufoo Ochoa, Diagnostics of Rotor Asymmetries in Inverter Fed Induction Machines, Dissertation, Siegen, Germany: Naturwissenschaftlich-Technische Fakultät der Universität Siegen, 2012.
- [86] E. T. Serna Calvo, Diagnostics of rotor asymmetries in inverter-fed, variable speed induction machines, Universität Siegen Diss., Germany: Logos-Verlag, 2009.
- [87] H. Haberhauer and F. Bodenstein, Maschinenelemente, Germany: Springer Vieweg, 2014.
- [88] G. Niemann, H. Winter and B.-R. Höhn, "Maschinenelemente," in *Band 1: Konstruktion und Berechnung von Verbindungen, Lagern, Wellen*, Würzburg, Springer, 2005, pp. 614 - 615.
- [89] T. A. Harris and M. N. Kotzalas, Essential Concepts of Bearing Technology, United States of America: Taylor and Francis Group, 2007.
- [90] T. A. Harris and M. N. Kotzalas, Advanced Concepts of Bearing Technology, United States of America: Taylor and Francis Group, 2007.
- [91] J. R. Stack, T. G. Habetler and R. G. Harley, "Fault Classification and Fault Signature Production," *IEEE Transactions on Industry Applications*, vol. 40, no. 3, pp. 735 - 739, 2004.
- [92] T. Thümmel, Experimentelle Mechanismendynamik, Habilitationsschrift, München: VDI-Verlag, 2008.
- [93] H. Dresig, Schwingungen mechanischer Antriebssysteme, Berlin: Springer Verlag, 2006.
- [94] A. Palmgren, Grundlagen der Wälzlagertechnik, Stuttgart: Franckh'sche Verlagshandlung, 1964.
- [95] W. Zientz, *Untersuchung des Betriebsverhaltens oszillierend drehend bewegter Wälzlager in den Gelenken von Mechanismen und Getrieben. Dissertation*, Universität Siegen: VDI-Verlag GmbH, 1989.
- [96] F. O. u. H. AG, *FAG Wälzlager Katalog WL 41 520/2 DB*, Schweinfurt: FAG, 1996.

- [97] M. Perdomo, M. Pacas, T. Eutebach and J. Immel, "Sensitivity analysis of the identification of variable inertia with an extended Kalman Filter," in *39th Annual Conference of the IEEE Industrial Electronics Society, IECON 2013*, Vienna, 2013.
- [98] H. a. H. F. Dresig, *Maschinendynamik*, Berlin: Springer-Verlag, 2005.
- [99] S. Beineke, *Online-Schätzung von Mechanischen Parametern, Kennlinien und Zustandsgrößen geregelter Elektrischer Antriebe*, Düsseldorf: VDI Verlag, 2000.
- [100] M. Perdomo, M. Pacas, T. Eutebach and J. Immel, "Identification of variable mechanical parameters using extended Kalman Filters," in *Diagnostics for Electric Machines, Power Electronics and Drives 9th IEEE International Symposium*, Valencia, 2013.
- [101] C. Fritzen, *Maschinendynamik*, Deutschland: Universität Siegen, 2012.
- [102] E. Kiel, *Antriebslösungen*, Berlin: Springer-Verlag, 2007.
- [103] G. Yujie, "Research on inertia identification and auto-tuning of speed controller for AC servo system," in *IEEE Proceedings of the Power Conversion Conference*, Osaka, 2002.